

University of Alberta

DEVELOPMENT, TESTING, AND APPLICATIONS OF NEW PSEUDOPOTENTIAL
METHODS FOR THE CALCULATION OF MOLECULAR STRUCTURES AND SPECTRA

by

Christopher Charles Lovallo



A thesis submitted to the Faculty of Graduate Studies and Research in partial fulfillment of the requirements for the degree of **Doctor of Philosophy**.

Department of Chemistry

Edmonton, Alberta
Spring 2004



Library and
Archives Canada

Bibliothèque et
Archives Canada

Published Heritage
Branch

Direction du
Patrimoine de l'édition

395 Wellington Street
Ottawa ON K1A 0N4
Canada

395, rue Wellington
Ottawa ON K1A 0N4
Canada

Your file *Votre référence*
ISBN: 0-612-96297-0
Our file *Notre référence*
ISBN: 0-612-96297-0

The author has granted a non-exclusive license allowing the Library and Archives Canada to reproduce, loan, distribute or sell copies of this thesis in microform, paper or electronic formats.

L'auteur a accordé une licence non exclusive permettant à la Bibliothèque et Archives Canada de reproduire, prêter, distribuer ou vendre des copies de cette thèse sous la forme de microfiche/film, de reproduction sur papier ou sur format électronique.

The author retains ownership of the copyright in this thesis. Neither the thesis nor substantial extracts from it may be printed or otherwise reproduced without the author's permission.

L'auteur conserve la propriété du droit d'auteur qui protège cette thèse. Ni la thèse ni des extraits substantiels de celle-ci ne doivent être imprimés ou autrement reproduits sans son autorisation.

In compliance with the Canadian Privacy Act some supporting forms may have been removed from this thesis.

Conformément à la loi canadienne sur la protection de la vie privée, quelques formulaires secondaires ont été enlevés de cette thèse.

While these forms may be included in the document page count, their removal does not represent any loss of content from the thesis.

Bien que ces formulaires aient inclus dans la pagination, il n'y aura aucun contenu manquant.

Canada



UNIVERSITY OF ALBERTA

25 November 2003

Transfer of Copyright

I hereby give permission for Christopher C. Lovallo to use copyrighted information in Chapters 2 – 7 of his Ph.D. Thesis. I should add that the full copyrights were transferred to the publishers of various journals.

Mariusz Klobukowski

Department of Chemistry

Edmonton • 114 Street – 91 Avenue • Alberta • Canada • T6G 2G2
Telephone: (780) 492-2568 • (780) 492-3477 • Fax: (780) 492-8231
E-mail: Mariusz.Klobukowski@ualberta.ca

Abstract

The desire to study larger compounds with advanced computational methods drives the need for faster and more accurate models. This thesis focuses on development and testing of two new pseudopotential methods: one accurate for smaller systems, and one faster for larger complexes.

Chapters 2 and 3 describe the project designed to update the Model Core Potentials. The improved Model Core Potentials (iMCPs) were developed for the transition metals and the elements that are often found in ligand groups. The iMCPs reproduce atomic all-electron calculations with great accuracy. Transition metal complexes from all groups were studied, and the results compared to experimental data. The iMCPs were superior to previous versions of the MCPs at reproducing both geometries and frequencies. The effects of relativity and electron correlation were also studied.

Results of iMCP tests on the structures and energetics of compounds containing xenon-carbon bonds are discussed in Chapter 4. Both geometries and energies of small organic complexes were well-described at correlated levels of theory with the iMCPs. Density functional theory calculations suggested a number of undiscovered compounds that are thermodynamically stable with respect to their reactants.

In Chapter 5, reparameterization of the well-tempered Model Core Potentials (wtMCPs) was done in order to study the interaction between the rare gases and coinage metal monohalides. The binding energies in these systems were found to range from the strength of a hydrogen bond to that of a weak covalent bond. Structural parameters were calculated in order to predict spectroscopic constants for previously unknown compounds of this type.

The final two chapters deal with accurate calculations on interactions between helium and alkaline earth metals. The wtMCP basis sets used are augmented with bond

functions. Chapter 6 presents results obtained with a smaller polarization space, in order to test the applicability of the pseudopotential method along with the coupled-cluster methods on these systems. In Chapter 7, the polarization space was expanded in order to study the systems near the basis set limit. Results for CaHe agreed well with previous high-level calculations; for SrHe and BaHe, the present results are the best yet available for these systems.

If we knew what we were doing, it wouldn't be called research, would it?

Albert Einstein

It is folly to use as one's guide in the selection of fundamental science the creation of utility. Not because (scientists)... despise utility. But because... useful outcomes are best identified after the making of discoveries, rather than before.

John Polanyi

...man will occasionally stumble over the truth, but usually manages to pick himself up, walk over or around it, and carry on.

Winston Churchill

Quantum mechanics: the dreams that stuff is made of.

Damon Runyon

On two occasions I have been asked [by members of Parliament!], 'Pray, Mr. Babbage, if you put into the machine wrong figures, will the right answers come out?' I am not able rightly to apprehend the kind of confusion of ideas that could provoke such a question.

Charles Babbage

To my mother and to Maria, who were always there for me.

Acknowledgements

First of all, I would like to thank my supervisor, Mariusz Klobukowski, for all of his help and support over the years. Through the ups and downs, successes and failures, computer glitches and user errors, he was always there with some good advice and ideas for another way to tackle the problem. I wouldn't be here today without him. Our group, although small, has also always been a great source of ideas and discussions throughout the years. I have had the opportunity to work with some great people here, including Dr. Steven Decker, Jonathan Mane, John Lo, and Lara Silkin.

I would also like to acknowledge the Department of Chemistry, the Faculty of Science, the Province of Alberta, and NSERC for my funding; and the Department of Chemistry and NSERC for the funding of workstations used in the calculations. Additional computer time was provided by the University of Alberta Computing and Network Services, who have been a huge help over the years; and the Multimedia Advanced Computing Infrastructure provided access to the SGI supercomputers.

The present work would not be possible without the computer programs that people around the world generously provided to us. I would like to thank Dr. Mark Gordon and Dr. Michael Schmidt for continually providing us with the latest version of the GAMESS program, along with invaluable technical support and suggestions. Dr. Roger Amos provided us with the CADPAC program, and was very helpful in explaining the implementations of various methods in CADPAC. Finally, not only did Dr. Robert LeRoy provide us with his LEVEL program, he even came to the university to give seminars on how best to use it.

I would like to thank all of my friends and family in Edmonton and beyond. This has been a wonderful experience in every way, and I have you to thank for that. You have taught me that sometimes the best way to solve a problem is to go out and leave

it behind for a bit. Lastly, I especially would like to say thank you to Maria and my Mom. They both know me well enough to understand that sometimes I need a kick to get going, and have always been there, day or night, to support me in every way possible. Believe it or not, it's actually done!

Table of Contents

1	Introduction	1
1.1	The Electronic Schrödinger Equation	2
1.2	The Hartree-Fock Method	4
1.3	Post-Hartree-Fock Methods	9
1.3.1	Configuration Interaction Method	9
1.3.2	Coupled-Cluster Theory	12
1.3.3	Møller-Plesset Perturbation Theory	13
1.4	Density Functional Theory	17
1.5	Pseudopotentials	21
1.5.1	Effective Core Potentials	23
1.5.2	Model Core Potentials	24
1.5.3	Relativistic Potentials	26
1.6	Relativistic Effects	26
1.7	Basis Sets	30
1.7.1	Slater- and Gaussian-Type Functions	31
1.7.2	Contracted Gaussian Functions	33
1.7.3	Well-Tempered Basis Sets	35
1.7.4	Polarization Functions	36
1.7.5	Bond Functions	36
1.8	Interpretation of the Wavefunction	37
1.8.1	Atomic Polarizabilities	37
1.8.2	Long-Range Dispersion Interactions	38
1.8.3	Potential Energy Surfaces	38
1.9	Scope of this Thesis	42
2	Improved Model Core Potentials for the First-Row Transition Metals	51
2.1	Introduction	51
2.2	Outline of the MCP Formalism	53
2.3	Determination of Potentials and Basis Sets	54
2.4	Computational Methods	59
2.5	Results and Discussion	59
2.6	Conclusions	68

3	Improved Model Core Potentials for the Second- and Third-Row Transition Metals	72
3.1	Introduction	72
3.2	Determination of Potentials and Basis Sets	73
3.3	Computational Methods	77
3.4	Results and Discussion	77
3.5	Conclusions	86
4	Application of the Improved Model Core Potentials to the Thermochemistry of Organoxenon Complexes	90
4.1	Introduction	90
4.2	Computational Methods	92
4.3	Results and Discussion	93
4.4	Conclusions	101
5	Transition Metal - Rare Gas Bonding: The Next Frontier	106
5.1	Introduction	106
5.2	Computational Methods	107
5.3	Results and Discussion	108
5.4	Conclusions	112
6	Accurate <i>ab initio</i> Alkaline Earth - Helium Pair Potentials	116
6.1	Introduction	116
6.2	Computational Methods	119
6.3	Results and Discussion	121
6.4	Conclusions	129
7	Accurate <i>ab initio</i> Pair Potentials Between Helium and the Heavier Group 2 Elements	134
7.1	Introduction	134
7.2	Computational Methods	136
7.3	Results and Discussion	139
7.4	Conclusions	149
8	Final Conclusions	152
8.1	Future Work	154
8.2	Final Comments	155
A	Parameterization and Testing Data for the Improved Model Core Potentials	158
A.1	Reference Data for the First-Row Transition Metals	158
A.2	Testing Data for the First-Row Transition Metals	163
A.3	Reference Data for the Second- and Third-Row Transition Metals	183
A.4	Testing Data for the Second- and Third-Row Transition Metals	185

List of Tables

1.1	DZ basis set for carbon (s space only)	34
1.2	cc-pVTZ basis set for carbon (s space only)	35
2.1	Partitioning of core and valence electrons and size of basis sets	55
2.2	Non-relativistic iMCP valence basis set for Ti atom ($f_{proj} = 4.5$)	58
2.3	Non-relativistic iMCP potential parameters for Ti atom ($f_{proj}=4.5$)	59
2.4	Calculated bond lengths, frequencies, and orbital energies for TiF_4^a	64
2.5	Bond lengths (in Å) and vibrational frequencies (in cm^{-1}) for VOF_3	65
2.6	Mean absolute errors in calculated bond lengths (Å)	65
2.7	Mean absolute errors in calculated vibrational frequencies (cm^{-1})	65
2.8	Timing results for MCP and all-electron molecular calculations	67
3.1	Partitioning of core and valence electrons and size of basis sets	74
3.2	Molecules included in training and test sets	76
3.3	Non-relativistic iMCP potential parameters for Au atom ($f_{proj}=1.3$)	76
3.4	Non-relativistic iMCP valence basis set for Au atom ($f_{proj}=1.3$)	76
3.5	Structural parameters for selected transition metal complexes ^a	81
3.6	Vibrational frequencies (in cm^{-1}) for selected transition metal complexes	82
3.7	Vibrational frequencies (in cm^{-1}) for selected transition metal complexes	83
3.8	Structural parameters and vibrational frequencies calculated using different DFT grids ^{a,b}	85
4.1	Structural parameters of CH_3 , CH_3^+ , and XeCH_3^+ ^{a,b}	94
4.2	Xe and CH_3 ionization energies and methyl cation affinity of Xe (eV). ^a	94
4.3	Bond lengths (in Å) of molecules potentially found as xenon ligands	96
4.4	Bond lengths (in Å) of xenon complexes	99
4.5	ΔG_{rxn} (kcal/mol) for reaction (1)	100
4.6	ΔG_{rxn} (kcal/mol) for reaction (2)	100
5.1	Contraction patterns for basis sets used in calculations ^a	109
5.2	MP2 Bond lengths of coinage metal monohalides (Å)	109
5.3	MP2 Bond lengths of argon - coinage metal monohalides (Å)	110
5.4	MP2 Bond lengths of krypton - coinage metal monohalides (Å)	110
5.5	MP2 bond lengths of xenon - coinage metal monohalides (Å) ^a	111
5.6	MP2 binding energies (BSSE-corrected) of Rg-MX complexes (kcal/mol)	111

6.1	Previous theoretical calculations of alkaline earth - helium pair potentials	118
6.2	Basis set contraction pattern used in calculations	120
6.3	Calculated atomic polarizabilities (in au)	122
6.4	He - He pair potential parameters (r_e in Å, ϵ in cm^{-1}).	126
6.5	Light alkaline earth (Be - Ca) - He pair potential parameters ^{a,b}	126
6.6	Sr - He pair potential parameters ^{a,b}	126
6.7	Ba - He pair potential parameters ^{a,b}	127
6.8	Calculated energies of bound rovibrational states for He ₂ and BeHe (in cm^{-1})	128
6.9	Calculated energies of bound rovibrational states for MgHe isotopomers (in cm^{-1})	128
6.10	Calculated energies of bound rovibrational states for CaHe isotopomers (in cm^{-1})	128
6.11	Calculated energies of bound rovibrational states for SrHe isotopomers (in cm^{-1})	129
6.12	Calculated energies of bound rovibrational states for BaHe isotopomers (in cm^{-1})	129
6.13	Calculated values of the Ancilotto parameter λ^a	130
7.1	Previous theoretical calculations of heavier alkaline earth - helium pair potential parameters	135
7.2	Basis set contraction pattern used in calculations	137
7.3	Polarization / correlating functions used in calculations	138
7.4	Calculated atomic polarizabilities (in au)	140
7.5	Experimental and calculated dispersion coefficients (in au)	141
7.6	CCSD(T) alkaline-earth metal - helium pair potential parameters ^{a,b}	143
7.7	Counterpoise-corrected CCSD(T) interaction energies (in cm^{-1})	144
7.8	Calculated energies (in cm^{-1}) and radial expectation values (in Å) of bound rovibrational states	146
7.9	Calculated values of the Ancilotto parameter λ (Eqn. 7.1)	147
B.1	Be-He CCSD(T) pair potentials	197
B.2	Mg-He CCSD(T) pair potentials	198
B.3	Ca-He CCSD(T) pair potentials	199
B.4	Sr-He CCSD(T) pair potentials	200
B.5	Ba-He non-relativistic CCSD(T) pair potentials	201
B.6	Ba-He scalar-relativistic CCSD(T) pair potentials	202
B.7	He-He CCSD(T) pair potentials	203

List of Figures

1.1	Interaction potential energy curve for MgHe	39
2.1	Deviation between MCPs and reference Cu core orbitals (1s, 2s, 3s) .	61
2.2	Deviation between MCPs and reference Cu valence orbitals (4s, 3p, 3d)	62
3.1	Deviation between iMCP and reference Au core orbitals (3s, 4s, 5s) .	79
3.2	Deviation between iMCP and reference Au valence orbitals (6s, 5p, 5d)	80
4.1	Sigma antibonding orbital of Xe(C ₆ F ₅) ₂	97
4.2	Pi bonding orbital of Xe(C ₆ F ₅) ₂	98
6.1	CCSD(T) Mg - He interaction potential (without bond functions) . .	124
7.1	Ba - He interaction potentials with respect to the dissociation limit .	142
7.2	Contour plot of the Ancilotto equation and the correlation between the well depths (in cm ⁻¹) and equilibrium interatomic distances (in Å) for the alkali and alkaline earth metals	148

List of Abbreviations

1-D	one-dimensional
ACCD	approximate coupled-cluster with double substitutions method
avg	average
B/B88	density exchange functional, due to Becke
B3	three-parameter hybrid density exchange-correlation functional, due to Becke
B3LYP	exchange-correlation density functional, comprised of B3 and LYP functionals
B3PW91	exchange-correlation density functional, comprised of B3 and PW91 functionals
BDE	bond dissociation energy
BF	bond functions
BLYP	exchange-correlation density functional, comprised of B88 and LYP functionals
BSSE	basis set superposition error
C	correlation
CADPAC	Cambridge Analytical Derivatives Package, a computational chemistry program
CC	coupled-cluster method
CC3	coupled-cluster method including single, double, and approximate triple excitations
CCSD	coupled-cluster method including single and double excitations
CCSD(T)	coupled-cluster method including single, double, and perturbative triple excitations
CCSDT	coupled-cluster method including single, double, and iterative triple excitations
CEP	Compact Effective Potential, a type of pseudopotential
cGTF	contracted Gaussian Type Function
CI	configuration interaction method
CIS	configuration interaction method including just single excitations
CISD	configuration interaction method including single and double excitations
CISDTQ	configuration interaction method including single, double, triple, and quadruple excitations
CP	counterpoise correction
deMon	densite de Montreal, a computational chemistry program
DFT	density functional theory
dppm	bis-(diphenylphosphino)methane, $(\text{C}_6\text{H}_5)_2\text{PCH}_2\text{P}(\text{C}_6\text{H}_5)_2$

ECP	Effective Core Potential
Eqn.	equation
Exp.	experiment
FC	frozen-core
GAMESS	General Atomic and Molecular Electronic Structure System, a computational chemistry program
GTF	Gaussian Type Function
GGA	generalized-gradient approximation
HF	Hartree-Fock
HFD	Hartree-Fock dispersion
HFRH	Hartree-Fock-Roothaan-Hall
iMCP	improved Model Core Potentials
KS	Kohn-Sham
LDA	local density approximation
LYP	density correlation functional, due to Lee, Yang, and Parr
MCP	Model Core Potential
MM	Molecular Mechanics
MP2	Møller-Plesset second-order perturbation theory
MP3	Møller-Plesset third-order perturbation theory
MP4	Møller-Plesset fourth-order perturbation theory
MRCI	multireference configuration interaction method
NMR	nuclear magnetic resonance
NR	non-relativistic
PCM	Polarizable Continuum Model, a solvation method
PES	potential energy (hyper)surface
pGTF	primitive Gaussian Type Function
PW91	density correlation functional, due to Perdew and Wang
QCISD(T)	quadratic configuration interaction including single, double, and perturbative triple excitations
QM	quantum mechanics
QM/MM	hybrid quantum mechanics / molecular mechanics model

RESC	Relativistic Elimination of the Small Component, a scalar-relativistic method
RHF	restricted Hartree-Fock
RMS	root-mean-square
ROHF	restricted open-shell Hartree-Fock
SCF	self-consistent field
SDB	Stuttgart-Dresden-Bonn, a family of pseudopotentials
SI	International System (of units)
sMCP	standard version of MCPs, due to Sakai <i>et al.</i>
SR	scalar-relativistic
TDHF	time-dependent Hartree-Fock method
UHF	unrestricted Hartree-Fock
WTBS	well-tempered all-electron basis set
wtMCP	well-tempered Model Core Potentials
X	exchange
XC	exchange-correlation

Chapter 1

Introduction

In recent years, the explosive growth in computing power has led to the rapid development of the burgeoning new field of computational chemistry. Many molecular properties can now be calculated to high accuracy on systems large enough to be of chemical interest. Computational papers can now commonly be found in general chemistry journals, and not only in those read by specialists. In addition, many largely experimental papers now also include a computational component. This increasing reliability of, and reliance on, theoretical methods was underlined by the awarding of the 1998 Nobel Prize in Chemistry to computational chemists John Pople and Walter Kohn [1].

Computational chemistry has become increasingly important to a number of different areas of chemistry. The pharmaceutical industry uses computational chemistry in areas such as protein folding [2] and molecular docking [3]. Computational chemistry has also become indispensable in the modeling of transition metal complexes and reaction mechanisms, as evidenced by a number of recent reviews [4, 5, 6].

As computing power has increased, very accurate (and time-consuming) computational methods have been applied to larger and larger systems. The desire to use these methods on larger systems, such as surfaces or biological molecules, means that newer and faster methods are always in demand. One method that has proven to be of great usefulness is the pseudopotential method. Details of this method, as well as a brief overview of all the computational methods used in this thesis, are included in the following sections. The discussion of the methods and concepts presented here

was collected from a variety of sources. The methods are presented in greater detail in several monographs and textbooks, written by Szabo and Ostlund [7], Jensen [8], McQuarrie [9], Parr and Yang [10], Faas [11], Greiner [12], Moss [13], and Levine [14].

1.1 The Electronic Schrödinger Equation

If we consider a spin-free, non-relativistic Hamiltonian, and neglect the effects of spin-orbit coupling, the time-independent Schrödinger equation for a molecule with N_e electrons and N_N nuclei can be written as:

$$\hat{H}\Psi(\vec{\xi}_1, \vec{\xi}_2, \dots, \vec{\xi}_{N_e}; \vec{R}_1, \vec{R}_2, \dots, \vec{R}_{N_N}) = E\Psi(\vec{\xi}_1, \vec{\xi}_2, \dots, \vec{\xi}_{N_e}; \vec{R}_1, \vec{R}_2, \dots, \vec{R}_{N_N}), \quad (1.1)$$

where the Hamiltonian operator in SI units is defined as:

$$\begin{aligned} \hat{H} = & -\frac{\hbar^2}{2} \sum_{A=1}^{N_N} \frac{1}{M_A} \nabla_A^2 - \frac{\hbar^2}{2m_e} \sum_{i=1}^{N_e} \nabla_i^2 \\ & + \frac{1}{4\pi\epsilon_0} \sum_{A=1}^{N_N} \sum_{B>A}^{N_N} \frac{Z_A Z_B e^2}{R_{AB}} - \frac{1}{4\pi\epsilon_0} \sum_{i=1}^{N_e} \sum_{A=1}^{N_N} \frac{Z_A e^2}{r_{iA}} + \frac{1}{4\pi\epsilon_0} \sum_{i=1}^{N_e} \sum_{j>i}^{N_e} \frac{e^2}{r_{ij}}, \end{aligned} \quad (1.2)$$

where $\vec{\xi}_i$ is a vector that denotes the three spatial (\vec{r}_i) and one spin (ω_i) coordinates of electron i (with charge $-e$ and mass m_e), \vec{R}_A is a vector denoting the coordinates of nucleus A (with charge $+e \times Z_A$ and mass M_A), \hbar is Planck's constant h divided by 2π , and $\frac{1}{4\pi\epsilon_0}$ is the permittivity of vacuum. The distances R_{AB} , r_{iA} , and r_{ij} are the distances between nuclei, between a nucleus and an electron, and between electrons, respectively. The first two terms in the Hamiltonian correspond to the kinetic energy of the nuclei and electrons. The third term is the repulsion energy between the nuclei. The fourth term is the electrostatic attraction between nuclei and electrons and the final term is the interelectronic repulsion.

To simplify this expression, we recognize that the nuclei are much heavier than the electrons, and thus they move more slowly. We can then separate the nuclear from

the electronic motion, and approximate the electronic motion as occurring in the field of stationary nuclei. This is known as the Born-Oppenheimer approximation [15] and it will be used in all of the calculations described in this thesis. This simplifies the Hamiltonian by eliminating the nuclear kinetic energy term and by reducing the internuclear repulsion term to a constant value, leading in consequence to an electronic-only Hamiltonian. In the system of atomic units, where the electronic mass m_e , Planck's constant \hbar , the electronic charge e , and the permittivity of vacuum $4\pi\epsilon_0$ are all set equal to 1 [14], we can write the electronic Hamiltonian as:

$$\hat{H}_{el} = -\frac{1}{2} \sum_{i=1}^{N_e} \nabla_i^2 + \sum_{i=1}^{N_e} \sum_{A=1}^{N_N} \frac{Z_A}{r_{iA}} + \sum_{i=1}^{N_e} \sum_{j>i}^{N_e} \frac{1}{r_{ij}} + V_{NN}, \quad (1.3)$$

where V_{NN} is now a constant which depends on the (fixed) positions of the nuclei. The electronic Schrödinger equation can now be written as:

$$\hat{H}_{el} \Psi_{el}(\vec{\xi}_1, \vec{\xi}_2, \dots, \vec{\xi}_{N_e}; \vec{R}) = E_{el} \Psi_{el}(\vec{\xi}_1, \vec{\xi}_2, \dots, \vec{\xi}_{N_e}; \vec{R}), \quad (1.4)$$

where \hat{H}_{el} is given in Eqn. 1.3. The electronic wavefunction Ψ_{el} now only depends parametrically on the nuclear coordinates (collectively designated by \vec{R}). Eqn. (1.4) allows us to define the concept of a potential energy surface (see Section 1.8.3) by calculating the electronic energy as a function of the nuclear positions.

We have now simplified the problem through the separation of the nuclear and the electronic coordinates, but we must now solve Eqn. (1.4) in order to find the wavefunction and the energy of the system. Unfortunately, the Schrödinger equation can only be solved exactly for very simple cases such as the hydrogen-like atomic systems (H, He⁺, ...), the harmonic oscillator, and the rigid rotor. For more complicated systems we must rely on approximate methods in order to obtain solutions for this equation. The most popular method to do this, and the basis for many of the more advanced methods in use today, is the Hartree-Fock method.

1.2 The Hartree-Fock Method

In the Hartree-Fock (HF) method, the form of the wavefunction Ψ_{el} is chosen to be a product of one-electron functions, known as orbitals. It is expressed in the form of a Slater determinant to ensure that, in accord with the Pauli Principle, the wavefunction is antisymmetric. This is a necessary requirement for the wavefunction due to the fermionic nature of electrons. In Slater-determinantal form, the wavefunction is written as:

$$\Psi_{el} = \frac{1}{\sqrt{N_e!}} \begin{vmatrix} \psi_1(\vec{\xi}_1) & \psi_1(\vec{\xi}_2) & \cdots & \psi_1(\vec{\xi}_{N_e}) \\ \psi_2(\vec{\xi}_1) & \psi_2(\vec{\xi}_2) & \cdots & \psi_2(\vec{\xi}_{N_e}) \\ \vdots & \vdots & \ddots & \vdots \\ \psi_{N_e}(\vec{\xi}_1) & \psi_{N_e}(\vec{\xi}_2) & \cdots & \psi_{N_e}(\vec{\xi}_{N_e}) \end{vmatrix}, \quad (1.5)$$

or in shorthand notation:

$$\Psi_{el} = \frac{1}{\sqrt{N_e!}} \det \left| \psi_1(\vec{\xi}_1) \quad \psi_2(\vec{\xi}_2) \quad \cdots \quad \psi_{N_e}(\vec{\xi}_{N_e}) \right|. \quad (1.6)$$

The ψ_i are known as spin orbitals and may be defined in terms of spatial orbitals ϕ_i as:

$$\psi_i(\xi_j) = \phi_i(\vec{r}_j) \times \begin{cases} \alpha(\omega_j) = \phi_i(\vec{r}_j) \\ \beta(\omega_j) = \bar{\phi}_i(\vec{r}_j) \end{cases}. \quad (1.7)$$

If we apply the variational method using the Hamiltonian of Eqn. (1.3) and the wavefunction of Eqn. (1.5) or (1.6), the problem of finding the wavefunction is reduced to the problem of solving N_e coupled one-electron integro-differential Hartree-Fock equations of the following form:

$$\hat{f}(\vec{r}_i)\psi_i(\vec{\xi}_i) = \varepsilon_i\psi_i(\vec{\xi}_i), \quad (1.8)$$

where $\hat{f}(\vec{r}_i)$ is a one-electron operator known as the Fock operator and ε_i is the (one-electron) orbital energy.

For a system in which N_e is an even number and each spatial orbital ϕ_i has two electrons associated with it (a closed-shell system), then we have a total of $N_e/2$ spatial orbitals $\phi_i(\vec{r}_i)$, each describing two electrons. After integrating the Hartree-Fock equations over the (orthonormal) spin functions α and β , we obtain the Fock operator in terms of the spatial orbitals:

$$\hat{f}(\vec{r}_1) = -\frac{1}{2}\nabla_1^2 - \sum_{A=1}^{N_n} \frac{Z_A}{r_{1A}} + \sum_{j=1}^{N_e/2} [2\hat{J}_j(\vec{r}_1) - \hat{K}_j(\vec{r}_1)], \quad (1.9)$$

where $\hat{J}_j(\vec{r}_1)$ and $\hat{K}_j(\vec{r}_1)$ are the Coulomb and exchange operators, respectively, and are defined as follows:

$$\hat{J}_j(\vec{r}_1)\phi_i(\vec{r}_1) = \left(\int \phi_j^*(\vec{r}_2) \frac{1}{r_{12}} \phi_j(\vec{r}_2) d\vec{r}_2 \right) \phi_i(\vec{r}_1), \quad (1.10)$$

$$\hat{K}_j(\vec{r}_1)\phi_i(\vec{r}_1) = \left(\int \phi_j^*(\vec{r}_2) \frac{1}{r_{12}} \phi_i(\vec{r}_2) d\vec{r}_2 \right) \phi_j(\vec{r}_1). \quad (1.11)$$

The Coulomb operator describes the electrostatic repulsion between electron 1 and a smeared-out charge distribution that corresponds to electron 2 (in orbital $\phi_j(\vec{r}_2)$). The instantaneous correlation between electron 1 (at \vec{r}_1) and electron 2 (at \vec{r}_2) is lost in this smearing process. The exchange operator arises due to the fact that the wavefunction must be antisymmetric, and has no classical interpretation.

If we combine the first two terms of Eqn. (1.9) (kinetic energy and electron-nuclear attraction terms), into the one-electron term $\hat{h}(\vec{r}_1)$, also called the bare nucleus or core Hamiltonian, we can express the HF equation as:

$$\left(\hat{h}(\vec{r}_1) + \sum_{j=1}^{N_e/2} [2\hat{J}_j(\vec{r}_1) - \hat{K}_j(\vec{r}_1)] \right) \phi_i(\vec{r}_1) = \varepsilon_i \phi_i(\vec{r}_1). \quad (1.12)$$

The solution of Eqn. (1.12) is complicated by the fact that both the Coulomb and exchange operators depend on the eigenfunctions $\phi_i(\vec{r}_1)$. Therefore, the HF equations are non-linear, and must be solved iteratively. A practical approach to solve the equations, the use of a basis set, was suggested by Roothaan [16] and Hall [17]. The (unknown) eigenfunctions are expanded in a set of K known basis functions $\chi_q(\vec{r})$:

$$\phi_i(\vec{r}_1) = \sum_{q=1}^K \chi_q(\vec{r}_1) c_{qi}. \quad (1.13)$$

If this expression is substituted into Eqn. (1.12), we obtain what are known as the Hartree-Fock-Roothaan-Hall (HFRH) equations:

$$\hat{f}(\vec{r}_1) \sum_{q=1}^K \chi_q(\vec{r}_1) c_{qi} = \varepsilon_i \sum_{q=1}^K \chi_q(\vec{r}_1) c_{qi}. \quad (1.14)$$

If we multiply both sides of this equation from the left by a basis function $\chi_p(\vec{r}_1)$ and integrate, we obtain the HFRH equations in the matrix form:

$$\mathbf{FC} = \mathbf{SCE}, \quad (1.15)$$

where \mathbf{F} is the Fock matrix, \mathbf{C} is a matrix containing the expansion coefficients, \mathbf{S} is the overlap matrix, and \mathbf{E} is the (diagonal) matrix of orbital energies. The elements of the Fock matrix are:

$$F_{pq} = \langle \chi_p(\vec{r}_1) | \hat{f}(\vec{r}_1) | \chi_q(\vec{r}_1) \rangle \quad (1.16)$$

$$= \int \chi_p^*(\vec{r}_1) \hat{f}(\vec{r}_1) \chi_q(\vec{r}_1) d\vec{r}_1 \quad (1.17)$$

$$= \int \chi_p^*(\vec{r}_1) \hat{h}(\vec{r}_1) \chi_q(\vec{r}_1) d\vec{r}_1 + \sum_{j=1}^{N_e/2} \left[2 \int \chi_p^*(\vec{r}_1) \hat{J}_j(\vec{r}_1) \chi_q(\vec{r}_1) d\vec{r}_1 - \int \chi_p^*(\vec{r}_1) \hat{K}_j(\vec{r}_1) \chi_q(\vec{r}_1) d\vec{r}_1 \right], \quad (1.18)$$

and the elements of the overlap matrix are defined as:

$$S_{pq} = \langle \chi_p(\vec{r}_1) | \chi_q(\vec{r}_1) \rangle = \int \chi_p^*(\vec{r}_1) \chi_q(\vec{r}_1) d\vec{r}_1. \quad (1.19)$$

Solving the HFRH equations has now been reduced to the problem of finding the matrices \mathbf{E} and \mathbf{C} . The matrix equation must be solved iteratively, as the Fock matrix elements depend on the expansion coefficients \mathbf{C} . An initial guess to the \mathbf{C} matrix is used to construct the Fock matrix, which is diagonalized to obtain a new \mathbf{C} matrix. This process is continued until the change in \mathbf{C} is less than a predetermined threshold. At this point, the wavefunction Φ_{el} and the orbitals ϕ_k are known, and the energy and any other desired properties of the system can be calculated from the wavefunction. The HF (electronic) energy can be very simply expressed in terms of spin orbitals as:

$$E_{el} = \sum_i^{N_e/2} \langle \psi_i(\vec{\xi}_1) | \hat{h}(\vec{r}_1) | \psi_i(\vec{\xi}_1) \rangle + \frac{1}{2} \sum_{i=1}^{N_e/2} \sum_{j=1}^{N_e/2} [\langle ij | ij \rangle - \langle ij | ji \rangle], \quad (1.20)$$

where the following shorthand notation has been used for the two-electron integrals (which come from the Coulomb and exchange operators):

$$\langle ij | kl \rangle = \int \int \psi_i^*(\vec{\xi}_1) \psi_j^*(\vec{\xi}_2) \frac{1}{r_{12}} \psi_k(\vec{\xi}_1) \psi_l(\vec{\xi}_2) d\vec{\xi}_1 d\vec{\xi}_2. \quad (1.21)$$

The value of any observable property (one that can be represented by a quantum mechanical operator) can be calculated by finding the expectation value of the operator:

$$\langle A \rangle = \langle \Phi_{el} | \hat{A} | \Phi_{el} \rangle = \int \Phi_{el}^* \hat{A} \Phi_{el} d\tau, \quad (1.22)$$

where τ represents all coordinates in space (*e.g.* $d\tau = d\vec{\xi}_1 d\vec{\xi}_2 \dots d\vec{\xi}_{N_e}$). The solution of Eqn. (1.15) gives $N_e/2$ occupied orbitals and $K - N_e/2$ virtual (unoccupied) orbitals.

The preceding discussion assumed a closed-shell system, and the above equations form the basis of the restricted Hartree-Fock method (RHF). For an open-shell system,

one with a different number of electrons of α and β spins, there are two methods available to treat the system. The first is the restricted open-shell Hartree-Fock method (ROHF) [18]. This builds on the RHF method by treating the paired electrons as in the RHF method, and puts the unpaired electrons into their own orbitals. The other method is the unrestricted Hartree-Fock method (UHF) [19]. The UHF method differs from the RHF and ROHF methods in the way it treats the so-called paired electrons. In the UHF method, Equation (1.7) does not apply. Each electron is in its own orbital, and does not share a spatial orbital with an electron of opposite spin. The method is equally applicable to closed-shell systems, but in those cases the UHF and RHF methods usually give identical results. For open-shell systems, the UHF method gives a wavefunction with greater variational flexibility, and thus will in general lead to a lower energy than the ROHF wavefunction. However, the UHF method does have its drawbacks. The resulting wavefunction is not an eigenfunction of the spin operator (\hat{S}^2), and states of higher spin multiplicity contaminate the wavefunction. For example, quartet or sextet states may contaminate a doublet wavefunction, resulting in an unphysical energy lowering.

The Hartree-Fock methods generally give results that are semiquantitative with respect to experiment, and important trends can be drawn from the HF results. Unfortunately, for many systems, *e.g.* transition metals, HF calculations can be completely in error [20], and even trends taken from the data may be incorrect. Other effects, such as the dispersion forces that hold van der Waals molecules together, are completely absent in the HF methods, and so HF calculations on these systems give only repulsive potential energy surfaces. Recall that in the HF methods, the instantaneous electron correlation between two electrons was replaced in a smeared-out electronic charge Eqn. (1.10). The lack of electron correlation is what causes these problems. It is thus necessary to go beyond the HF methods for such systems. The calculated properties for all systems almost always improve with respect to experiment as we move beyond the HF methods. This can be done in two ways; either by using the HF orbitals to build better wavefunctions, as in the post-HF methods (Section 1.3) or by abandoning the wavefunction theory completely, as in density functional theory (Section 1.4).

1.3 Post-Hartree-Fock Methods

The post-HF methods are methods that start with an initial HF calculation in order to obtain the HF orbitals, and then use those orbitals to build better wavefunctions. This can be done in a two different ways, either in a perturbational method such as Møller-Plesset perturbation theory, or via a variational method such as in configuration interaction (CI) or coupled-cluster (CC) theory.

1.3.1 Configuration Interaction Method

In order to improve the flexibility of the wavefunction, one can go beyond the single-determinant HF approximation and build a wavefunction made of many determinants. These additional determinants can be formed by exciting electrons from the HF occupied orbitals to virtual orbitals. The wavefunction is approximated by the sum of these determinants, which can be written in symbolic form as:

$$\Psi_{CI}(\vec{\xi}_1, \vec{\xi}_2, \dots, \vec{\xi}_{N_e}) = \sum_I c_I D_I(\vec{\xi}_1, \vec{\xi}_2, \dots, \vec{\xi}_{N_e}), \quad (1.23)$$

where:

$$D_I(\vec{\xi}_1, \vec{\xi}_2, \dots, \vec{\xi}_{N_e}) = \frac{1}{\sqrt{N_e!}} \det \left| \begin{array}{cccc} \psi_{I1}(\vec{\xi}_1) & \psi_{I2}(\vec{\xi}_2) & \cdots & \psi_{IN_e}(\vec{\xi}_{N_e}) \end{array} \right|. \quad (1.24)$$

Eqn. (1.23) is then used in a variational scheme in order to find the expansion coefficients in front of each term and then the energy.

To form an excited determinant, one or more electrons are promoted from occupied orbitals to unoccupied ones. The orbitals themselves stay fixed during the procedure, the only variational degrees of freedom in this procedure, known as configuration interaction (CI), are the expansion coefficients c_I in front of the determinants D_I . A series of determinants can be formed, starting from those in which only a single electron is excited, to those where all of the electrons are excited. A CI wavefunction where all possible excited determinants are included is called a full-CI wavefunction, and it provides the exact energy in the basis set used (see Section 1.7). In the limit

of an infinite basis set, full-CI gives the exact non-relativistic energy. The form of the full-CI wavefunction, that improves the HF wavefunction Ψ_0 , can be written as:

$$\begin{aligned} \Psi = c_0\Psi_0 + & \sum_a \sum_b \sum_c \sum_d c_{abcd}^r \Psi_{abcd}^r + \sum_a \sum_b \sum_c \sum_d \sum_r \sum_s \sum_t c_{abcd}^{rs} \Psi_{abcd}^{rstu} + \dots + \sum_r \sum_s \sum_t c_{abc}^{rst} \Psi_{abc}^{rst} \\ & + \sum_a \sum_b \sum_c \sum_d \sum_r \sum_s \sum_t \sum_u c_{abcd}^{rstu} \Psi_{abcd}^{rstu} + \dots, \end{aligned} \quad (1.25)$$

where the sums over a, b, c , and d run over the occupied spin orbitals and the sums over r, s, t , and u run over the unoccupied spin orbitals. The determinant Ψ_{ab}^{rs} is formed by exciting two electrons (one from orbital a and one from orbital b) to the (formerly unoccupied) orbitals r and s . In practice, full-CI calculations are only performed for the smallest systems due to the very large number of determinants this method entails. For a closed-shell system of N_e electrons and K basis functions, the number of possible determinants is [21]:

$$N_{det} = \left(\frac{K!}{(N_e/2)!(K - (N_e/2))!} \right)^2. \quad (1.26)$$

This means that even for a small molecule, the number of determinants can be staggering. For example, in the case of ammonia with a modest basis set (leading to ten electrons in thirty orbitals), a full-CI wavefunction will contain nearly twenty-nine billion determinants!

For this reason, CI expansions of less than full-CI quality are generally used. The lowest quality CI expansion is CIS (CI singles), where the CI expansion contains the HF determinant and all of the singly-excited determinants. This is very useful for the excited states and for some of the molecular properties, but the energy of the ground state is unchanged by the interaction with the singly-excited determinants. This is known as Brillouin's theorem [22]:

$$\langle \Psi_0 | \hat{H} | \Psi_a^r \rangle = 0. \quad (1.27)$$

It can be shown that it is the doubly-excited determinants that contribute the most to the energy, followed by the quadruply-excited ones [7]. For this reason, the most commonly used CI expansion includes all the single and double excitations, also known as CISD. The number of determinants for the CISD method is of the order $\mathcal{O}(N_{occ}^2 N_{virt}^2)$ where N_{occ} is the number of occupied orbitals and N_{virt} is the number of virtual orbitals, so this is easily done for systems of moderate size. The effect of the quadruple excitations can be approximated in several ways. The simplest is the correction introduced by Langhoff and Davidson [23]:

$$E_q = [1 - (c_0)^2] E_{corr}, \quad (1.28)$$

where E_{corr} is the CISD correlation energy ($E_{CISD} - E_{HF}$) and c_0 is the coefficient in front of the Hartree-Fock determinant Ψ_0 in the CI expansion.

A far superior method is multi-reference CI (MRCI). In MRCI, a small number of determinants are chosen as the reference set, and then a CI calculation is performed using all unique singly- and doubly-excited configurations obtained from the reference set. This allows for higher-order excitations because the determinants that are used as the reference are excited determinants. For example, a double excitation from a doubly-excited determinant results in a quadruply-excited determinant with respect to Ψ_0 . If the reference determinants are carefully chosen, the most important higher excitations will be included in the wavefunction.

CI-based methods have two major drawbacks. They are quite computationally demanding. The CISD method formally scales as K^6 where K is the number of basis functions, and the higher-order methods scale upwards from there (CISDTQ scales as K^{10}). In addition, any level of CI other than full-CI is not size-consistent, as it does not reach the proper limit as the system is stretched. For example, in a system AB, as the bond is stretched, the energy of A \cdots B should converge to the sum of the energies of isolated A and B as the interaction disappears. Methods, such as CISD, that are not size-consistent do not exhibit such behavior. This complicates their use for certain studies, like the calculation of potential energy surfaces for stretched molecules. It also makes it impossible to perform counterpoise calculations (Section

1.8.3). The size-consistency problem (but not the computational demands) can be rectified by using the coupled-cluster methods.

1.3.2 Coupled-Cluster Theory

In the coupled-cluster (CC) theory, the wavefunction is written in an exponential form:

$$\Psi = e^{\hat{T}} \Psi_0, \quad (1.29)$$

where Ψ_0 represents the HF determinant and \hat{T} , the cluster operator, is defined as:

$$\hat{T} = \hat{T}_1 + \hat{T}_2 + \cdots + \hat{T}_{N_e}. \quad (1.30)$$

The definitions of the excitation operators that make up the cluster operator are as follows:

$$\hat{T}_1 \Psi_0 = \sum_a^{\text{occ}} \sum_r^{\text{unocc}} t_a^r \psi_a^r, \quad \hat{T}_2 = \sum_a^{\text{occ}} \sum_b^{\text{occ}} \sum_r^{\text{unocc}} \sum_s^{\text{unocc}} t_{ab}^{rs} \Psi_{ab}^{rs}. \quad (1.31)$$

So \hat{T}_1 creates all of the singly-excited determinants, \hat{T}_2 the doubly-excited ones, *etc.* The exponential in the wavefunction can be expanded as:

$$e^{\hat{T}} = 1 + \hat{T} + \frac{\hat{T}^2}{2!} + \frac{\hat{T}^3}{3!} + \cdots = \sum_{k=0}^{\infty} \frac{\hat{T}^k}{k!}. \quad (1.32)$$

The effect of the cluster operator is to express the wavefunction as a sum of the ground-state and all excited determinants, so it is fully equivalent to a full-CI wavefunction. As was discussed in Section 1.3.1, such a calculation is too large to be tractable, so the size of the cluster operator must be reduced. If only the first two terms of the cluster operator are retained:

$$\hat{T} = \hat{T}_1 + \hat{T}_2, \quad (1.33)$$

from Eqn. (1.32), we obtain:

$$e^{\hat{T}_1 + \hat{T}_2} = 1 + \hat{T}_1 + \hat{T}_2 + \frac{1}{2}\hat{T}_1^2 + \frac{1}{6}\hat{T}_1^3 + \hat{T}_1\hat{T}_2 + \frac{1}{2}\hat{T}_2^2 + \dots \quad (1.34)$$

The terms have been grouped into excitation levels; the first term is the zeroth-order excitation (HF determinant), the second term will yield all of the singly-excited determinants, the third and fourth terms yield all of the doubly-excited determinants, and so on. The advantage of this CC method, called the coupled-cluster singles and doubles (CCSD) method is that even though the cluster operator only goes to second order, the resulting wavefunction includes the effects of higher order terms. For example, the last term in Eqn. (1.34) describes a quadruple excitation. However, it does not include all of the quadruple excitations, for example, there will not be a term corresponding to \hat{T}_4 . In addition, the coefficients t (or amplitudes as they are usually called in CC theory) of the quadruple excitations are not found independently, instead they are products of the amplitudes of lower-order excitations. The last term of Eqn. (1.34) will give a quadruple excitation whose amplitude will be the square of the amplitude of the relevant double excitation (from \hat{T}_2).

Coupled-cluster theory has several advantages over CI expansions of nominally the same order. Both CCSD and CISD formally scale as K^6 , so computational times should be approximately equal for the two methods, but the coupled-cluster expansion contains more terms, such as the last term in Eqn. (1.34). Not only does this mean that CCSD should recover more of the correlation energy than CISD, it also has the important consequence of making CCSD size-consistent. Procedures have also been developed that allow for the effect of triple excitations to be estimated in a perturbative manner. This method, known as CCSD(T), is one of the most commonly used methods for very high accuracy calculations of structures and energetics of molecules.

1.3.3 Møller-Plesset Perturbation Theory

Perturbation theory is widely used throughout chemistry and physics to solve problems that can be related to simpler ones that have already been solved. The

basic idea is to take a problem that has already been solved, and then expressing the new problem as a perturbation of that system. The approach works best if the perturbation is small compared to the unperturbed problem. In the sense of an eigenvalue problem, if one has already solved the following problem:

$$\hat{A}\Phi_i = a_i\Phi_i, \quad (1.35)$$

and found the function(s) Φ_i and the eigenvalue(s) a_i , then the perturbed problem would be expressed as:

$$(\hat{A} + \hat{A}')\Phi'_i = a'_i\Phi'_i. \quad (1.36)$$

The desire is to solve this perturbed problem and find the values of Φ'_i and a'_i .

Perturbation theory leads to an infinite series of corrections to both the eigenvalues and eigenfunctions:

$$\Phi' = \Phi^{(0)} + \Phi^{(1)} + \Phi^{(2)} + \dots, \quad (1.37)$$

$$a' = a^{(0)} + a^{(1)} + a^{(2)} + \dots, \quad (1.38)$$

where $\Phi^{(0)} = \Phi$ and $a^{(0)} = a$ (the unperturbed values), $\Phi^{(1)}, \Phi^{(2)}, \dots$ are the first-, second-, and higher-order corrections to the eigenfunctions, and the $a^{(1)}, a^{(2)}, \dots$ are the first-, second-, and higher-order corrections to the eigenvalues. Unlike the variational methods, there is no lower bound, so the corrections may overshoot the correct result. In addition, the corrections (in particular the lower-order ones) may not be in the proper direction, so the “corrected” eigenvalue or eigenfunction may actually be further away from the correct value than the uncorrected one.

For a general Hamiltonian \hat{H} partitioned as follows:

$$\hat{H} = \hat{H}_0 + \hat{H}', \quad (1.39)$$

where the (non-degenerate) eigenvalues and eigenvectors of \hat{H}_0 are known:

$$\hat{H}_0 \Psi_i^{(0)} = E_i^{(0)} \Psi_i^{(0)}, \quad (1.40)$$

perturbation theory gives us the following expressions for the first- and second-order corrections to the energy:

$$E_i^{(1)} = \langle \Psi_i^{(0)} | \hat{H}' | \Psi_i^{(0)} \rangle, \quad (1.41)$$

$$E_i^{(2)} = \langle \Psi_i^{(0)} | \hat{H}' | \Psi_i^{(1)} \rangle, \quad (1.42)$$

where the first-order correction to the wavefunction $\Psi_i^{(1)}$ can be shown to be:

$$\Psi_i^{(1)} = \sum_{n \neq i} | \Psi_n^{(0)} \rangle \langle \Psi_n^{(0)} | \Psi_i^{(1)} \rangle, \quad (1.43)$$

and:

$$\langle \Psi_n^{(0)} | \Psi_i^{(1)} \rangle = \frac{\langle \Psi_n^{(0)} | \hat{H}' | \Psi_i^{(0)} \rangle}{E_i^{(0)} - E_n^{(0)}}. \quad (1.44)$$

The final general expression for the second-order correction to the energy is:

$$E_i^{(2)} = \sum_{n \neq i} \frac{\langle \Psi_i^{(0)} | \hat{H}' | \Psi_n^{(0)} \rangle \langle \Psi_n^{(0)} | \hat{H}' | \Psi_i^{(0)} \rangle}{E_i^{(0)} - E_n^{(0)}}, \quad (1.45)$$

and since \hat{H}' is Hermitian (and real):

$$E_i^{(2)} = \sum_{n \neq i} \frac{\langle \Psi_i^{(0)} | \hat{H}' | \Psi_n^{(0)} \rangle^2}{E_i^{(0)} - E_n^{(0)}}, \quad (1.46)$$

In the Møller-Plesset perturbation theory [24], \hat{H}_0 is the Hartree-Fock Hamiltonian:

$$\hat{H}_0 = \sum_{i=1}^{N_e} \hat{f}(i), \quad (1.47)$$

and the perturbation is the difference between the exact instantaneous electron correlation and the smeared-out version found in Hartree-Fock theory:

$$\hat{H}' = \sum_i \sum_{j>i} \frac{1}{r_{12}} - \sum_{i=1}^{N_e/2} [2\hat{J}_i(\vec{r}_1) - \hat{K}_i(\vec{r}_1)]. \quad (1.48)$$

From this partitioning, we can see that the zeroth-order (unperturbed) ground-state energy is just:

$$E_0^{(0)} = \langle \Psi_0 | \hat{H}_0 | \Psi_0 \rangle = \sum_a \varepsilon_a. \quad (1.49)$$

The first-order energy correction is:

$$E_0^{(1)} = \langle \Psi_0 | \hat{H}' | \Psi_0 \rangle = \langle \Psi_0 | \sum_i \sum_{j>i} \frac{1}{r_{12}} | \Psi_0 \rangle - \langle \Psi_0 | \sum_{i=1}^{N_e/2} [2\hat{J}_i(\vec{r}_1) - \hat{K}_i(\vec{r}_1)] | \Psi_0 \rangle, \quad (1.50)$$

This can be expressed in terms of the two-electron integrals defined in Eqn. (1.21):

$$E_0^{(1)} = -\frac{1}{2} \sum_a \sum_b \langle ab || ab \rangle, \quad (1.51)$$

where:

$$\langle ab || ab \rangle \equiv \langle ab | ab \rangle - \langle ab | ba \rangle. \quad (1.52)$$

The sum of the zeroth-order energy and the first-order correction is just the Hartree-Fock energy:

$$E_0^{(0)} + E_0^{(1)} = \sum_a \varepsilon_a - \frac{1}{2} \sum_a \sum_b \langle ab || ab \rangle. \quad (1.53)$$

The first correction to the energy beyond the HF energy is thus the second-order energy correction. From Eqn. (1.46), we can see that the energy correction is expressed as a sum over excited states. The singly-excited determinants need not be included because of Brillouin’s theorem Eqn. (1.27). Triply- and higher-excited determinants do not interact with the ground-state determinant because of the two-electron nature of the Hamiltonian. In consequence, the summation in Eqn. (1.53) runs over only the doubly-excited determinants. After summing over all possible double excitations, the second-order energy correction can be expressed in terms of the two-electron integrals and orbital energies (both occupied and unoccupied):

$$E_0^{(2)} = \sum_a \sum_{b>a} \sum_r \sum_{s>r} \frac{| \langle ab || rs \rangle |^2}{\epsilon_a + \epsilon_b - \epsilon_r - \epsilon_s}. \quad (1.54)$$

Møller-Plesset perturbation theory is size-consistent at all levels (MP2, MP3, MP4, *etc.*). It is not as effective as coupled-cluster theory at recovering correlation energy, and the energetics and structures of molecules are not as accurately calculated, but MP2 formally scales as K^5 , so much larger systems can be treated than with CC theory. It is still computationally too demanding to be used on larger systems though, and so we must abandon the wavefunction approach in order to treat the correlation energy in these systems.

1.4 Density Functional Theory

The post-Hartree-Fock methods are very effective for the calculation of energies and properties of molecular systems, but they are very computationally demanding. A less demanding alternative is available: density functional theory (DFT). DFT has several advantages over the post-HF methods, firstly it formally scales only as K^3 , so it can be even faster than HF theory itself, which formally scales as K^4 . However, this is highly dependent on the implementation, and in general, DFT calculations may take several times longer than the same calculation performed at the HF level. Secondly, in the DFT method, we deal only with the electron density, and not the positions of the individual electrons. This reduces the number of variables from $3N_e$

(x, y, and z coordinates for each electron) to just the three variables of the electron density in three-dimensional space. No matter how large the system is, the problem remains a three-dimensional one. This makes the DFT method the method of choice for large systems when the HF approximation is not sufficient.

In 1964, Hohenberg and Kohn [25] published a paper that proved that for a system in its non-degenerate ground-state, the energy could be uniquely determined by its electron density and there exists a universal functional of the electron density:

$$E_0 = F[\rho(\vec{r})]. \quad (1.55)$$

Note that this was only a proof of existence, as Hohenberg and Kohn only showed that such a functional existed, but not what it was, nor any prescription for finding it. In addition, there was no way to find the electron density needed for the functional without resorting to wavefunction methods.

A year later, Kohn and Sham [26] solved the second problem by devising a practical way to find $\rho(\vec{r})$. The equation that they derived is known as the Kohn-Sham (KS) equation, and it is very similar to the Hartree-Fock equation:

$$\hat{F}^{KS}(\vec{r}_1)\phi_i^{KS}(\vec{r}_1) = \varepsilon_i^{KS}\phi_i^{KS}(\vec{r}_1), \quad (1.56)$$

where \hat{F}^{KS} is the Kohn-Sham operator and ϕ_i^{KS} and ε_i^{KS} are the Kohn-Sham orbitals and orbital energies respectively. The electron density is defined through the Kohn-Sham orbitals:

$$\rho(\vec{r}) = 2 \sum_{i=1}^{N_e/2} |\phi_i^{KS}(\vec{r})|^2, \quad (1.57)$$

and the Kohn-Sham operator is defined as:

$$\hat{F}^{KS}(\vec{r}_1) = -\frac{1}{2}\nabla_i^2 - \sum_{A=1}^{N_N} \frac{Z_A}{r_{iA}} + \hat{J}(\vec{r}_1) + V_{XC}(\vec{r}_1). \quad (1.58)$$

The operator $\hat{J}(\vec{r}_1)$ is just the Coulomb operator, which in DFT is expressed as:

$$\hat{J}(\vec{r}_1) = \int \frac{\rho(\vec{r}_2)}{r_{12}} d\vec{r}_2, \quad (1.59)$$

and the last term $V_{XC}(\vec{r}_1)$ is the exchange-correlation potential term. This operator yields the following expression for the DFT energy (in terms of the electron density):

$$E_0 = - \sum_{i=1}^{N_e/2} \langle \phi_i(\vec{r}_i) | \nabla_i^2 | \phi_i(\vec{r}_i) \rangle - \sum_{A=1}^{N_N} \int \frac{Z_A}{r_{iA}} d\vec{r}_1 + \frac{1}{2} \int \int \frac{\rho(\vec{r}_1)\rho(\vec{r}_2)}{r_{12}} d\vec{r}_1 d\vec{r}_2 + E_{XC}[\rho(\vec{r})]. \quad (1.60)$$

If the correct expression for the energy functional $E_{XC}[\rho(\vec{r})]$ is used, the KS equations will result in the exact ground-state energy and electron density (within the basis set employed). However, the exact functional is not known and so approximations to it are used. Generally the first step is to separate $E_{XC}[\rho(\vec{r})]$ into two parts, a purely exchange part and a purely correlation part:

$$E_{XC}[\rho(\vec{r})] = E_X[\rho(\vec{r})] + E_C[\rho(\vec{r})]. \quad (1.61)$$

The approximation can be done in one of a number of ways. The simplest is the local density approximation (LDA). In this approximation, the energy functional is expressed as:

$$E_{XC}[\rho(\vec{r})] = \int \varepsilon_{XC}[\rho(\vec{r})]\rho(\vec{r}) d\vec{r}, \quad (1.62)$$

where $\varepsilon_{XC}[\rho(\vec{r})]$ is the energy density (exchange-correlation energy per particle) of a homogeneous electron gas of density $\rho(\vec{r})$. The values of the energy density $\varepsilon_{XC}[\rho(\vec{r})]$ are obtained via Monte Carlo calculations [27] and then analytically interpolated [28]. The main drawback of LDA is that it is based on a system with a constant density. The electron density of molecules is obviously not uniform over the range of the molecule, and this inhomogeneity results in overbinding in molecules when studied

using the LDA approach (*e.g.* bond lengths are too short and binding energies are much too large).

Since the problems with LDA stem from the fact that it assumes that the electron density is constant throughout the molecule, including information not only about the electron density at each point but also about the gradient of the electron density could help correct for the inhomogeneity inherent in molecular systems. This approach is known as the generalized-gradient approximation (GGA). The energy function now takes the general form:

$$E_{XC}[\rho(\vec{r})] = \int \varepsilon_{XC}[\rho(\vec{r})]\rho(\vec{r})d\vec{r} + \int G_{XC}[\rho(\vec{r}), \nabla\rho(\vec{r})]d\vec{r}, \quad (1.63)$$

where $G_{XC}[\rho(\vec{r}), \nabla\rho(\vec{r})]$ is a term that involves both the electron density and its gradient. This term helps correct for the inadequacies of the LDA approximation, but there is no set form for this term, so there are many suggestions in the literature. One commonly used example is an exchange functional due to Becke [29], known as B or B88 in the literature. It includes a correction to the LDA exchange density:

$$\varepsilon_X^{B88}[\rho(\vec{r}), \nabla\rho(\vec{r})] = \varepsilon_X^{LDA}[\rho(\vec{r})] + \Delta\varepsilon_X^{B88}[\rho(\vec{r}), \nabla\rho(\vec{r})], \quad (1.64)$$

where:

$$\Delta\varepsilon_X^{B88}[\rho(\vec{r}), \nabla\rho(\vec{r})] = -\beta\rho(\vec{r})^{\frac{1}{3}} \frac{x^2}{1 + 6\beta x \sinh^{-1}(x)}, \quad (1.65)$$

$$x = \frac{|\nabla\rho(\vec{r})|}{\rho(\vec{r})^{\frac{4}{3}}}, \quad (1.66)$$

and β is a parameter obtained by fitting to known atomic data. This functional shows one of the characteristics of most modern DFT functionals: they contain variational parameters that are found by fitting to experimental data. This enables functionals that may not have the correct functional form to still yield good results, but it may

also reduce the applicability of functionals, as they may not perform well on systems outside their range of parameterization. Functionals without parameters exist [30], as do functionals that involve not only the electron density and its gradient, but also the Laplacian (second derivative) of the electron density [31]; however, these functionals are not as widely used.

Another class of functionals are the hybrid functionals. These functionals incorporate a certain amount of exact (Hartree-Fock) exchange into the exchange-correlation functional. The most widely known (and used) of these is the Becke three parameter (B3) exchange-correlation functional [32], which is based on the B88 exchange functional (Eqns. (1.64) - (1.66)), discussed above:

$$E_{XC}^{B3} = (1 - a)E_X^{LDA} + aE_X^{HF} + b\Delta E_X^{B88} + (1 - c)E_C^{LDA} + c\Delta E_C^{GGA}, \quad (1.67)$$

where a , b , and c are parameters that are found by fitting to experimental data and depend on the GGA correlation functional used. In the B3LYP functional [33], the values of a , b , and c are 0.20, 0.72, and 0.81 respectively. The hybrid functionals tend to be among the most accurate of the DFT functionals [34], but due to the necessity of calculating Hartree-Fock exchange, they are also much slower.

Since all computational methods scale as some power of the number of basis functions, a simple way of speeding up computations is simply by reducing the number of basis functions. The use of pseudopotentials allows us to reduce the number of basis functions without significantly lowering the quality of our wavefunction.

1.5 Pseudopotentials

To understand the concept of pseudopotentials, one must only look at the Periodic Table. Elements exist in groups, such as the halogens, whose members share many atomic properties and reactivity. The reason that fluorine and iodine are quite similar chemically is that in both cases the valence p shell is one electron short of being full, whereas the core electrons ($1s^22s^2$ for fluorine and $1s^22s^22p^63s^23p^64s^23d^{10}4p^65s^24d^{10}$ for iodine) are only secondary to the chemical properties. In a molecular environment,

it is the valence electrons that undergo the greatest change upon chemical bonding, while the core electron density changes only slightly. The core electron density can be approximated as being fixed when an atom enters a molecular environment (frozen-core approximation). This electron density can then be replaced by a potential, known as a pseudopotential, that, when added to the Hamiltonian, will give (only) the valence orbitals as solutions.

The pseudopotential idea is not a new one. It was introduced by Hellman [35] in the 1930s. He expressed the potential energy of the alkali metals as:

$$U(r) = -\frac{1}{r} + \frac{A}{r}e^{-2\kappa r}. \quad (1.68)$$

where the first term represents the Coulomb attraction of the single valence electron to the core (with charge +1), and the second term is the pseudopotential. In effect the alkali metal atom was reduced to a one-electron hydrogen-like system. The fundamental equation for the creation of one type of pseudopotentials, the effective core potentials, is the Phillips-Kleinman [36] transformation. It describes the development of a pseudopotential through inversion of the wavefunction:

$$(\hat{T} + \hat{V})\phi_i = \varepsilon_i\phi_i, \quad (1.69)$$

$$V(r) = \frac{(\varepsilon_i - \hat{T})\phi_i(r)}{\phi_i(r)}. \quad (1.70)$$

In general, the wavefunction for the core and valence electrons can be written as:

$$\Psi_{total} = \mathcal{A}[\Psi_{core}(\vec{\xi}_1, \vec{\xi}_2, \dots, \vec{\xi}_{N_c})\Psi_{val}(\vec{\xi}_1, \vec{\xi}_2, \dots, \vec{\xi}_{N_v})], \quad (1.71)$$

where Ψ_{core} and Ψ_{val} are antisymmetrized wavefunctions for the N_c and N_v core and valence electrons respectively, and \mathcal{A} is an antisymmetrizer that allows permutations between the core and valence electrons. Only approximate wavefunctions, such as the HF wavefunction, can be factored in this manner [37]. The valence-only Hamiltonian can now be written as:

$$\hat{H}^{val}(\vec{r}_1, \vec{r}_2, \dots, \vec{r}_{N_v}) = \sum_{i=1}^{N_v} \left(\hat{h}(\vec{r}_i) + \sum_{j>i}^{N_v} \frac{1}{r_{ij}} \right), \quad (1.72)$$

where the second term represents the electron-electron repulsion between pairs of valence electrons and the one-electron operator $\hat{h}(\vec{r}_i)$ is defined as:

$$\hat{h}(\vec{r}_i) = -\frac{1}{2}\nabla_i^2 - \frac{Z - N_c}{|\vec{r}_i|} + V_{core}. \quad (1.73)$$

The first term corresponds to the kinetic energy of the valence electrons, the second term is the attraction between the valence electrons and the nucleus, whose nuclear charge has been reduced by the number of core electrons. Pseudopotential methods assume perfect screening of the nucleus by the core electrons, which of course is never the case. Since penetration into the core region by the valence electrons occurs, the pseudopotential approximation should lead to valence electrons that are less bound than they should be (since they are experiencing a lower effective nuclear charge than the imperfectly screened electrons in the real system). This could have an effect on calculated molecular properties. The final term, V_{core} , is the core potential, and it represents everything else, in particular, the Coulomb and exchange interactions between the valence and the core electrons. Due to the exchange interaction, this term is non-local in nature, but most pseudopotential methods replace it with a local potential for ease of use. There are two classes of pseudopotentials in common use, the effective core potentials (ECPs) and the Model Core Potentials (MCPs). They differ in how the V_{core} term is represented.

1.5.1 Effective Core Potentials

In the ECP method, the nodal structure of the valence orbitals is dropped. Nodeless pseudo-orbitals are formed by fitting to the outer lobe of the valence orbitals. This gives an excellent representation of the reference orbital in the valence region, while neglecting the density in the core region. For example, the 5s valence orbital in

xenon should contain four nodes, the ECP pseudo-orbital has none. These pseudo-orbitals and corresponding orbital energies ε_i are then used in the Phillips-Kleinman transformation, Eqn. (1.70), in order to produce a numerical pseudopotential. Note that nodeless orbitals are necessary for Eqn. (1.70) to be valid, due to the presence of ϕ_i in the denominator. Finally, this numerical potential is transformed to an analytical potential of the form:

$$r^2 V_l(r) = \sum_k A_{l,k} r^{n_{l,k}} e^{-B_{l,k} r^2}, \quad (1.74)$$

where n and l are the principal and angular momentum quantum numbers respectively, and A_l and B_l are the (ECP) core potential parameters.

The optimization of the A_l and B_l parameters has been done in a number of ways, and this defines the difference between the different types of ECPs. A simple least-squares fit of the numerical potential to the analytical form was done both by Hay and Wadt [38, 39, 40, 41] and by Ermler, Christiansen, Ross, and others [42, 43, 44, 45, 46]. Unfortunately, an accurate fit can result in a large number of terms, which reduces the computational efficiency of the potential. The compact effective core potentials (CEPs), due to Stevens and others [47, 48, 49], were parameterized in a different manner. They performed HF calculations using a large valence basis set, and varied the potential parameters until the calculated valence orbitals and orbital energies matched the reference valence orbitals and energies to within a threshold. This allows for a small number of core parameters. For example, the CEP [48] for xenon has twenty core parameters, whereas the potential for xenon by Hurley *et al.* [43] has forty-four. A third method, used to develop the Stuttgart potentials [50, 51, 52, 53, 54] varies the parameters to best fit the valence electron excited state spectrum of the atom.

1.5.2 Model Core Potentials

This is a brief overview of the MCP method, for more detail, especially in how the parameters and basis sets were derived, see Chapters 2 and 3. The MCP method was developed by Bonifacic and Huzinaga [55, 56, 57, 58, 59] in the mid-1970s. A

recent review of the development of the MCP method was written by Klobukowski *et al.* [60]. In the MCP method, the one-electron operator $\hat{h}(\vec{r}_i)$ is defined as:

$$\hat{h}(\vec{r}_i) = -\frac{1}{2}\nabla_i^2 - \frac{Z - N_c}{r_i} + V_{core}^{MCP}(\vec{r}_i) + \hat{\Omega}^{MCP}(\vec{r}_i). \quad (1.75)$$

The last term $\hat{\Omega}^{MCP}(\vec{r}_i)$ is a projection operator, included to maintain orthogonality between the core and valence orbitals. This prevents the valence orbitals from collapsing into the core. The form of the projection operator is:

$$\hat{\Omega}^{MCP} = \sum_{c=1}^{N_c} B_c |\bar{\phi}_c\rangle \langle \bar{\phi}_c|, \quad (1.76)$$

where $\bar{\phi}_c$ are the (fixed) frozen-core orbitals obtained from the reference atomic calculations, and the B_c are numerical constants defined in terms of the core orbital energies:

$$B_c = -f_{proj}\varepsilon_c. \quad (1.77)$$

The values of f_{proj} are constant for all of the orbitals in an atom, with values from about one to five, with the exact value depending on the parameterization method employed.

The projection operator shifts the core orbitals up into the virtual space, leaving the valence orbitals as the lowest energy solutions. Since the valence orbitals maintain orthogonality to the core orbitals, they exhibit the correct nodal structure, *e.g.* the 5s MCP orbital of xenon will have the desired four nodes. This has both advantages and drawbacks. The correct nodal structure allows for more accurate calculations of properties that depend on the electron density near the nucleus. This includes certain expectation values of r , spin-orbit coupling properties, and NMR properties such as chemical shifts. It may also give more accurate values of the valence correlation energy [61], as the electron density is described better when spread-out throughout the orbital, and not just concentrated in the outer lobe. However, calculations take

longer with the MCPs because a larger valence basis set is necessary in order to correctly describe the nodal structure. For example, the CEP basis set for radon [48] contains five functions in the s and p space, whereas the iMCP for radon has eight functions in each space. In addition, studies [62, 63] have failed to show an advantage of including the correct nodal structure for valence electron properties such as bond lengths and orbital energies.

1.5.3 Relativistic Potentials

When studying heavy atoms, it is necessary to include relativistic effects in order to obtain accurate results. It is very time-consuming to include relativistic effects in all-electron calculations (see next section), but the most important effects can be easily included with pseudopotentials. The pseudopotential core parameters depend on the reference function that they attempt to reproduce. If the reference function includes relativistic effects, then so can the pseudopotential. By using relativistic reference functions, relativistic pseudopotentials can be derived. The resulting valence orbitals and orbital energies will be non-relativistic, but since the relativistic effects are much more prominent in the core orbitals, this will be a minor effect. If greater accuracy is needed, it is possible to use a relativistic Hamiltonian with a pseudopotential, but the effect is too small to be noticeable in most cases [64].

1.6 Relativistic Effects

According to the Bohr model of the atom, the speed at which an electron in the 1s orbital moves (in atomic units) is equal to the atomic number of the atom. Since the speed of light in atomic units is equal to the inverse of the fine-structure constant α (in atomic units):

$$c = \alpha^{-1} = 137.039 \text{ au}, \quad (1.78)$$

then the electrons in the 1s orbital of lead (atomic number 82) travel at approximately 60% of the speed of light. Therefore, relativistic effects are very important when studying heavy atoms, in particular for the core orbitals. The relativistic effects cause

the core electrons to become heavier, and their orbits contract to become closer to the nucleus. This effect is most prevalent for the s electrons, which have the greatest penetration into the core area, but it also effects the p electrons to a lesser extent. The opposite effect is seen for the d and f electrons. Due to their lower penetration, the contraction effect is less noticeable for them, but they feel a strong indirect effect from the s and p electrons. When the s and p orbitals contract, the screening of the nucleus is more efficient, and the d and f electrons feel less net nuclear charge. This causes these orbitals to expand relative to the non-relativistic case. The effect on the valence orbitals is more subtle. There are essentially no direct relativistic effects on the valence orbitals of an atom. However, the indirect relativistic effects [65] can be quite significant. As the s and p core orbitals contract, the valence orbitals become better screened and they tend to expand. This is opposed by the expansion of the d and f orbitals which results in the partial descreening of the nucleus and a contraction of the valence orbitals.

This is the cause of the so-called “relativistic contraction”, where bond lengths decrease as one goes down a group. For example, the experimental equilibrium bond length of AgH is 1.618 Å, for AuH, it is 1.524 Å [66]. Note that the relativistic effects do not always have to decrease the bond length, if the bonding is mainly through the d or f orbitals (which expand with relativity), then the relativistic bond length will be longer than the non-relativistic one.

The basis of relativistic quantum mechanics is the (time-dependent) Dirac equation:

$$i\hbar \frac{\partial \Psi}{\partial t} = \left[-ic\hbar \left(\alpha_1 \frac{\partial}{\partial x_1} + \alpha_2 \frac{\partial}{\partial x_2} + \alpha_3 \frac{\partial}{\partial x_3} \right) + \beta m_e c^2 \right] \Psi, \quad (1.79)$$

where i is the imaginary unit, c is the speed of light, m_e is the (rest) mass of an electron, and α_i and β are 4×4 matrices defined as follows:

$$\alpha_i = \begin{pmatrix} \mathbf{0} & \sigma_i \\ \sigma_i & 0 \end{pmatrix} \quad (\mathbf{i} = \mathbf{x}, \mathbf{y}, \mathbf{z}), \quad (1.80)$$

with $\sigma_{x,y,z}$ denoting the 2×2 Pauli spin matrices, and:

$$\beta = \begin{pmatrix} \mathbf{1} & \mathbf{0} \\ \mathbf{0} & -\mathbf{1} \end{pmatrix}, \quad (1.81)$$

built from 2×2 unit ($\mathbf{1}$) and null ($\mathbf{0}$) matrices. The wavefunction Ψ must then have four components. Ψ is usually split into two two-component parts:

$$\Psi = \begin{pmatrix} \phi \\ \chi \end{pmatrix}, \quad (1.82)$$

where ϕ and χ are two-component vectors. Due to the relative magnitudes of the two components, these are commonly known as the large-component and small-component of the wavefunction respectively. For electronic states, ϕ is much larger than χ :

$$\phi \approx c\chi. \quad (1.83)$$

If the external potential is not changing with time, we can separate the time and space variables to obtain a form of the time-independent Dirac equation:

$$\begin{pmatrix} V & c\boldsymbol{\sigma} \cdot \hat{\mathbf{p}} \\ c\boldsymbol{\sigma} \cdot \hat{\mathbf{p}} & -2c^2 + V \end{pmatrix} \begin{pmatrix} \phi \\ \chi \end{pmatrix} = E \begin{pmatrix} \phi \\ \chi \end{pmatrix}, \quad (1.84)$$

where $\hat{\mathbf{p}}$ is the linear momentum operator and V is the potential. Since there are four components in the wavefunction, all of which must be solved for, the solution of this equation is difficult and time-consuming. Separate basis sets are needed for the large- and small-component parts, and since solving via the Hartree-Fock (or here the Dirac-Fock) approximation scales as K^4 in the number of basis functions, doubling K results in a sixteen-fold increase in computing time. A way to simplify this problem would be very useful. One common way of doing this is to invoke the Foldy-Wouthuysen [67] transformation which decouples the large- and small-components of the wavefunction. Note that since the small-component is approximately c times smaller than the large-component, its effect is expected to be small in comparison.

Once this is done, there are a number of ways to obtain Hartree-Fock-like equations to solve the two-component relativistic problem. The two remaining components are the spin-orbit-coupled components, and they can be averaged-out (by neglecting the spin-orbit coupling), resulting in a one-component wavefunction. This is called the scalar-relativistic (SR) method.

One SR method in common use is the RESC [68] method of Nakajima and Hirao. The scalar (spin-free) RESC Hamiltonian can be written as:

$$\hat{H}_{RESC}^{sf} = \hat{T} + \hat{O}\hat{Q}\hat{p} \cdot V\hat{p}\hat{Q}\hat{O}^{-1} + 2m_e c \hat{O}\hat{Q}^{1/2}V\hat{Q}^{1/2}\hat{O}^{-1}, \quad (1.85)$$

where \hat{T} is the classical relativistic kinetic energy:

$$\hat{T} = \sqrt{m_e^2 c^4 + \hat{p}^2 c^2} - m_e c^2, \quad (1.86)$$

\hat{p} is the linear momentum operator:

$$\hat{p}^2 = -\hbar^2 \left(\frac{\partial^2}{\partial x^2} + \frac{\partial^2}{\partial y^2} + \frac{\partial^2}{\partial z^2} \right), \quad (1.87)$$

and the \hat{O} and \hat{Q} operators are defined as:

$$\hat{O} = \frac{1}{E_p + m_e c^2} \left[1 + \frac{\hat{p}^2 c^2}{(E_p + m_e c^2)^2} \right]^{-\frac{1}{2}}, \quad (1.88)$$

$$\hat{Q} = \frac{c}{E_p + m_e c^2}, \quad (1.89)$$

and:

$$E_p = \sqrt{m_e^2 c^4 + \hat{p}^2 c^2}. \quad (1.90)$$

The RESC method is used to calculate scalar-relativistic atomic reference data for the parameterization of the wtMCPs.

For the iMCPs, numerical reference calculations are used in the parameterization. The scalar-relativistic corrections to the numerical wavefunction are the mass-variation term [69], which describes the dependence of the mass of the electron on its velocity:

$$\hat{H}_{mv} = -\frac{\hat{p}^4}{8m_e^3c^2}, \quad (1.91)$$

and the Darwin term:

$$\hat{H}_D = \frac{Z\pi\delta(r)}{2m_e^2c^2}. \quad (1.92)$$

Since it is only the s orbitals that have any amplitude at the nucleus, the Dirac δ term in the Darwin formula ensures that it only affects the s orbitals.

Now that we have discussed the various methods used in this thesis to calculate energies and molecular properties, we must discuss the use of basis sets to describe the system under study.

1.7 Basis Sets

To obtain the exact energy and properties, a complete basis set is needed, that is, one of infinite size. This is obviously impossible, so the science of basis sets is using the best basis set for your problem that you can afford. This is complicated by the fact that there are literally hundreds of basis sets to choose from. Some are obviously better than others, and some are even derived specifically for certain properties (*e.g.* Sadlej's basis sets, optimized for molecular polarizabilities [70]). In theory, any form of basis functions that spans the space could be used, but in practice, only two forms of basis functions are in common use: Gaussian functions and Slater functions.

1.7.1 Slater- and Gaussian-Type Functions

Slater functions are radial functions of the form:

$$R_n^S(\zeta, r) = N^S r^{n-1} e^{-\zeta r}, \quad (1.93)$$

where n is the principal quantum number, ζ is the Slater exponent and the normalization constant N^S is:

$$N^S = (2\zeta)^{n+\frac{1}{2}} [(2n)!]^{-\frac{1}{2}}. \quad (1.94)$$

The basis function χ is just this radial function multiplied by the relevant spherical harmonic:

$$\chi^S(\zeta, n, l, m, r, \theta, \phi) = R_n^S(\zeta, r) Y_{lm}(\theta, \phi), \quad (1.95)$$

where l and m are the angular momentum and magnetic quantum numbers respectively, and $Y_{lm}(\theta, \phi)$ are the spherical harmonics.

The Gaussian radial function also has an exponential form, it varies as e^{-r^2} :

$$R_n^G(\alpha, r) = N^G r^{n-1} e^{-\alpha r^2}, \quad (1.96)$$

where α is the Gaussian exponent. There are two types of Gaussian functions in use. The first is the spherical Gaussian function, where the basis function is made by multiplying the Gaussian radial function by a spherical harmonic:

$$\chi^{Gsph}(\alpha, n, l, m, r, \theta, \phi) = R_n^G(\alpha, r) Y_{lm}(\theta, \phi), \quad (1.97)$$

and the normalization constant N^G in this case is:

$$N^G = 2^{n+1} [(2n-1)!!]^{-\frac{1}{2}} (2\pi)^{-\frac{1}{4}} \alpha^{\frac{2n+1}{2}}. \quad (1.98)$$

Alternatively, Cartesian Gaussian functions can be used. In this form, the radial function is expressed in Cartesian coordinates. The Cartesian basis function takes the form:

$$\chi^{GCart}(\alpha, i, j, k, x, y, z) = N^G e^{-\alpha r^2} x^i y^j z^k, \quad (1.99)$$

where x , y , and z are Cartesian coordinates, $r^2 = x^2 + y^2 + z^2$, i , j , and k are integer exponents, and the normalization constant is:

$$N^G = (2\pi)^{\frac{3}{4}} [(2i+1)!!(2j+1)!!(2k+1)!!]^{-\frac{1}{2}} \alpha^{\frac{i+j+k+\frac{3}{2}}{2}}. \quad (1.100)$$

The sum of the integer exponents allows for the description of the orbital shapes:

$$L = i + j + k. \quad (1.101)$$

Functions where $L = 0$ correspond to s functions, $L = 1$ to p-type functions, $L = 2$ to d-type functions, *etc.* Note that there are six Cartesian d Gaussians: xx , xy , xz , yy , yz , and zz , giving rise to the five spherical d Gaussians (xy , xz , yz , $x^2 - y^2$, and $3z^2 - r^2$) plus an additional function of spherical (s) symmetry: $x^2 + y^2 + z^2$. This function may be either kept to improve the description of the s space, or removed by suitable transformation. Similarly, the ten Cartesian f Gaussians contain a set of three p functions in addition to the familiar seven f orbitals.

Slater-type functions have the correct functional form; for example the analytical solution to the Schrödinger equation for the $1S$ state of the hydrogen atom is:

$$\Phi_{1s} = \frac{1}{\sqrt{\pi a_o^3}} e^{-r/a_o}, \quad (1.102)$$

where a_o is the Bohr radius. Gaussian functions flatten out at the nucleus (their derivative at $r = 0$ is zero), instead of exhibiting the cusp of the Slater functions. In addition, due to their e^{-r^2} dependence, Gaussian functions also die off at long range

sooner than Slater functions. However, Gaussian functions are much more widely used because of their mathematical properties. It is very difficult and time-consuming to evaluate the two-electron integrals Eqn. (1.21) with Slater functions. The great advantage of Gaussian functions is that the product of two Gaussian functions centered at different points A and B is a Gaussian function centered at a third point C between A and B [71]. This allows us to reduce all of the three-center and four-center two-electron integrals to two-center integrals which are much easier to calculate.

1.7.2 Contracted Gaussian Functions

To improve the performance of Gaussian functions, we can take linear combinations of Gaussian functions to better approximate a Slater function. For example, a Gaussian function with a large exponent can help improve the description around the nuclei (although the correct cusp will never be achieved), and functions with very small exponents can improve the description of the long-range tail. The great increase in efficiency in integral evaluation provided by Gaussian functions allows us to use many more Gaussian functions than Slater functions and obtain similar accuracy with less computing time. These linear combinations are known as contracted Gaussian functions (cGTFs):

$$\chi_{j,L}^{cGTF} = \sum_{i=1}^K d_{i,j} \chi_{L,i}^{pGTF}, \quad (1.103)$$

where L is the type of function (s, p, d, *etc.*) described above and pGTF is shorthand notation for a primitive Gaussian-type function. The expansion coefficients $d_{i,j}$ in the contracted function are fixed when the basis set is made, and do not change during calculations using the basis set.

There are two ways to contract basis functions: segmented and general. In a segmented contraction, a set of primitives is grouped into a number of cGTFs with differing number of functions. For example, in the DZ basis of Dunning [72] for carbon (see Table 1.1), nine pGTFs of s symmetry are grouped into four cGTFs as (6111). The first cGTF is a sum of six pGTFs, and is used to describe the core 1s orbital. The remaining three cGTFs are each “sums” of only one pGTF each and are

used to describe the 2s orbital. The general contraction scheme was first used by Raffanetti [73]. In this scheme, the same pGTFs are used to make several cGTFs, but the expansion coefficients $d_{i,j}$ differ. This is often used in conjunction with some segmented contraction as well. As example of such a mixed basis set is Dunning's [74] cc-pVTZ basis set for carbon, shown in Table 1.2. The 1s and 2s orbital are each described by a set of eight pGTFs contracted to two cGTFs with different expansion coefficients. There are also two additional cGTFs of one pGTF each added in a segmented contraction.

Table 1.1: DZ basis set for carbon (s space only)

Function	Exponent	Coefficient	
		1s	2s
1	4232.61	0.002029	
	634.882	0.015535	
	146.097	0.075411	
	42.4974	0.257121	
	14.1892	0.596555	
	1.96660	0.242517	
2	5.14770		1.000000
3	0.49620		1.000000
4	0.15330		1.000000

Table 1.2: cc-pVTZ basis set for carbon (s space only)

Function	Exponent	Coefficient	
		1s	2s
1, 2	8236.0	0.0005310	-0.000113
	1235.0	0.0041080	-0.000878
	280.80	0.0210870	-0.004540
	79.270	0.0818530	-0.018130
	25.590	0.2348170	-0.055760
	8.9970	0.4344010	-0.126895
	3.3190	0.3461290	-0.170352
	0.3643	-0.008983	0.598684
3	0.9059		1.000000
4	0.1285		1.000000

There are several ways to obtain the exponents and the expansion coefficients needed for a basis set. Often, a basis set size is chosen, and the expansion coefficients and exponents are varied in order to minimize the HF energy. In some cases, in particular with pseudopotential basis sets, the basis sets are determined by least-squares fitting to some reference data (see Chapter 1). Sometimes, as in the well-tempered basis sets, the exponents are functionally related to each other.

1.7.3 Well-Tempered Basis Sets

The well-tempered basis sets (WTBS) were developed by Huzinaga and Klobukowski [75]. A large number of exponents ($N = 20 - 30$) were chosen for each atom, and the exponents themselves are generated via the following formulae:

$$\alpha_0 = \alpha, \quad (1.104)$$

$$\alpha_1 = \alpha\beta, \quad (1.105)$$

$$\alpha_k = \alpha_{k-1}\beta \left[1 + \gamma \left(\frac{k}{N} \right)^\delta \right], \quad k = 2, \dots, N, \quad (1.106)$$

where the parameters α , β , γ , and δ were optimized by minimizing the ground-state energy of the atom. The same exponents are shared by all of the angular

symmetries (s, p, d, *etc.*) The WTBS is a very large basis set designed for accurate all-electron calculations, and so it is used as the reference atomic data needed for the parameterization of the wtMCPs. For molecular calculations, basis sets need to be improved, either by expanding the atom-centered basis set with polarization functions or by adding bond functions between the atoms.

1.7.4 Polarization Functions

Even large basis sets like the WTBS cannot correctly describe the electron distribution in a molecular environment. When an atom is put into a molecule, the electron density is polarized. This can be modeled by adding functions of higher angular momentum to the basis set. For example, one or more d functions can be added to a carbon atom basis set. Note that the addition of these functions does not mean that carbon has d electrons or that electron density is being shifted to the unoccupied higher energy orbitals. The polarization set needs to be quite large for very accurate calculations; thus in Chapter 7, a polarization set of five p functions, four d functions, three f functions, and two g functions is added to the helium atom. All of the basis functions described thus far have been centered on the atoms in a molecule. However, it is also possible to place basis functions between atoms to improve the description of the electron density between atoms.

1.7.5 Bond Functions

Bond functions are basis functions that are located somewhere other than on atoms. They are often placed on a bond between two atoms, thus their name. They are usually placed at the midpoint of a bond, as it has been shown that their exact position does not have a great effect on the calculated energies. They are very useful in reducing the number of atom-centered basis functions necessary for a given accuracy (see Chapter 6). To describe the electron density at a certain point between two atoms, one s bond function could replace two atom-centered p functions (one on each atom), saving five basis functions. When going beyond diatomics, the placement of bond functions becomes much more problematic. In addition, bond functions greatly increase basis set superposition error, so if they are used, the counterpoise correction

(Section 1.8.3) becomes very important.

1.8 Interpretation of the Wavefunction

Once a wavefunction is obtained, it can be used to calculate various molecular properties such as dipole moments, polarizabilities, *etc.* A series of calculations can be used to map out the potential energy (hyper)surface of the molecule. The next few sections will briefly discuss the properties calculated in this thesis, as well as the potential energy surface as it pertains to geometry optimization and vibrational frequencies.

1.8.1 Atomic Polarizabilities

When an atom or molecule is placed into an external electric field \vec{F} , the electron density changes or polarizes. The energy of this polarization can be expanded in a Taylor series:

$$E(\vec{F}) = E(\vec{0}) + \frac{\partial E}{\partial \vec{F}} \vec{F} + \frac{1}{2} \frac{\partial^2 E}{\partial \vec{F}^2} \vec{F}^2 + \frac{1}{6} \frac{\partial^3 E}{\partial \vec{F}^3} \vec{F}^3 + \dots, \quad (1.107)$$

$$E(\vec{F}) = E(\vec{0}) - \vec{\mu}_0 \vec{F} - \frac{1}{2} \alpha \vec{F}^2 - \frac{1}{6} \beta \vec{F}^3 - \frac{1}{24} \gamma \vec{F}^4 - \dots, \quad (1.108)$$

where α , β , and γ are the (dipole) polarizability, (first) hyperpolarizability, and second hyperpolarizability respectively, and $\vec{\mu}_0$ is the (permanent) dipole moment of the molecule. Note that all of these quantities are tensor quantities; the dipole moment is a first-rank tensor (a three-element column vector), the polarizability is a second-rank tensor (a three by three matrix), the hyperpolarizability is third-rank (a three by three by three matrix), and so on. This equation holds for both molecules and atoms (where of course the permanent dipole moment is zero). In addition, atoms are spherically symmetric, so if the applied electric field is chosen to be in the z direction, only one element of this tensor needs to be calculated to give the polarizability (α_{zz}). The first correction to the energy of an atom is the polarizability:

$$\alpha = -\frac{\partial^2 E}{\partial \vec{F}^2}. \quad (1.109)$$

To calculate the polarizability, we need the second derivative of the energy with respect to an external field. This may be done either analytically, such as through the time-dependent Hartree-Fock (TDHF) method, or more generally, numerically via finite differencing of the energy at several values of the external field. Both methods are used in this thesis, but since analytical methods were not available for post-HF methods, the finite-field method was most commonly used.

1.8.2 Long-Range Dispersion Interactions

The interaction between two neutral atoms at long range is entirely due to dispersion forces. These forces can be described by a series expansion, with the leading term dying off as r^{-6} :

$$E_{int} = \sum_{i=1}^{\infty} \frac{C_{2i+4}}{r^{2i+4}}. \quad (1.110)$$

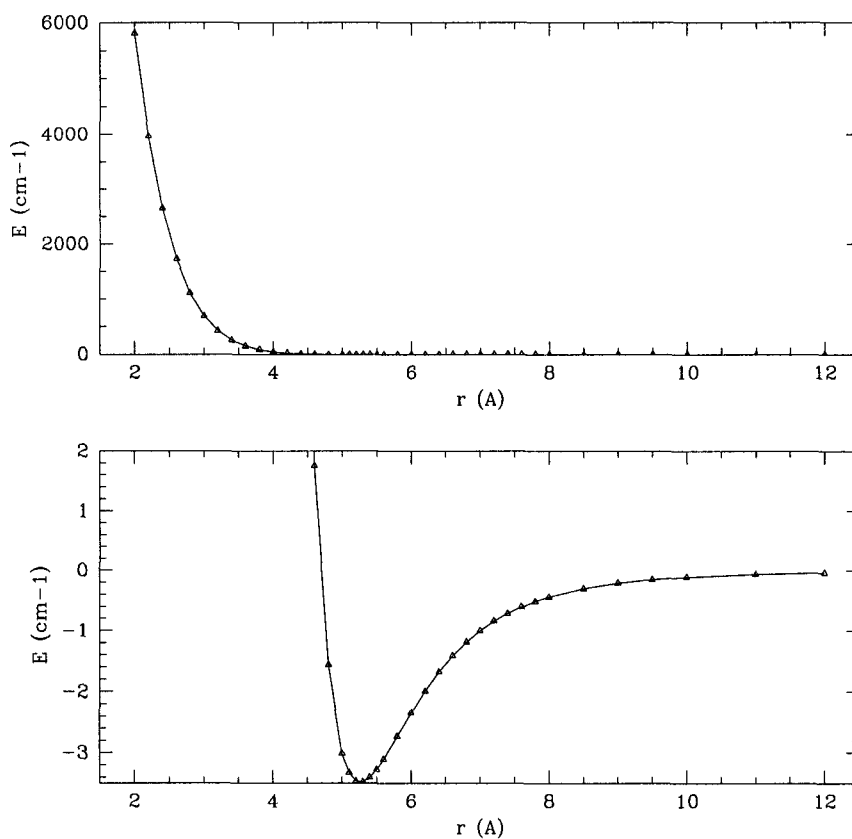
In theory, this sum goes to infinity, but in practice it is difficult to determine with any degree of accuracy coefficients beyond the first few. The dispersion coefficients (C_{2i+4}) can be determined experimentally, or by fitting to *ab initio* data. The data must be chosen such that no other effects are influencing the energy, such as exchange-repulsion or electrostatic attraction. In Chapter 7, *ab initio* data is used to fit values of C_6 and C_8 as a test of the calculated pair-potential interaction energies.

1.8.3 Potential Energy Surfaces

The potential energy surface (PES or hypersurface if in many dimensions), a consequence of the Born-Oppenheimer approximation is one of the most important concepts in computational chemistry. It allows for the description of the energy changes and barriers in chemical reactions. In addition, the concepts of an optimized geometry and harmonic vibrational frequencies can also be defined in terms of a PES.

An example of the simplest PES, that of a diatomic molecule, is shown in Figure 1.1. Here, the PES is simply a one-dimensional (1-D) curve of the interaction energy against the internuclear distance. Most of the following discussion will be based on a 1-D PES, but the concepts can easily be extended to multiple dimensions.

Figure 1.1: Interaction potential energy curve for MgHe



Interaction Energy

The interaction energy is defined as the change in the energy of a complex A-B when the components are brought together:

$$E_{int}(r_{AB}) = E_{AB}(r_{AB}) - E_A - E_B, \quad (1.111)$$

where E_{AB} is the energy of the A-B complex, E_A and E_B are the energies of system A and system B respectively, and r_{AB} is the distance between A and B (the internuclear distance where A and B are both atoms). Note that this equation cannot be used for non-size-consistent methods like CISD, since we should have:

$$\lim_{r_{AB} \rightarrow \infty} E_{int}(r_{AB}) = 0, \quad (1.112)$$

and this is not true for such methods. When systems A and B are not atoms, the interaction energy as a function of distance becomes more difficult to define, and the interaction energies reported in such a case are usually the maximum interaction energies, obtained from values for the minimum-energy structure of the complex and for the separated pieces. The PES also allows us to determine this minimum-energy structure.

Basis Set Superposition Error and the Counterpoise Correction

A complete basis set would allow for the most accurate calculation of the interaction energy possible within the theoretical method used, but since this is not feasible, the use of smaller basis sets is necessary. Unfortunately, smaller basis sets come with a drawback. If the basis set on system A is not fully saturated (which, unless a complete basis is used, is always the case), it can “steal” some of the basis set centered on system B to better describe its own electron density and thus lower the energy. This is especially problematic with very small basis sets, or basis sets that involve bond functions or diffuse functions (basis functions with very small exponents). This effect is known as basis set superposition error. To correct for it, Boys and Bernardi [76] suggested the counterpoise procedure. Instead of calculating the energy of system A by itself, the energy of system A is calculated in the presence of the basis set (but not the nuclei or electrons) of system B. The same is done for system B. The expression for the interaction energy, Eqn. (1.111), is thus modified:

$$E_{int}(r_{AB}) = E_{AB}(r_{AB}) - E_A\{AB\} - E_B\{AB\}, \quad (1.113)$$

where $E_A\{AB\}$ and $E_B\{AB\}$ are the energies of system A and B calculated with the combined basis set of both A and B.

Geometry Optimization and First Derivatives of the PES

The minimum-energy structure of a complex is known as its optimized geometry. Since the energy at the optimized geometry is a stationary point on the PES, we know that:

$$\left(\frac{dE}{dr}\right)_{r_e} = 0, \quad (1.114)$$

where r_e is the equilibrium internuclear distance between the atoms A and B. In a multidimensional case, the gradient will be zero in all of the dimensions. This point can be found in one of three ways. If an analytical expression for the gradient is available, then the gradient is calculated at a certain point. Based on the signs of the gradient, we move along each of the conjugate (orthogonal) directions in the direction that lowers the energy and calculate the gradient again. This is repeated until the gradient in all directions is less than a threshold. If an analytical expression is not available for the method, there remain two choices. The gradient can be calculated by doing a finite-differencing of energies calculated along a small step in each conjugate direction. This gradient can then be used in the automatic routine that decides on the size and direction of the geometry steps. A third option is simply to calculate the energy at a certain geometry and then at another geometry and so on. With a sufficiently intelligent minimizer, this trudge along the PES can find a minimum of the function.

This procedure is not foolproof. If the surface is multidimensional, any of these methods can get stuck in a local minimum, especially if the initial guess to the minimum-energy structure is quite poor. After such an optimization, the nature of the stationary point found should be tested.

Nature of the Stationary Point and Vibrational Frequencies

To determine the nature of the stationary point, the second derivative of the energy is needed. The second derivative describes the curvature of the stationary

point. If it is positive, then the stationary point is a minimum, if it is negative, then the stationary point is a maximum. In the multidimensional case, the stationary point may be a minimum in some directions and a maximum in others. To calculate the vibrational frequencies, the PES at the stationary point is approximated as a number of uncoupled harmonic oscillators, one in each conjugate direction. The vibrations along the conjugate directions are known as the normal modes of vibration. For small enough displacements from the minimum, any surface can be modeled as harmonic. From the quantum mechanics of the harmonic oscillator, we know that the vibrational frequency (in wavenumbers) can be expressed as:

$$\omega = \tilde{\omega} = \frac{1}{2\pi c} \left(\frac{k}{\mu} \right)^{\frac{1}{2}}, \quad (1.115)$$

where μ is the reduced mass and k , the force constant, is defined as:

$$k = \frac{d^2 E}{dr^2}. \quad (1.116)$$

Since the frequency varies as the square root of the second derivative, two cases are possible. If the second derivative is positive, then its square root is a real number and the frequency is real. If the second derivative is negative, then its square root, and thus the vibrational frequency, are imaginary. This allows us to classify the stationary point. If all of the vibrational frequencies are real, then the point is a true minimum on the PES. If one frequency is imaginary, then the stationary point is a (first-order) saddle point on the PES. These saddle points are known as transition states as they connect two minima on the PES along a path known as the reaction coordinate. If there are more than one imaginary frequency, then the stationary point is a higher-order saddle point on the PES, and is probably not chemically relevant.

1.9 Scope of this Thesis

This thesis is concerned with the development of pseudopotential methods to accelerate the calculation of molecular systems that involve heavy atoms, and to increase

the accuracy of such calculations. The research was intended to produce methods usable by the scientific community that provided results that were as accurate, or more so than currently available with other methods, but with less computational effort. The thesis is divided into three parts. The next two chapters deal with the development of the improved Model Core Potentials (iMCPs) for all of the transition metal atoms. Chapter 4 presents an application of the iMCPs to an area of great chemical interest. The final three chapters deal with the reparameterization and application of the well-tempered Model Core Potentials (wtMCPs) for systems containing rare gases. The final chapter, in particular, shows the ability of the wtMCPs to provide results superior to any previous calculations on the systems.

Chapters 2 and 3 are very similar in design, and describe the development of the iMCPs for the transition metals. Chapter 2 goes through the method in more detail, and compares the performance of the iMCPs to previous versions of the MCPs. Calculations were performed on a number of small to medium-sized first-row transition metal complexes at the RHF and DFT levels. The bond lengths and vibrational frequencies calculated at both levels of theory were compared to experimental values, as well as to those calculated using the older version of the MCPs. Reasons for reparameterizing the MCPs are discussed, including a study of the speed of calculations performed with both the iMCPs and the previous versions of the MCPs.

Chapter 3 is concerned with the development of the iMCPs for the second- and third-row transition metals. Fewer complexes of these elements (in particular smaller ones) have been experimentally studied, and so the focus has been shifted off extensive comparisons to experimental data, and towards a study of the effect of differing DFT functionals on the calculations. Two functionals were studied in order to determine which one was superior in the determination of bond lengths and vibrational frequencies for these compounds. In addition, the effect of the DFT integration grid on the results from calculations using both the non-relativistic and scalar-relativistic potentials was studied.

Chapter 4 is the first application of the iMCPs to a system of chemical interest. The field of rare gas chemistry has exploded in recent years, and many new compounds have been synthesized. Calculations were performed at the RHF, DFT, and

MP2 levels on a number of small organic compounds that mimic ligands commonly found in organoxenon complexes in order to determine the ability of the iMCPs to model geometries of such complexes. The energy changes of a number of reactions to synthesize organoxenon compounds are studied at the RHF and DFT levels of theory and several new energetically stable compounds are predicted.

Reparameterization of the newly developed wtMCPs was undertaken to improve the description of the electron density near the nuclei, and the first test of these new potentials is the subject of Chapter 5. This was a project inspired by an unresolved issue in experimental spectroscopy. Geometries and binding energies were calculated at the MP2 level for the complexes formed by the interaction between a rare gas and the coinage metal monohalides. The geometries can then be used to determine the spectroscopic constants for as yet unknown complexes.

The final two chapters deal with the application of the wtMCPs to weakly-bound complexes between the Group 2 metals and helium. Chapter 6 describes calculations with a medium-size basis set on all of the Group 2 complexes. The polarizabilities of the Group 2 atoms, the pair potential parameters, and the bound rovibrational states were calculated at the CCSD(T) level of theory. The results were compared to all-electron WTBS results. The effect of bond functions on the results was also studied.

Chapter 7 is more specialized, as it deals with only the heavier Group 2 elements. The basis sets have been augmented with additional polarization and bond functions; the pair potentials, calculated using the CCSD(T) method, are the most accurate available for these complexes. The bound rovibrational levels are studied, and an attempt is made to determine whether or not these metal atoms would be found inside a helium nanodroplet, or on the surface.

The common theme among the chapters is the development of the Model Core Potentials and their application to a wide variety of chemical systems. Most of the applications in the thesis involve transition metals and/or rare gases, which are of specific interest to me, but the breadth of applications possible for the MCP method, which ranges from large clusters for the iMCPs to near-basis-set limit accuracy calculations on small systems for the wtMCPs, shows that these methods can be used

in all areas of chemistry.

Bibliography

- [1] Obtained from <http://www.nobel.se/chemistry/laureates/1998/index.html> on September 29, 2003.
- [2] J.-E. Shea and C. L. Brooks III *Ann. Rev. Phys. Chem.* **52** (2001) 499.
- [3] N. Brooijmans and I. D. Kuntz *Ann. Rev. Biophys. Biomol. Struct.* **32** (2003) 335.
- [4] N. Fey *J. Chem. Technol. Biotechnol.* **74** (1999) 852.
- [5] *Chem. Rev.* **100** (2000).
- [6] *Coord. Chem. Rev.* **238-9** (2003).
- [7] A. Szabo and N. S. Ostlund *Modern Quantum Chemistry: Introduction to Advanced Electronic Structure Theory* Dover Publications: Mineola, N.Y., 1996.
- [8] F. Jensen *Introduction to Computational Chemistry* John Wiley & Sons: Chichester, U.K., 1999.
- [9] D. A. McQuarrie *Quantum Chemistry* University Science Books: Sausalito, CA, 1983.
- [10] R. G. Parr and W. Yang *Density-Functional Theory of Atoms and Molecules* Oxford University Press: New York, 1989.
- [11] S. Faas, Ph.D. Thesis, Utrecht University, The Netherlands, 2000.
- [12] W. Greiner *Relativistic Quantum Mechanics: Wave Equations 3rd ed.* Springer: Berlin, 2000.

- [13] R. E. Moss *Advanced Molecular Quantum Mechanics: An Introduction to Relativistic Quantum Mechanics and the Quantum Theory of Radiation* Chapman and Hall: London, 1973.
- [14] I. N. Levine *Quantum Chemistry 5th ed.* Prentice Hall: Upper Saddle River, N.J., 2000.
- [15] B. T. Sutcliffe *J. Chem. Soc. Faraday Trans.* **89** (1993) 2321.
- [16] C. C. Roothaan *Rev. Mod. Phys.* **23** (1951) 69.
- [17] G. G. Hall *Proc. Roy. Soc. A* **205** (1951) 541.
- [18] C. C. Roothaan *Rev. Mod. Phys.* **32** (1960) 179.
- [19] J. A. Pople and R. K. Nesbet *J. Chem. Phys.* **22** (1954) 571.
- [20] E. R. Davidson in *The Challenge of d and f Electrons: Theory and Computation* D. R. Salahub and M. C. Zerner, eds. American Chemical Society: Washington, 1989; p. 153.
- [21] R. McWeeny *Methods of Molecular Quantum Mechanics 2nd ed.* Academic Press: San Diego, 1992.
- [22] L. Brillouin, *J. Phys.* **3** (1932) 373.
- [23] S. R. Langhoff and E. R. Davidson *Int. J. Quantum Chem.* **8** (1974) 61.
- [24] C. Møller and M. S. Plesset *Phys. Rev.* **46** (1934) 618.
- [25] P. Hohenberg and W. Kohn *Phys. Rev. B* **136** (1964) 864.
- [26] W. Kohn and L. J. Sham *Phys. Rev. A* **140** (1965) 1133.
- [27] D. M. Ceperley and B. J. Alder *Phys. Rev. Lett.* **45** (1980) 566.
- [28] S. J. Vosko, L. Wilk, and M. Nusair *Can. J. Phys.* **58** (1980) 1200.
- [29] A. D. Becke *Phys. Rev. B* **38** (1988) 3098.

- [30] J. P. Perdew, M. Ernzerhof, and K. Burke *J. Chem. Phys.* **105** (1996) 9982.
- [31] E. I. Proynov, S. Sirois, and D. R. Salahub *Int. J. Quant. Chem.* **64** (1997) 427.
- [32] A. D. Becke *J. Chem. Phys.* **98** (1993) 5648.
- [33] P. J. Stephens, F. J. Devlin, C. F. Chabalowski, and M. J. Frisch *J. Chem. Phys.* **98** (1994) 11623.
- [34] L. A. Curtiss, K. Raghavachari, P. C. Redfern, and J. A. Pople *J. Chem. Phys.* **106** (1997) 1063.
- [35] H. Hellmann *J. Chem. Phys.* **3** (1935) 61.
- [36] J. C. Phillips and L. Kleinman *Phys. Rev.* **116** (1959) 880.
- [37] S. Huzinaga *Can. J. Chem.* **73** (1995) 619.
- [38] T. H. Dunning, Jr. and P. J. Hay in *Methods of Electronic Structure Theory Vol. 2* H. F. Schaefer III, ed. Plenum Press: New York (1977).
- [39] P. J. Hay and W. R. Wadt *J. Chem. Phys.* **82** (1985) 270.
- [40] P. J. Hay and W. R. Wadt *J. Chem. Phys.* **82** (1985) 284.
- [41] P. J. Hay and W. R. Wadt *J. Chem. Phys.* **82** (1985) 299.
- [42] L.F. Pacios and P. A. Christiansen *J. Chem. Phys.* **82** (1985) 2664.
- [43] M. M. Hurley, L. F. Pacios, P. A. Christiansen, R. B. Ross, and W. C. Ermler *J. Chem. Phys.* **84** (1986) 6840.
- [44] L. A. LaJohn, P. A. Christiansen, R. B. Ross, T. Atashroo, and W. C. Ermler *J. Chem. Phys.* **87** (1987) 2812.
- [45] R. B. Ross, J. M. Powers, T. Atashroo, W. C. Ermler, L. A. LaJohn, and P. A. Christiansen *J. Chem. Phys.* **93** (1990) 6654.
- [46] S. A. Wildman, G. A. DiLabio, and P. A. Christiansen *J. Chem. Phys.* **107** (1997) 9975.

- [47] W. J. Stevens, H. Basch, and M. Krauss *J. Chem. Phys.* **81** (1984) 6026.
- [48] W. J. Stevens, M. Krauss, H. Basch, P. G. Jasien, *Can. J. Chem.* **70** (1992) 612.
- [49] T. R. Cundari and W. J. Stevens *J. Chem. Phys.* **98** (1993) 5555.
- [50] P. Fuentealba, H. Preuss, H. Stoll, and L. v. Szentpaly *Chem. Phys. Lett.* **89** (1982) 418.
- [51] P. Fuentealba, L. v. Szentpaly, H. Preuss, and H. Stoll *J. Phys. B* **18** (1985) 1287.
- [52] G. Igel-Mann, H. Stoll, and H. Preuss *Mol. Phys.* **65** (1988) 1321.
- [53] W. Kuechle, M. Dolg, H. Stoll, and H. Preuss *Mol. Phys.* **74** (1991) 1245.
- [54] A. Bergner, M. Dolg, W. Kuechle, H. Stoll, and H. Preuss *Mol. Phys.* **80** (1993) 1431.
- [55] V. Bonifacic and S. Huzinaga *J. Chem. Phys.* **60** (1974) 2779.
- [56] V. Bonifacic and S. Huzinaga *J. Chem. Phys.* **62** (1975) 1507.
- [57] V. Bonifacic and S. Huzinaga *J. Chem. Phys.* **62** (1975) 1509.
- [58] V. Bonifacic and S. Huzinaga *J. Chem. Phys.* **64** (1976) 956.
- [59] V. Bonifacic and S. Huzinaga *J. Chem. Phys.* **65** (1976) 2332.
- [60] M. Klobukowski, S. Huzinaga, and Y. Sakai in *Computational Chemistry: Reviews of Current Trends Vol. 3* World Scientific: Singapore, 1999; Chapter 2.
- [61] B. Pittel and W. H. E. Schwarz *Chem. Phys. Lett.* **46** (1977) 121.
- [62] G. Frenking, I. Antes, M. Bohme, S. Dapprich, A. W. Ehlers, V. Jonas, A. Neuhaus, M. Otto, R. Stegmann, A. Veldkamp, and S. F. Vyboishchikov in *Reviews in Computational Chemistry Vol. 8* K. B. Lipkowitz and D. B. Boyd, eds. VCH Publishers: New York, 1996; p. 63.

- [63] M. Klobukowski *Theor. Chim. Acta* **83** (1992) 239.
- [64] C. C. Lovallo, unpublished data.
- [65] J.-P. Desclaux *Int. J. Quant. Chem.* **6** (1972) 25.
- [66] K. P. Huber and G. Herzberg "Constants of Diatomic Molecules" (data prepared by J.W. Gallagher and R.D. Johnson, III) in NIST Chemistry WebBook, NIST Standard Reference Database Number 69, Eds. P.J. Linstrom and W.G. Mallard, March 2003, National Institute of Standards and Technology, Gaithersburg MD, 20899 (<http://webbook.nist.gov>).
- [67] L.L. Foldy and S.A. Wouthuysen *Phys. Rev.* **78** (1950) 29.
- [68] T. Nakajima and K. Hirao *Chem. Phys. Lett.* **302** (1999) 383.
- [69] R. D. Cowan and D. C. Griffin *J. Opt. Soc. Am.* **66** (1976) 1010.
- [70] A. J. Sadlej *Collec. Czech. Chem. Commun.* **53** (1988) 1995.
- [71] S. F. Boys *Proc. Roy. Soc. A* **200** (1950) 542.
- [72] T. H. Dunning, Jr. *J. Chem. Phys.* **53** (1970) 2823.
- [73] R. C. Raffanetti *J. Chem. Phys.* **58** (1973) 4452.
- [74] T. H. Dunning, Jr. *J. Chem. Phys.* **90** (1989) 1007.
- [75] S. Huzinaga and M. Klobukowski *Chem. Phys. Lett.* **212** (1993) 260.
- [76] S. F. Boys and F. Bernardi *Mol. Phys.* **37** (1979) 1529.

Chapter 2

Improved Model Core Potentials for the First-Row Transition Metals*

2.1 Introduction

Pseudopotential methods have long been used to simplify calculations of systems that contain many chemically inert core electrons. The Model Core Potential (MCP) formalism, developed by Huzinaga and coworkers [1], differs from other commonly used pseudopotentials, such as the compact effective potentials of Stevens *et al.* [2, 3] or the pseudopotentials of the Stuttgart group [4], by the inclusion of a projection operator defined in terms of the atomic core orbitals. The operator ensures that the resulting valence orbitals may retain the correct nodal structure. For a summary of the past refinements and extensions to the MCP method, see the review by Klobukowski *et al.* [5]

Pseudopotentials can also reproduce relativistic effects in atoms and molecules if relativistic all-electron results are used as the reference set in the parameter optimization. In this way, the relativistic effects embedded in the core orbitals, valence orbitals, and the valence orbital energies are eventually reflected in the potential parameters and valence basis sets. The major relativistic effects that are usually taken into account in most calculations are the scalar relativistic effects (mass-variation and Darwin terms). This allows taking into account most of the relativistic effects, without resorting to computationally expensive four-component Dirac-Hartree-Fock

*A version of this chapter was published as: C. C. Lovallo and M. Klobukowski *J. Comput. Chem.* **24** (2003) 1009.

calculations.

Calculations on transition metals have garnered great interest due to their importance both in the field of material science and in a wide variety of catalytic processes, in both industrial and biological settings. The field has matured in recent years, with an entire special issue of Chemical Reviews devoted to the field [6]. Pseudopotentials are often used in the study of transition metal complexes in order to take advantage of the speed and relativistic corrections that pseudopotentials can provide [7, 8].

The most recent version of the MCPs for the main group atoms was published by Sakai *et al.* [9] in 1997; however, for the transition metal atoms, the potentials were parameterized in 1987 [10, 11]. The potentials derived in the present paper for the first-row transition metals and the atoms most often present as ligands in transition metal complexes (C, N, O, F, and Cl) were reparameterized using a method different from the one used by Sakai *et al.* [9]. We have called these new potentials the improved Model Core Potentials (iMCPs). The performance of the new potentials is compared with the previous standard version of the MCPs (denoted here as sMCPs) in calculations on a number of complexes containing first-row transition metals in order to study their ability to reproduce experimental bond lengths and harmonic vibrational frequencies. Timing calculations were also performed to determine whether calculations with the new iMCPs were as fast as those with the sMCPs, as well as to see the speedup over all-electron calculations.

Reparameterization of the MCPs was undertaken in order to introduce L-shell structure (where the s and p basis functions share common exponents) into the basis sets of the main group elements. The use of L-shells has been shown to be very effective in reducing the time of the evaluation of the 2-electron integrals [12, 13]. We also changed the parameterization process, both by increasing the number of parameters fitted as well as through the use of tighter convergence criteria and better fitting procedures, in order to obtain improved orbital energies. For better internal consistency of the method, we reparameterized the transition metals so that the new metal potentials would match the accuracy of the new main group potentials. In addition, in order to improve the description of the d valence shell, we increased the size of the valence basis set in the d space from five primitive Gaussian functions to

six. Furthermore, both non-relativistic and scalar-relativistic iMCPs were made for each transition metal atom. (The only sMCPs available for the first-row transition metals are non-relativistic). Therefore, the new iMCPs are the first MCPs for these atoms that incorporate relativistic effects.

2.2 Outline of the MCP Formalism

In order to establish the notation, the fundamental equations of the MCP method are reviewed; for more details, see Section 1.5.2 and the review [5]. For any closed-shell atom of nuclear charge Z , with N_c core electrons, the (one-electron) core-valence Hamiltonian operator can be expressed as:

$$\hat{h} = -\frac{1}{2}\nabla^2 - \frac{Z}{r} + \sum_c (2\hat{J}[\bar{\phi}_c] - \hat{K}[\bar{\phi}_c] + B_c|\bar{\phi}_c\rangle\langle\bar{\phi}_c|), \quad (2.1)$$

$$= -\frac{1}{2}\nabla^2 - \frac{Z - N_c}{r} + \hat{V}_C^{core} + \hat{V}_X^{core} + \hat{\Omega}, \quad (2.2)$$

where \hat{J} and \hat{K} are the Coulomb and exchange operators respectively, $\bar{\phi}_c$ are the (frozen) core orbitals, B_c are numerical constants, and the sum runs over all core orbitals. There are three core operators: the core-valence Coulomb interaction operator \hat{V}_C^{core} , the core-valence exchange interaction operator \hat{V}_X^{core} , and the projection (shift) operator $\hat{\Omega}$:

$$\hat{V}_C^{core} = -\frac{N_c}{r} + 2\sum_c \hat{J}[\bar{\phi}_c], \quad (2.3)$$

$$\hat{V}_X^{core} = -\sum_c \hat{K}[\bar{\phi}_c], \quad (2.4)$$

$$\hat{\Omega} = \sum_c B_c|\bar{\phi}_c\rangle\langle\bar{\phi}_c|, \quad (2.5)$$

where the sums run over the core orbitals on the atom. In the MCP approximation, the exact frozen-core operator (the sum of the Coulomb and exchange parts above) is approximated by a sum of Gaussian type functions:

$$\hat{V}^{core} \equiv -\frac{Z - N_c}{r} + \hat{V}_C^{core} + \hat{V}_X^{core} \approx \tilde{V}^{core}, \quad (2.6)$$

where:

$$\tilde{V}^{core} \equiv -\frac{Z - N_c}{r_i} \left[1 + \sum_l A_l r_i^{n_l} \exp(-\alpha_l r_i^2) \right], \quad (2.7)$$

$$n_l = 0 \text{ or } 1; l = 1, 2, \dots, N.$$

The MCP parameters are the set of A_l , α_l , and B_c . Note that the explicit form of the atomic core orbitals must be known for use in the projection operator. In contrast to previous versions of the MCP implementation, in the iMCP approach the B_c values are optimized during the parameterization procedure.

2.3 Determination of Potentials and Basis Sets

In order to obtain atomic numerical reference data, Hartree-Fock calculations were performed using the program of Froese-Fischer [14]. The calculations were done for the state-averaged energy for the ground-state electronic configuration for the ligand atoms. For the transition metals, state-averaged calculations were done for the $s^1 d^{n+1}$ configuration, except for Zn where the $4s^2 3d^{10}$ ground-state configuration was used. Most of the transition metals have a $s^2 d^n$ ground state (except for Cr and Cu) [15], however the orbitals obtained from this state are too compact to properly describe the more diffuse orbitals obtained in molecular systems [10]. Both non-relativistic (NR) and Cowan-Griffin [16] scalar-relativistic (SR) calculations were done for all of the atoms.

To obtain the core atomic orbitals needed for the projection operator, the core reference orbitals (defined on the numerical grid from the atomic Hartree-Fock program) were fit to Gaussian functions. The Gaussian exponents chosen were those of the well-tempered basis sets (WTBS) of Huzinaga *et al.* [17] In the iMCPs, unlike in the sMCPs, the size of the core basis set that defines the projector operators is not constant among all the orbitals with the same angular momentum: it varies in size, with the core 3s orbital being the largest. Table 2.1 shows the size of the core basis sets. For the transition metals, the penultimate p orbital (3p) was considered to be a valence orbital. Calculations have shown, especially for the early transition

metals, that including this orbital in the valence space improves the reliability of the calculations [11]. Therefore, no large-core (sd only) iMCP potentials were developed. The inclusion of penultimate orbitals in the iMCPs is a constant feature of their development; the iMCPs for the second and third row transition metals also consider the 4p or 5p orbitals as valence (see Chapter 3), and the iMCPs for the main group elements of the third-row and beyond (Ga - Rn) include the penultimate d shell in the valence space (see Chapter 4 and ref. [18]).

Table 2.1: Partitioning of core and valence electrons and size of basis sets

Atom	Valence Electrons	Core Electrons	Valence Basis Sets	Core Basis Sets
C, N	$2s^2 2p^n$	$1s^2$	(5s/5p) - as 5L	(14)
O, F	$2s^2 2p^n$	$1s^2$	(5s/5p) - as 5L	(16)
Cl	$3s^2 3p^5$	$1s^2 2s^2 2p^6$	(5s/5p) - as 5L	(13,16/16)
Sc	$3p^6 4s^1 3d^2$	$1s^2 2s^2 2p^6 3s^2$	(5s/4p/6d)	(13,16,19/13)
Ti, Fe, Co, Ni	$3p^6 4s^1 3d^{n+1}$	$1s^2 2s^2 2p^6 3s^2$	(5s/4p/6d)	(13,16,19/15)
V, Cr, Mn	$3p^6 4s^1 3d^{n+1}$	$1s^2 2s^2 2p^6 3s^2$	(5s/4p/6d)	(13,16,19/16)
Cu	$3p^6 4s^1 3d^{10}$	$1s^2 2s^2 2p^6 3s^2$	(5s/4p/6d)	(12,15,20/14)
Zn	$3p^6 4s^2 3d^{10}$	$1s^2 2s^2 2p^6 3s^2$	(5s/4p/6d)	(13,16,19/15)

The iMCPs are designed for use on larger transition metal clusters, so it is desirable that the sizes of the valence basis sets remain fairly small. A set of five s, four p, and six d primitive Gaussian functions was chosen in order to balance the considerations of speed and accuracy. This is a very similar size to the sMCP basis sets, which consist of six s, four p, and five d primitive Gaussian functions. The values of the exponents were determined by fitting them to the reference numerical orbitals.

One of the ways in which the iMCPs differ from the sMCPs is that all of the parameters of the MCP formalism are systematically optimized. The values of the B_c constants are generally given as a constant multiplied by the orbital energy $\bar{\epsilon}_c$ corresponding to that (frozen) core orbital. Usually that constant is the same for all the core orbitals in the atom:

$$B_c = -f_{proj} \bar{\epsilon}_c, \quad (2.8)$$

$c = 1, 2, \dots, C$ core levels.

The f_{proj} parameter can change the hardness of the potential, with a larger value of f_{proj} leading to a harder potential and thus longer bond lengths. In the sMCPs, the value of f_{proj} is usually 2.0, with only the third-row transition metals and heavier main-group atoms having values less than 2.0. For these atoms, a value of 1.0 - 1.5 was used. For the iMCPs, each atom had a value of f_{proj} optimized separately by scaling the potential so that it reproduced all-electron molecular Hartree-Fock calculations on several small training systems.

Once the test value of f_{proj} is chosen, the remaining MCP parameters (A_l and α_l) are found by minimizing the following sum over the valence orbitals j :

$$\Delta_{val} = \sum \left\{ W_j^\epsilon |\epsilon_j^{REF} - \epsilon_j^{MCP}| + W_j^P \sum_m [P_j^{REF}(r_m) - P_j^{MCP}(r_m)]^2 \right\}, \quad (2.9)$$

so that both the valence orbital energies ϵ and the orbital radial distribution functions P (defined on the grid r_m) are used to fit the potential. For the first-row ligand atoms (C, N, O, and F), a total of two terms with $n_l=0$ are used, leading to two A_l and two α_l parameters. For all other atoms, three terms with $n_l=0$ and three terms with $n_l=1$ are used, giving six A_l and six α_l parameters. The expansion coefficients for the valence basis sets are determined in this step by least-squares fitting to the reference valence orbitals. The valence exponents do not change in this step.

The potentials are tested in molecular calculations against an all-electron basis set. Geometry optimizations for several (3-5) molecules per atom were done using a modified version of the well-tempered basis set [17]. The standard Raffenetti [19] general contraction was used; the five smallest exponents in the s and d spaces for the transition metal and s and p spaces for the ligand atom(s) were added uncontracted. Two p polarization functions were added on the transition metal atom and one d polarization function was added to the ligand atom(s), with the exponents derived for the iMCPs (see below). This resulted in a basis set size of (26,26,26,26,1,1,1,1,1/17,17,1*,1*/13,1,1,1,1) for the transition metal and (20,20,1,1,1,1,1/13,1,1,1,1,1/1*) for the ligand atoms. The notation used here indicates that the s space for the transition metal consists of four contracted Gaussian

functions (each a sum of twenty-six Gaussian primitive functions), and five uncontracted Gaussian functions. Similarly, the p space consists of two contracted Gaussian functions which are sums of seventeen primitives each, and two uncontracted polarization functions, which are indicated by asterisks. The d space contains one contracted Gaussian function and five uncontracted Gaussian primitives. The geometry of the same molecules was then optimized using the iMCP basis set contracted to triple zeta in the valence spaces, and single zeta in the metal p space. The same polarization set was used, resulting in a basis set size of (3,1,1/4,1*, 1*/4,1,1) for the transition metal and (3,1,1/3,1,1/1*) for the ligand atoms. New values of f_{proj} were chosen, and the other parameters were reoptimized until the bond lengths obtained from the iMCP matched those obtained with the all-electron basis set. For the first-row elements, changing the value of f_{proj} made no change in the bond lengths (which already reproduced the all-electron values very well), and the value of f_{proj} was fixed at 2.0. The values obtained for the other atoms varied between 1.05 and 5.0. A complete set of all data used to parameterize the iMCPs is available in Appendix A.

It should be noted that the values of f_{proj} were fit in molecular calculations on a small number of molecules (although the same value of f_{proj} seemed to fit the best for just about all of the molecules for one atom), and only at the NR-RHF level. Transferability of the MCPs was assumed, and the same values of f_{proj} were used for the scalar-relativistic potentials, as well as in correlated molecular calculations for molecules beyond the training set. This may introduce some error into our calculations, as the values of f_{proj} could be different if they were determined with DFT reference calculations, or at the scalar-relativistic level. However, this error is expected to be small when compared to the errors introduced by basis set incompleteness for these small valence basis sets, or by the use of an approximate DFT functional. Previous work [20] has shown that pseudopotentials optimized at the RHF level can be used to reproduce both structural parameters and energetics at the DFT level for transition metal carbonyl systems.

It is well known that polarization functions are needed to properly represent the electron density changes that occur when an atom is brought into a molecular environment. Polarization functions are often determined by minimizing the energy for a

correlated atomic or molecular system; however, in the present work, the exponents of polarization functions were determined by maximizing the overlap between the desired polarization set and the numerical valence orbitals of the atom. Since the iMCPs have small basis sets, large polarization spaces are not needed because the error due to incomplete valence basis representation may be greater than from the incomplete polarization space. Therefore, only a 2d1f polarization set was prepared for the main-group elements (fit to the valence s and p orbitals), and a 2p1f set was derived for the transition metals, with the 2p set fit to the 4s orbital and 1f function fit to the 3d orbital. The resulting polarization exponents are very similar to those derived by Huzinaga *et al.* [21] using a similar method. As an example of the results obtained, the MCP basis set and parameters for the Ti atom are tabulated in Tables 2.2 and 2.3. The complete set of parameters and basis sets is available as a preprint.

Table 2.2: Non-relativistic iMCP valence basis set for Ti atom ($f_{proj} = 4.5$)

Type	Exponent	Contraction coefficient
s	89.921039	-0.033582
	8.060620	0.129304
	0.698601	-0.408426
	0.053015	0.816888
	0.020247	0.279522
p	55.390012	-0.098019
	13.806964	-0.253735
	1.412692	0.673867
	0.449784	0.416957
d	25.152514	0.023164
	6.476645	0.109500
	2.121343	0.301560
	0.726617	0.417022
	0.241276	0.375489
	0.075095	0.181225
p*	0.084	1.0
	0.027	1.0
f*	1.445	1.0

Table 2.3: Non-relativistic iMCP potential parameters for Ti atom ($f_{proj}=4.5$)

	n=0		
A	0.2761343	0.0733203	0.0842194
α	118.46509	4.0254606	1.2867193
	n=1		
A	219.27556	5.5457705	0.0533082
α	1400.9783	28.598178	1.0073688

2.4 Computational Methods

Most calculations were done using CADPAC [22] except for the all-electron reference calculations and the timing calculations, which were done with the GAMESS program [23]. Calculations were done at the restricted Hartree-Fock (RHF) as well as at the density functional theory (DFT) level using the B3P86 [24, 25] hybrid functional. All structures were optimized using analytic gradients, and some were verified by performing non-gradient minimization. Harmonic vibrational analysis was performed using analytic second derivatives whenever possible, but when software limitations prevented their use, second derivatives were calculated numerically using a two-point difference model with the default step size ($0.001 a_0$). Cartesian Gaussian functions were used in the MCP calculations, spherical Gaussians in the all-electron ones.

2.5 Results and Discussion

An initial comparison between the old and new MCPs can be made using the results from atomic calculations. Figures 2.1 and 2.2 display how the non-relativistic iMCPs and the sMCPs represent the s-type core orbitals and valence orbitals for the Cu atom, shown as the difference between the reference (numerical) orbital and the MCP core orbital (notice the logarithmic scale of the abscissa). The larger basis set size for the core levels in the iMCPs is obviously important, as the maximum error in the orbital is reduced by more than an order of magnitude. In addition, the errors

in the orbitals decrease as r increases, indicating a better fit in the outer core region, which should have the greatest effect on the valence orbitals. The basis set size for the valence space is very similar; 6s4p5d primitives for the sMCPs and 5s4p6d primitives for the iMCPs, so it may be expected that the errors in the p orbital should be about the same between the two potentials, the error in the d orbital should be less for the iMCPs, and the error in the s orbital should be smaller for the sMCPs. This is what is seen; the root-mean-square (RMS) deviation in the sMCP p orbital is 6% higher than that in the iMCP p orbital, but the difference in the d orbital is much greater. Here, the RMS error is decreased by almost a factor of 3 from the sMCP to the iMCP. The RMS error in the iMCP s orbital is almost twice as large than that of the sMCP orbital, but if we only consider the outermost part of electron density (outside the furthest node), the errors are essentially equal. Therefore, the extra exponent in the sMCP basis set is used mostly to fit the innermost part of the electron density. This can be seen by inspecting the exponents, the largest exponent in the s space for the sMCP basis set is 314.09, whereas it is 154.58 for the iMCP basis set. Since this inner electron density is chemically insignificant for the structural parameters and vibrational frequencies studied in this work, we can expect that the iMCPs represent an improvement over the sMCPs in the d space without sacrificing any accuracy in the s and p spaces.

Differences also appear when the valence orbital energies are inspected. The sMCP valence orbital energies generally match the numerical reference energies with errors up to a few millihartrees. The largest energy differences in each orbital symmetry are 1.5 mE_h for the 3p orbital of Mn, 5 mE_h for the 3d orbital of Mn, and 4 mE_h for the 4s orbital of Sc [11]. Within the iMCP parameterization, the differences between the iMCP and reference orbital energies were always smaller than 0.5 μE_h .

Figure 2.1: Deviation between MCPs and reference Cu core orbitals (1s, 2s, 3s)

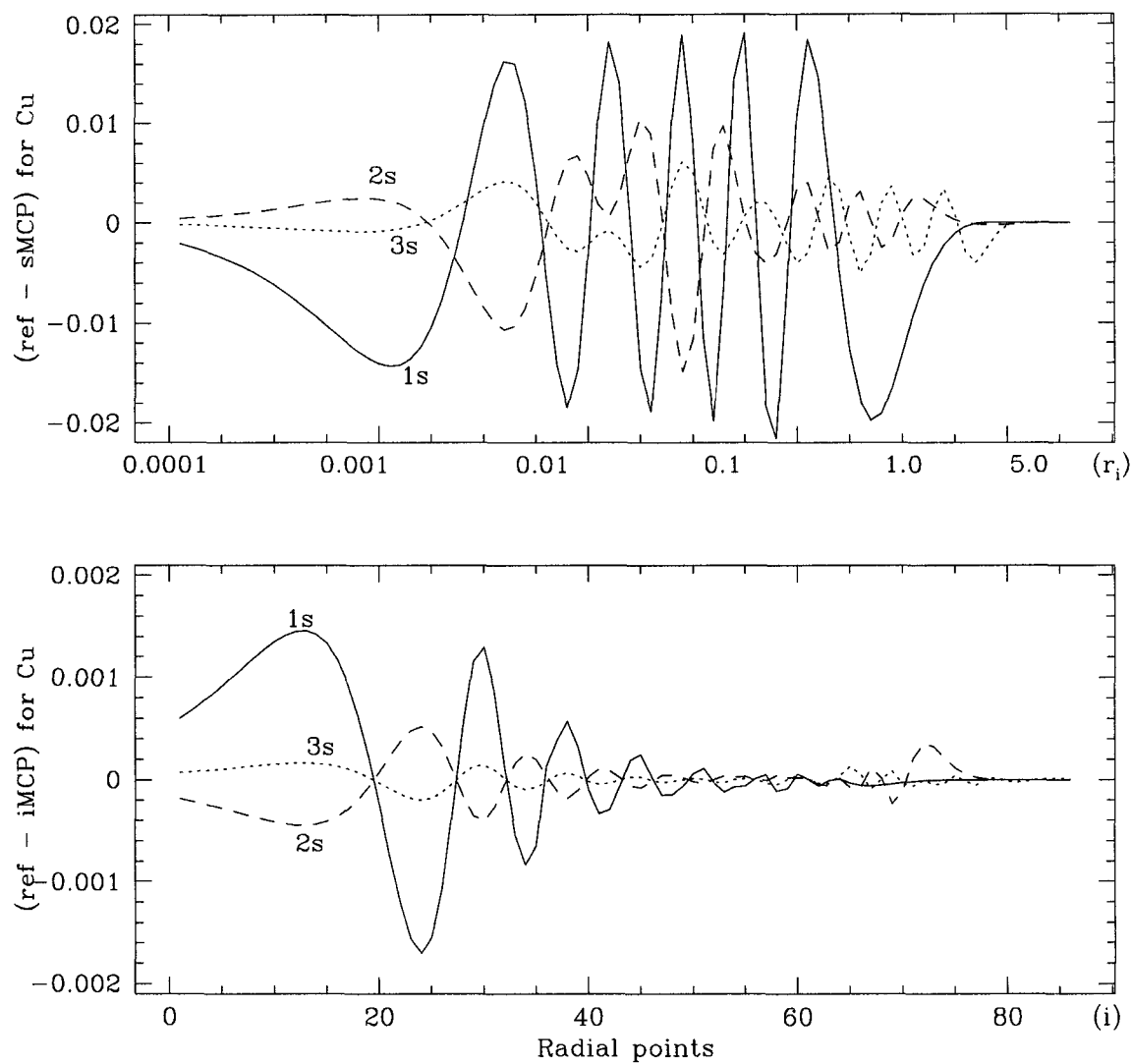
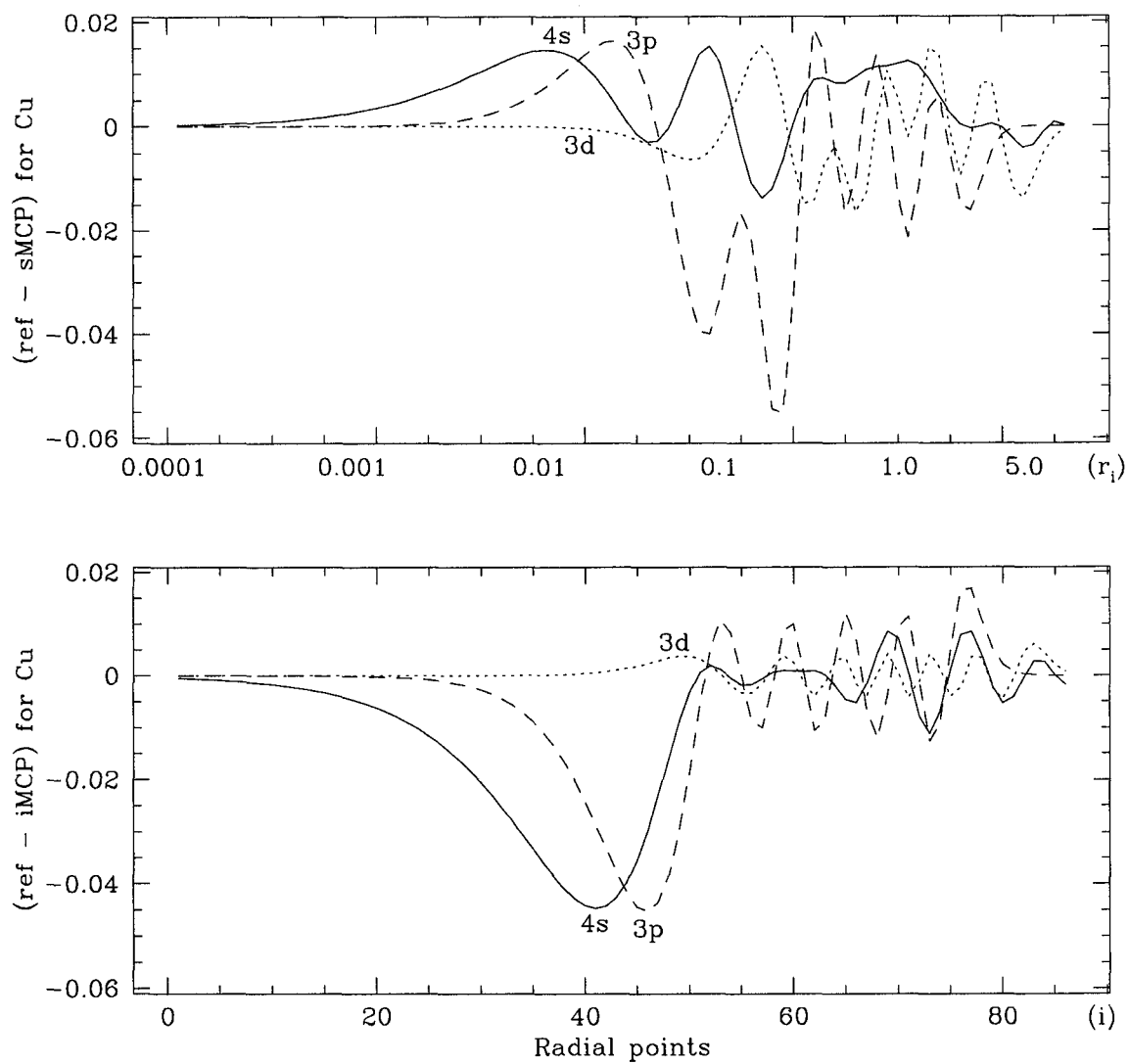


Figure 2.2: Deviation between MCPs and reference Cu valence orbitals (4s, 3p, 3d)



Molecular calculations were done to test the performance of the iMCPs in a molecular environment. The molecule TiF_4 was chosen for further comparison of the iMCP and all-electron methods at the RHF level. The valence basis set used here (and in the rest of the calculations in this chapter) was a triple-zeta expansion in the valence space (s and d for the transition metals, s and p for the main-group elements, and s for hydrogen) and a complete contraction of the penultimate 3p shell for the transition metals. Two p polarization functions were then added to the transition metal basis set, two d polarization functions for the main-group elements, and one p polarization function for the hydrogen atoms. The results are shown in Table 2.4. The bond lengths are very nearly equal, demonstrating that we can expect structural parameters to closely replicate the all-electron values. The harmonic vibrational frequencies overestimate the all-electron values by about 10%. This not only indicates that we might expect molecular properties that we did not explicitly consider in the fitting of the iMCPs to be fairly well reproduced, but also that we should expect that our RHF frequencies will be somewhat higher than usually expected from the RHF method. The iMCP orbital energies are also very close to the all-electron values, with a difference of no more than 5 mE_h , almost half of what we see with the sMCPs. Compared to the experimental values, the bond lengths are too short and the harmonic frequencies too high, as is usually seen at the RHF level. Note that when we compare our iMCP results to experimental values, any errors our iMCPs may exhibit with respect to experiment may be due to the fact that the all-electron calculations (that the iMCPs are designed to replicate) cannot accurately predict the experimental bond lengths and vibrational frequencies for these compounds. The results for the sMCPs are much more scattered. The bond length is not reproduced as accurately, and the orbital energies are not as close to the all-electron ones, with errors of up to 9 mE_h . The harmonic frequencies are more scattered than the iMCP ones, with the lower (bending) frequencies being larger than the all-electron and iMCP values, and the higher (stretching) frequencies being smaller than the all-electron values, making it more difficult to devise a common scaling factor to improve the results relative to experiment.

A total of 20 first-row transition metal compounds were studied, ranging in size

Table 2.4: Calculated bond lengths, frequencies, and orbital energies for TiF_4^a

	sMCP	iMCP	all e ⁻	Exp.
r_e	1.715	1.727	1.729	1.75 ^b
$\omega_1(\text{E})$	206	201	196	185 ^c
$\omega_2(\text{T}_2)$	241	238	232	209
$\omega_3(\text{A}_1)$	772	822	779	712
$\omega_4(\text{T}_2)$	816	878	840	793
$\varepsilon_{\text{t}2}$	-0.7376	-0.7289	-0.7289	
ε_e	-0.7250	-0.7156	-0.7163	
$\varepsilon_{\text{a}1}$	-0.7071	-0.7014	-0.7068	
$\varepsilon_{\text{t}2}$	-0.6858	-0.6784	-0.6829	
$\varepsilon_{\text{t}1}$	-0.6674	-0.6600	-0.6618	

a) r_e in Å, ω in cm^{-1} , ε in E_h b) [26] c) [27]

from CuH to $\text{Zn}(\text{CH}_3)_4^{2-}$. The optimized bond lengths and harmonic vibrational frequencies were compared to the experimental values at both the RHF and DFT levels. A total of 32 bond lengths and 71 vibrational frequencies were studied. A complete set of all the data for the bond lengths and frequencies can be found in Appendix A. A representative set of data (VOF_3) is shown in Table 2.5. It can be seen that all three sets of potentials predict the bond lengths of VOF_3 to about the same accuracy. This is very similar to what is seen across the Periodic Table in general: the new iMCPs are as good or slightly better than the previous version, and the scalar-relativistic corrections generally lead to predicted bond lengths that are closer to experiment at the RHF level. At the B3P86 level, the predicted lengths are closer to experiment, and again there is little to distinguish the three potentials. The harmonic vibrational frequencies are all 10-25% larger than experiment at the RHF level; at the B3P86 level, the frequencies are still too high by about 4-8%. The frequencies calculated with the scalar-relativistic potential tend to be a little larger than those calculated with the non-relativistic potentials, so as a whole, the frequencies are less accurately calculated with the relativistic potential. The mean absolute errors in bond lengths and in frequencies were calculated, and the results are tabulated in Tables 2.6 and 2.7.

Table 2.5: Bond lengths (in Å) and vibrational frequencies (in cm^{-1}) for VOF_3

	NR iMCP		SR iMCP		sMCP		Exp. ^a
	RHF	B3P86	RHF	B3P86	RHF	B3P86	
r(V-O)	1.504	1.542	1.509	1.542	1.477	1.520	1.569
r(V-F)	1.686	1.695	1.693	1.694	1.700	1.695	1.729
$\omega_1(A_1)$	829	781	833	785	780	765	720
$\omega_2(A_1)$	1307	1178	1313	1185	1332	1184	1055
$\omega_3(A_1)$	300	266	301	268	292	272	256
$\omega_4(E)$	889	854	894	859	841	845	801
$\omega_5(E)$	369	326	363	327	379	335	304
$\omega_6(E)$	237	212	238	214	235	221	204

a) [28]

Table 2.6: Mean absolute errors in calculated bond lengths (Å)

	NR iMCP	SR iMCP	sMCP
RHF (all)	0.078	0.069	0.082
RHF (M-L)	0.089	0.078	0.091
B3P86 (all)	0.028	0.029	0.033
B3P86 (M-L)	0.032	0.033	0.037

Table 2.7: Mean absolute errors in calculated vibrational frequencies (cm^{-1})

	NR iMCP	SR iMCP	sMCP
RHF	106	106	108
B3P86	44	46	42

The B3P86 results are clearly better than the RHF ones, both for geometries and for frequencies. Semiquantitative agreement with experimental data is possible with the B3P86 functional for all of the compounds studied in this work. Both sets of new potentials give a small improvement in the predicted geometries, and predict vibrational frequencies about as well as the previous MCPs. The new parameterization protocol did not improve the results as much as was hoped, but the addition of scalar-relativistic potentials, which were not previously available for the first-row transition metals, and the new L-shell structure of the basis sets are improvements to the method.

Table 2.6 shows two results for each method and potential used. Separate values of the mean absolute error with respect to the experimental values are given for the complete set of 32 bond lengths, and for the subset of 27 bond lengths that describe transition metal - ligand bonds. This subset ignores the variation inside the ligands themselves, such as carbon - oxygen bonds in carbonyls or carbon - hydrogen bonds in methyl groups. Since these bond lengths are predicted much more accurately, excluding them results in a larger mean absolute error, and a more correct estimate of the expected error in bond lengths that involve the metal atoms. Using these potentials, a bond length error of 0.08 - 0.09 Å is expected at the RHF level, and 0.03 - 0.04 Å at the B3P86 level. The errors in the vibrational frequencies appear quite large, with a mean absolute error of over 100 cm⁻¹ at the RHF level for all of the potentials. However, the order of the predicted frequencies is usually correct, and a scaling factor may be applied to improve the agreement between calculated and experimental results. A scaling factor of approximately 0.89 is often applied to frequencies calculated at the RHF level to improve the agreement with experiment, and note that the expected error of only about 10% in a frequency can be 200 - 300 cm⁻¹ if that frequency is a carbonyl or methyl stretching frequency. At the B3P86 level, the predicted frequencies already show semiquantitative agreement with respect to experiment, and scaling would further improve the results. Some frequencies, notably the high-frequency stretches, are still predicted to be somewhat too large, but the error is less than half of what it was at the RHF level.

Pseudopotentials are often used in order to accelerate calculations. To demonstrate how much calculations could be accelerated by using iMCPs instead of the all-electron basis set, the larger system Ti₈C₁₂ was chosen. A single-point direct RHF calculation was done on this system, ignoring molecular symmetry. The time required for one SCF iteration is shown in Table 2.8. Compared to the large all-electron calculation that the iMCPs attempt to mimic, we achieve a speedup of over 600 times with our iMCP calculation. This suggests that the iMCP method should be able to accurately reproduce results from large basis set all-electron calculations, but at a fraction of the cost. By introducing the L-shell structure into the iMCPs, we hoped that calculations using these new pseudopotentials would also be faster than those performed

using the previous versions of the MCPs. The L-shell structure is only found in the basis sets of the main-group elements, so systems with many ligand atoms would be the most affected. To determine this effect, a calculation was done on the $(\text{CO})_{10}$ system, with the carbonyls fixed to the positions that they occupy in the $\text{Mn}_2(\text{CO})_{10}$ eclipsed conformer, and C_1 (no) molecular symmetry was assumed. The time required for a single SCF iteration is shown in Table 2.8. The new pseudopotential requires about one-third less time than the previous MCPs. The iMCP basis sets for the transition metals are actually larger than the sMCP basis sets as they contain six d primitives as opposed to five; consequently calculations involving transition metals should be slightly slower with these basis sets. In order to elucidate the effect this would have on calculation time, the complete $\text{Mn}_2(\text{CO})_{10}$ system was studied. The results are shown in Table 2.8. The effect of the transition metals is quite noticeable, but the iMCP calculation is still faster, albeit by only about 5%. As the primary application of the iMCPs is in the study of large organometallic clusters, a final test calculation was done on a large system of chemical interest, the $\text{Mn}_2(\text{CO})_6(\text{dppm})_2$ cluster. This system has a large ratio of ligand atoms to transition metal atoms, so the iMCPs are expected to be more efficient than the sMCPs. From Table 2.8 it can be seen that the iMCP calculations are about 25% faster.

Table 2.8: Timing results for MCP and all-electron molecular calculations

System	Method	Iteration time ^a
Ti_8C_{12}	iMCP	19.3 mins.
	all-electron	8.5 days
$(\text{CO})_{10}$	iMCP	88 s
	sMCP	130 s
$\text{Mn}_2(\text{CO})_{10}$	iMCP	258 s
	sMCP	273 s
$\text{Mn}_2(\text{CO})_6(\text{dppm})_2$	iMCP	27871 s
	sMCP	36642 s

^a) Calculations performed on a 1.2GHz Athlon PC running Red Hat Linux 6.2

2.6 Conclusions

The new iMCPs that we have developed can be used to give semiquantitative agreement with experimental data for the first-row transition metal complexes with accuracy comparable to that of much more expensive all-electron calculations. The new potentials also improve upon previous versions of MCPs in both speed and reproduction of atomic properties. They are very effective at reproducing molecular geometries and vibrational frequencies, and they are the first MCPs available for these elements that incorporate scalar-relativistic effects into the potentials.

Bibliography

- [1] V. Bonifacic and S. Huzinaga *J. Chem. Phys.* **60** (1974) 2779.
- [2] W. J. Stevens, H. Basch, and M. Krauss *J. Chem. Phys.* **81** (1984) 6026.
- [3] W. J. Stevens, M. Krauss, H. Basch, and P. G. Jasien *Can. J. Chem.* **70** (1992) 612.
- [4] M. Dolg, U. Wedig, H. Stoll, and H. J. Preuss, *J. Chem. Phys.* **86** (1987) 866.
- [5] M. Klobukowski, S. Huzinaga, and Y. Sakai in *Computational Chemistry: Reviews of Current Trends Vol. 3* World Scientific: Singapore, 1999; Chapter 2.
- [6] *Chem. Rev.* **100** (2000).
- [7] G. Frenking, I. Antes, M. Böhme, S. Dapprich, A. W. Ehlers, V. Jonas, A. Neuhaus, M. Otto, R. Stegmann, A. Veldkamp, and S.F. Vyboishchikov in *Reviews in Computational Chemistry Vol. 8* VCH: New York, 1996; Chapter 2.
- [8] T. R. Cundari, M. T. Benson, M. Leigh Lutz, and S. O. Sommerer in *Reviews in Computational Chemistry Vol. 8* VCH: New York, 1996; Chapter 3.
- [9] Y. Sakai, E. Miyoshi, M. Klobukowski, and S. Huzinaga, *J. Chem. Phys.* **106** (1997) 8084.
- [10] Y. Sakai, E. Miyoshi, M. Klobukowski, and S. Huzinaga *J. Comput. Chem.* **8** (1987) 226.
- [11] Y. Sakai, E. Miyoshi, M. Klobukowski, and S. Huzinaga, *J. Comput. Chem.* **8** (1987) 256.

- [12] W. J. Hehre, R. F. Stewart, and J. A. Pople *J. Chem. Phys.* **51** (1967) 2657.
- [13] J. A. Pople and W. J.; Hehre *J. Comput. Phys.* **27** (1978) 161.
- [14] C. Froese-Fischer *Comp. Phys. Comm.* **4** (1972) 107.
- [15] W. C. Martin, A. Musgrove, and S. Kotochigova “Ground Levels and Ionization Energies for the Neutral Atoms” (Web Version 1.2.2), [Online]. Available: <http://physics.nist.gov/IonEnergy> [2003, September 24]. National Institute of Standards and Technology, Gaithersburg, MD.
- [16] R. D. Cowan and D. C. Griffin *J. Opt. Soc. Am.* **66** (1976) 1010.
- [17] S. Huzinaga and M. Klobukowski *Chem. Phys. Lett.* **212** (1993) 260.
- [18] C. C. Lovallo and M. Klobukowski *Int. J. Quant. Chem.* **90** (2002) 1099.
- [19] R. C. Raffanetti *J. Chem. Phys.* **58** (1973) 4452.
- [20] C. van Wüllen, *Int. J. Quant. Chem.* **58** (1996) 147.
- [21] S. Huzinaga, J. Andzelm, M. Klobukowski, E. Radzio-Andzelm, Y. Sakai, and H. Tatewaki *Gaussian Basis Sets for Molecular Calculations* Elsevier: Amsterdam, 1984.
- [22] CADPAC version 6.3: The Cambridge Analytic Derivatives Package Issue 6, Cambridge, 1995. A suite of quantum chemistry programs developed by R. D. Amos with contributions from I. L. Alberts, J. S. Andrews, S. M. Colwell, N. C. Handy, D. Jayatilaka, P. J. Knowles, R. Kobayashi, K. E. Laidig, G. Laming, A. M. Lee, P. E. Maslen, C. W. Murray, J. E. Rice, E. D. Simandiras, A. J. Stone, M.-D. Su, and D. J. Tozer.
- [23] M. W. Schmidt, K. K. Baldrige, J. A. Boatz, S. T. Elbert, M. S. Gordon, J. J. Jensen, S. Koseki, N. Matsunaga, K. A. Nguyen, S. Su, T. L. Windus, M. Dupuis, and J. A. Montgomery, *J. Comput. Chem.* **14** (1993) 1347.
- [24] A. D. Becke *J. Chem. Phys.* **98** (1993) 5648.

- [25] J. P. Perdew *Phys. Rev. B* **33** (1986) 8822.
- [26] G. V. Girshev and N. I. Girsheva *Russ. J. Struct. Chem.* **24** (1983) 11.
- [27] L. E. Alexander and I. R. Beattie *J. Chem. Soc. Dalton Trans.* (1972) 1745.
- [28] A. Almenningen, S. Samdal, and D. Christen *J. Mol. Struct.* **48** (1978) 69.

Chapter 3

Improved Model Core Potentials for the Second- and Third-Row Transition Metals*

3.1 Introduction

This chapter will describe the development and testing of the improved Model Core Potentials (iMCPs) for the second- and third-row transition metals. The development is very similar to our work on the iMCPs for the first-row transition metals (see last chapter and ref. [1]). The largest difference between the first-row and heavier transition metals is that due to the large atomic number of the heavier transition metals, in particular those of the third-row, calculations are complicated both by the large number of electrons and by the necessity of incorporating relativistic effects into the calculations. For this reason, pseudopotentials, which can deal with both of these problems simultaneously, are widely used [2, 3] and more accurate versions are always needed.

The use of the Model Core Potential (MCP) formalism allows the valence orbitals to retain the correct nodal structure. This can be very important for the calculation of properties that depend on the electron density near the nucleus, like spin-orbit coupling, which can be very large in the heavier transition metals.

The most recent version of the MCPs for the second- and third-row transition

*A version of this chapter was submitted to the *Journal of Computational Chemistry* on September 30, 2003.

metal atoms was published by Sakai *et al.* [4, 5] in 1987. We have shown in the last chapter that the iMCPs reproduce both atomic and molecular data more accurately than the previous standard version of the MCPs; in addition, they are also faster. We now wish to bring these qualities to the heavier transition metals.

Reparameterization of the MCPs was initially undertaken in order to introduce L-shell structure (where the s and p basis functions share common exponents) into the basis sets of the main group elements. The use of L-shells has been shown to be very effective in reducing the time of the evaluation of the 2-electron integrals [6, 7]. We also improved the parameterization process, both by increasing the number of parameters fitted as well as through the use of tighter convergence criteria and better fitting procedures, in order to obtain improved orbital energies. We then undertook the reparameterization of the transition metals to have better internal consistency of the method, *i.e.* to obtain potentials for the transition metals that were as accurate as those newly developed for the main group elements.

We increased the size of the valence basis set in the d space from five primitive Gaussian functions to six in order to improve the description of the valence d orbital. Both non-relativistic and scalar-relativistic iMCPs were made for each transition metal atom. This allows for the study of relativistic effects on the structures and frequencies of transition metal compounds.

In this chapter, the focus is less on the testing of the iMCPs against the previous (sMCP) version of the potentials, but instead on the study of the effect of changing DFT functionals and grid sizes on the molecular calculations.

3.2 Determination of Potentials and Basis Sets

The notation used here follows that of Section 2.3. Only the aspects of the parameterization and development of the iMCPs that differ are shown here. State-averaged atomic calculations were done using the program of Froese-Fischer [8] for the $(n+1)s^1nd^{k+1}$ configuration, except for Cd and Hg where the ground-state $(n+1)s^2nd^{10}$ configuration was used. Most of the second- and third-row transition metals have a $(n+1)s^2nd^k$ ground state (although some are $(n+1)s^1nd^{k+1}$, and Pd is $5s^04d^{10}$) [9],

Table 3.1: Partitioning of core and valence electrons and size of basis sets

Atom	Valence Electrons	Core Electrons	Valence Basis Sets	Core Basis Sets
Y	4p ⁶ 5s ¹ 4d ²	[Ar] 4s ² 3d ¹⁰	(6s/5p/6d)	(11,14,17,20/14,15/15)
Zr	4p ⁶ 5s ¹ 4d ³	[Ar] 4s ² 3d ¹⁰	(6s/5p/6d)	(11,14,17,20/12,15/17)
Nb	4p ⁶ 5s ¹ 4d ⁴	[Ar] 4s ² 3d ¹⁰	(6s/5p/6d)	(11,14,17,20/12,15/15)
Mo	4p ⁶ 5s ¹ 4d ⁵	[Ar] 4s ² 3d ¹⁰	(6s/5p/6d)	(13,14,17,20/14,15/15)
Tc	4p ⁶ 5s ¹ 4d ⁶	[Ar] 4s ² 3d ¹⁰	(6s/5p/6d)	(12,15,17,20/13,14/15)
Ru	4p ⁶ 5s ¹ 4d ⁷	[Ar] 4s ² 3d ¹⁰	(6s/5p/6d)	(12,15,18,20/12,16/14)
Rh	4p ⁶ 5s ¹ 4d ⁸	[Ar] 4s ² 3d ¹⁰	(6s/5p/6d)	(12,15,18,20/12,16/15)
Pd	4p ⁶ 5s ¹ 4d ⁹	[Ar] 4s ² 3d ¹⁰	(6s/5p/6d)	(12,15,17,20/12,14/14)
Ag	4p ⁶ 5s ¹ 4d ¹⁰	[Ar] 4s ² 3d ¹⁰	(6s/5p/6d)	(12,14,17,20/14,15/13)
Cd	4p ⁶ 5s ² 4d ¹⁰	[Ar] 4s ² 3d ¹⁰	(6s/5p/6d)	(12,16,17,20/13,15/13)
Hf	5p ⁶ 6s ¹ 5d ³	[Kr] 5s ² 4d ¹⁰	(7s/6p/6d)	(11,14,16,18,20/11,13,16/13,16/12)
Ta	5p ⁶ 6s ¹ 5d ⁴	[Kr] 5s ² 4d ¹⁰	(7s/6p/6d)	(10,13,15,20,20/13,15,16/12,15/12)
W	5p ⁶ 6s ¹ 5d ⁵	[Kr] 5s ² 4d ¹⁰	(7s/6p/6d)	(11,14,16,19,20/12,14,18/13,16/12)
Re	5p ⁶ 6s ¹ 5d ⁶	[Kr] 5s ² 4d ¹⁰	(7s/6p/6d)	(10,13,15,18,20/12,14,18/13,16/12)
Os	5p ⁶ 6s ¹ 5d ⁷	[Kr] 5s ² 4d ¹⁰	(7s/6p/6d)	(10,13,15,18,20/12,14,18/13,16/12)
Ir	5p ⁶ 6s ¹ 5d ⁸	[Kr] 5s ² 4d ¹⁰	(7s/6p/6d)	(10,13,15,18,20/12,14,18/13,16/12)
Pt	5p ⁶ 6s ¹ 5d ⁹	[Kr] 5s ² 4d ¹⁰	(7s/6p/6d)	(10,13,15,18,20/12,14,18/13,16/12)
Au	5p ⁶ 6s ¹ 5d ¹⁰	[Kr] 5s ² 4d ¹⁰	(7s/6p/6d)	(10,13,15,18,20/12,14,18/13,18/12)
Hg	5p ⁶ 6s ² 5d ¹⁰	[Kr] 5s ² 4d ¹⁰	(7s/6p/6d)	(11,14,16,19,20/12,14,18/13,16/13)

$$[\text{Ar}] = 1s^2 2s^2 2p^6 3s^2 3p^6; [\text{Kr}] = 1s^2 2s^2 2p^6 3s^2 3p^6 4s^2 3d^{10} 4p^6$$

but the orbitals obtained from the states of the s² configuration are too compact to properly describe the more diffuse orbitals required in molecular environments [4].

The core reference orbitals (from the numerical calculations) were represented by a sum of Gaussian functions, with the exponents taken from the well-tempered basis sets [10] of Huzinaga *et al.* and coefficients determined by least-squares fitting. The actual size of the core basis sets was chosen by means of a cutoff of the expansion coefficient in the sum (2×10^{-5}), so the sizes are not constant from atom to atom. The size of the core basis sets is shown in Table 3.1. In all cases, the penultimate p orbital (4p or 5p for second- and third-row atoms, respectively) was considered a valence orbital. No large-core iMCPs were developed.

One of the desired qualities of the iMCPs is that the valence basis sets remain

quite small, as they are intended for use in larger transition metal clusters. A new set of MCPs, the wtMCPs, is being developed for very accurate calculations on smaller systems (see Chapters 5 - 7). A set of six d Gaussian primitives was chosen to expand the d orbitals for all of the transition metals, as it allows us to represent the outer lobe of either the 4d and 5d orbitals with four primitive Gaussians, while two primitive Gaussians are used for the description of the inner part of the valence d orbital. To represent the s and p spaces, a number of primitives was chosen equal to one greater than the principal quantum number of the shell. This yields an expansion for the gold atom of seven s (to describe the 6s orbital), six p (to describe the 5p orbital), and six d (to describe the 5d orbital) primitive functions. The exponents were determined by a least-squares fit to the reference valence orbitals.

As was done previously [1], by varying the f_{proj} parameter (Eqn. (1.77)), the potentials were scaled to reproduce non-relativistic all-electron Hartree-Fock results. The potentials were calibrated in molecular calculations for molecules in the training set, which generally contained one molecule for each transition metal (Table 3.2), against a modified version of the all-electron well-tempered basis set [10]. The same type of basis set contraction as in Chapter 2 was used for the reference calculations. The parameters were reoptimized in order to find the optimum value of f_{proj} as was done previously, but it should be noted that the values here were fit in molecular calculations to just one (or two in the case of Cd) molecule(s) in the training set, as opposed to 3 - 5 as was done for the first-row transition metals. The work done in Chapter 2 showed that the same value of f_{proj} worked best for several molecules in the training set, so it was decided that only one molecule in the training set per atom would be necessary. Again, we assumed transferability of the f_{proj} values to the scalar-relativistic and correlated cases. This error is expected to be small in comparison to the other errors introduced by a small valence basis set and an approximate DFT functional.

A set of two p and one f polarization functions was derived for the transition metals, with the set of the two p functions fit to the valence s orbital, and the f function fit to the valence d orbital. The iMCP parameters and valence basis set obtained for the Au atom are shown in Tables 3.3 and 3.4, respectively. The complete

set of parameters and basis sets is available as a preprint.

Table 3.2: Molecules included in training and test sets

Training Set	Test Set
YO, ZrN, NbN, MoO ₂ , TcO, RuCO ⁻ , RhC, PdCO, AgH, CdH, CdH ⁺ , HfF ₄ , TaO, WF ₆ , ReClO ₃ , OsO ₄ , IrC, PtC, AuH, HgCl ₂	YF, ZrF ₄ , ZrCl ₄ , Mo(CO) ₆ , Ag(N ₃) ₄ ⁻ , Cd(CH ₃) ₂ , HfF ₄ , HfCl ₄ , TaO ₃ ⁻ , W(CO) ₆ , ReO ₄ ⁻ , OsO ₄ , Ir(CO) ₂ ⁻ , Pt(O ₂), Au(N ₃) ₄ ⁻ , Hg(CH ₃) ₂

Table 3.3: Non-relativistic iMCP potential parameters for Au atom ($f_{proj}=1.3$)

	n=0			n=1		
A	1.7448436	0.8142287	0.0429711	614.48760	13.936815	0.5025112
α	120.07499	4.6399712	0.7444906	11620.269	61.851708	5.6955606

Table 3.4: Non-relativistic iMCP valence basis set for Au atom ($f_{proj}=1.3$)

Type	Exponent	Contraction coefficient
s	1322.738265	-0.009858
	132.700310	0.046979
	23.325589	-0.146807
	5.740453	0.282221
	0.851791	-0.512233
	0.074502	0.739994
	0.028186	0.377788
p	989.799389	-0.022348
	277.084038	-0.073113
	39.873908	0.267072
	7.199227	-0.602480
	1.259409	0.832087
	0.468605	0.304490
d	104.996651	0.105633
	9.324712	-0.276093
	1.393626	0.504102
	0.528742	0.454296
	0.201643	0.208445
	0.078376	0.024862
p*	0.101	1.0
	0.031	1.0
f*	1.031	1.0

3.3 Computational Methods

Most calculations were done using CADPAC [11] except for the all-electron reference calculations which were done with the GAMESS program [12]. Calculations were done at the restricted Hartree-Fock (RHF) as well as at the density functional theory (DFT) level using the gradient-corrected BLYP [13, 14] and hybrid B3LYP [14, 15, 16] functionals. All structures were optimized using analytic gradients. Harmonic vibrational analysis was performed using analytic second derivatives whenever possible, but when software limitations prevented their use, second derivatives were calculated numerically using a two-point differencing of analytical gradients with the default step size ($0.001 a_0$). Cartesian Gaussian functions were used in the MCP calculations, spherical Gaussians in the all-electron ones.

3.4 Results and Discussion

An initial indication of the quality of the iMCPs is the appearance of the orbitals as compared to the reference orbitals. Figures 3.1 and 3.2 show how the non-relativistic iMCPs represent the highest three (3s, 4s, and 5s) s-type core orbitals and valence orbitals (6s, 5p, and 5d) for the Au atom, shown as the difference between the reference (numerical) orbital and the MCP orbital (note the logarithmic scale of the abscissa). The higher core orbitals (such as the 5s) have a smaller error than the deep core orbitals (such as the 3s). For the series 3s to 5s, the mean absolute error in the fitted versus the reference function drops by a factor of 2 from the 3s to the 4s, and another factor of two from the 4s to the 5s. Much of this is due to the greater magnitude of the 3s orbital near the nucleus where most of the error occurs. The error in the orbitals decreases as r increases, indicating a better fit in the outer core region, which should have the greatest effect on the valence orbitals. The initially large error in the 3s orbital has been greatly decreased by $r=0.01 a_0$, and by about $0.1 a_0$ the errors in all core orbitals are essentially the same. If we look at the valence orbitals, we see that the error has increased by an order of magnitude with respect to the reference functions. This is to be expected due to the small valence basis set we are using. All of the valence orbitals show a poorer fit in the core region, in particular

the 5d orbital. The errors in the 6s and 5p orbitals decrease faster than that for the 5d orbital, but are all approximately equal by about $r=0.5 a_0$, which is still well into the core region of the Au atom. The atomic calculations give the expectation value of r for the 5d orbital to be about $1.55 a_0$, and the maximum of the 5d orbital (for both the reference function and the iMCP orbital) lies at about $1.2 a_0$.

In order to test the reliability of the iMCPs (and, indirectly, their transferability), a total of 16 second- and third-row transition metal compounds were used as a test set (Table 3.2), covering all of the transition metal groups. A selected set of structural parameters is shown in Table 3.5. In general, the DFT functionals used provide a good description of the bond lengths in these compounds. The B3LYP functional gives calculated bond lengths that are slightly better than the BLYP functional, with the absolute error in bond lengths reduced by approximately 25%. The relativistic effects bring the calculated bond lengths closer to the experimental values in almost all cases, reducing the absolute error in the bond lengths by about 45%. The bond angles are fairly well reproduced at the DFT level as well, but are generally slightly too large.

Harmonic vibrational frequencies were also determined for these complexes, and a selected set is shown in Tables 3.6 and 3.7. Again, the addition of relativistic effects is quite important, reducing the error with respect to experiment by about 25%. The BLYP functional is better at predicting the vibrational frequencies. Much of this difference, however, can be attributed to the C-H stretching frequencies in dimethylcadmium, which the B3LYP functional badly overestimates. If these frequencies are removed, then the difference between the two functionals is reduced to just a few percent.

Figure 3.1: Deviation between iMCP and reference Au core orbitals (3s, 4s, 5s)

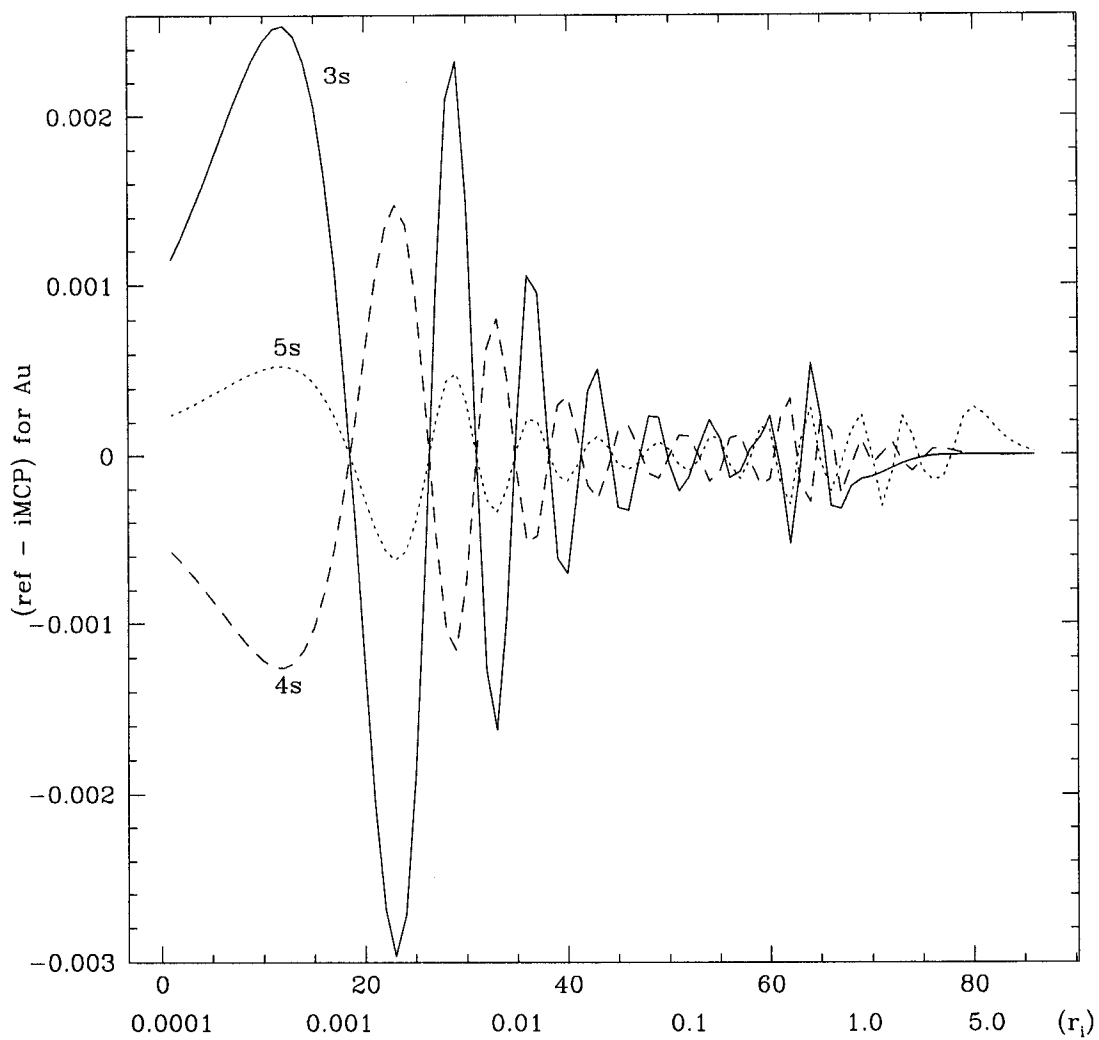


Figure 3.2: Deviation between iMCP and reference Au valence orbitals (6s, 5p, 5d)

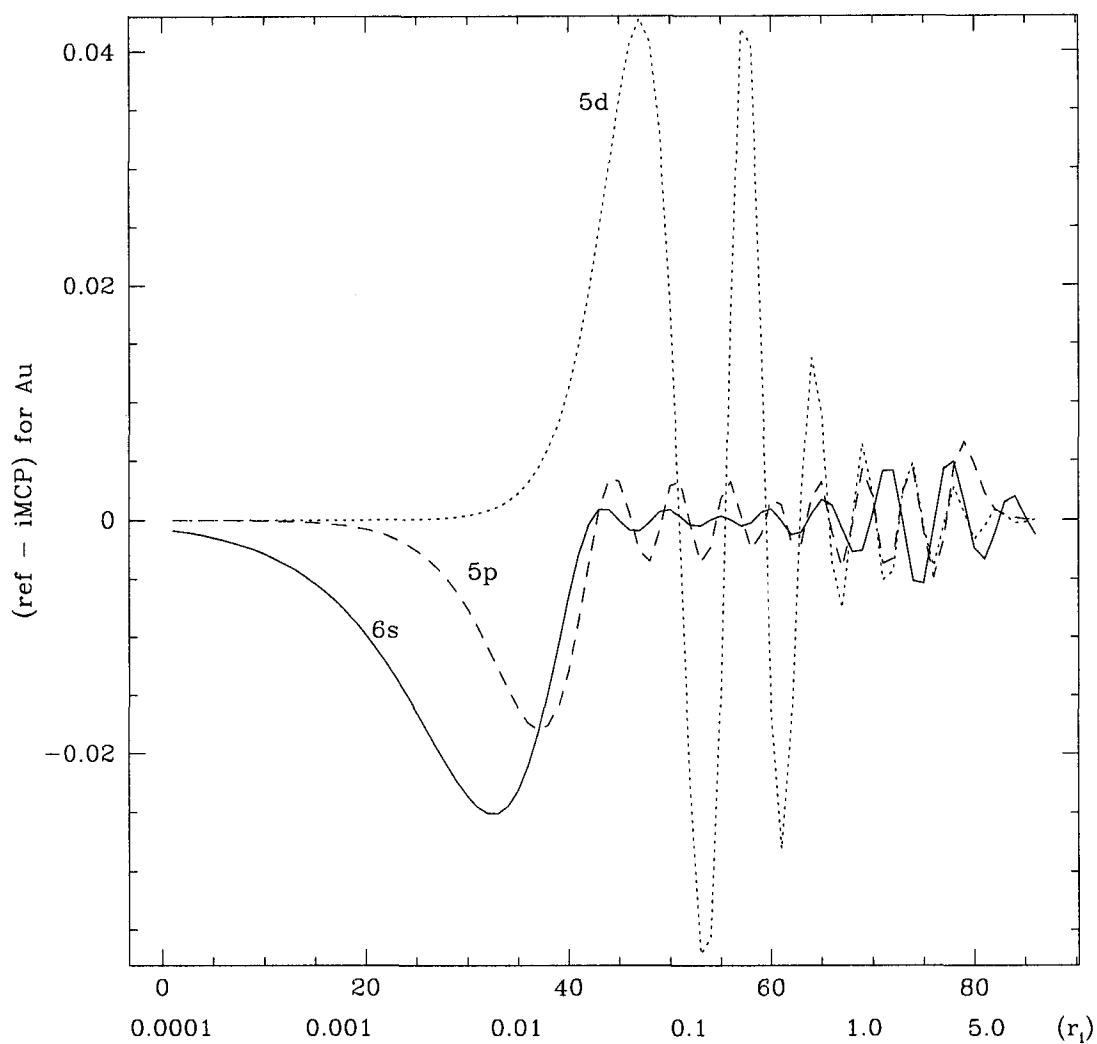


Table 3.5: Structural parameters for selected transition metal complexes^a

Compound	Symmetry	Parameter	BLYP		B3LYP		Exp.
			NR	SR	NR	SR	
YF	C_{4v}	r(Y-F)	1.904	1.915	1.907	1.914	1.926 ^b
ZrCl ₄	T_d	r(Zr-Cl)	2.327	2.324	2.322	2.321	2.32 ^c
HfF ₄	T_d	r(Hf-F)	1.926	1.903	1.916	1.895	1.89 ^d
Mo(CO) ₆	O_h	r(Mo-C)	2.067	2.056	2.069	2.057	2.063 ^e
		r(C-O)	1.149	1.150	1.137	1.138	1.145
Au(N ₃) ₄ ⁻	C_{4h}	r(Au-N1)	2.213	2.127	2.191	2.093	2.03 ^f
		r(N1-N2)	1.217	1.224	1.206	1.212	1.22
		r(N2-N3)	1.165	1.160	1.148	1.143	1.15
		<(Au-N1-N2)	117.3	117.2	116.8	117.3	116
		<(N1-N2-N3) ^g	175.5	173.8	176.2	174.6	172
OsO ₄	T_d	r(Os-O)	1.776	1.734	1.752	1.713	1.711 ^h
Cd(CH ₃) ₂	D_{3h}	r(Cd-C)	2.195	2.157	2.182	2.141	2.112 ⁱ
		r(C-H)	1.098	1.098	1.093	1.093	1.09
		<(Cd-C-H)	110.2	109.8	110.5	110.1	108.4

^{a)} Bond lengths in Å, angles in degrees ^{b)} [17] ^{c)} [18] ^{d)} [19] ^{e)} [20] ^{f)} [21]

^{g)} Dihedral Au-N1-N2-N3 is 180° ^{h)} [22] ⁱ⁾ [23]

All of the preceding calculations were performed with the standard “MEDIUM” grid in CADPAC. To test the effect of grid size on the calculations, several complexes were studied using the “HIGH” grid size. The results can be seen in Table 3.8. For the lightest complex studied (ZrF₄), very little effect was seen, just a slight shrinking in the bond length in the non-relativistic case, and a resulting small increase in the stretching frequencies. For the third-row complexes, different behavior emerged. For HfF₄, a pronounced shrinking of the bond length is seen at the non-relativistic level, resulting in a fairly large increase in the stretching frequencies. At the scalar-relativistic level, essentially no change in the bond length is observed. In fact, with the high grid, all relativistic contraction has disappeared, and the bond length in the non-relativistic case is actually shorter. For dimethylmercury, the opposite effect is observed. Again there is essentially no change in the bond lengths at the scalar-relativistic level, but now there is a bond lengthening when the non-relativistic potential is used. Interestingly, when the medium grid is used, there is an imaginary frequency (ω_4), indicating that the eclipsed D_{3h} conformer is not a minimum

Table 3.6: Vibrational frequencies (in cm^{-1}) for selected transition metal complexes

Compound	Symmetry	Vibration	BLYP		B3LYP		Exp.
			NR	SR	NR	SR	
ZrF ₄	T _d	$\omega_1(A_1)$	605	621	634	647	600 ^a
		$\omega_2(E)$	152	156	154	158	150
		$\omega_3(T_2)$	608	625	635	650	668
		$\omega_4(T_2)$	155	158	161	164	190
HfF ₄	T _d	$\omega_1(A_1)$	617	650	649	675	677 ^b
		$\omega_2(E)$	162	182	164	183	173
		$\omega_3(T_2)$	590	623	614	645	650
		$\omega_4(T_2)$	155	166	158	169	164
W(CO) ₆	O _h	$\omega_1(A_{1g})$	2059	2058	2166	2166	2126 ^c
		$\omega_2(A_{1g})$	384	412	386	418	426
		$\omega_3(E_g)$	1967	1962	2073	2066	2021
		$\omega_4(E_g)$	365	395	368	401	410
		$\omega_5(T_{1g})$	301	333	268	302	362
		$\omega_6(T_{1u})$	1942	1933	2049	2036	1998
		$\omega_7(T_{1u})$	318	336	327	350	374
		$\omega_8(T_{1u})$	567	587	555	582	587
		$\omega_9(T_{1u})$	76	83	78	86	82
		$\omega_{10}(T_{2g})$	457	471	471	489	482
		$\omega_{11}(T_{2g})$	75	82	68	73	81
		$\omega_{12}(T_{2u})$	514	523	524	539	521
		$\omega_{13}(T_{2u})$	57	60	60	63	61
TaO ₃ ⁻	C _{3v}	$\omega_1(A_1)$	841	884	860	894	
		$\omega_2(A_1)$	228	273	186	245	
		$\omega_3(E)$	752	784	737	767	807 ^d
		$\omega_4(E)$	282	316	270	310	

a) [24] b) [25] c) [26] d) [27]

Table 3.7: Vibrational frequencies (in cm^{-1}) for selected transition metal complexes

Compound	Symmetry	Vibration	BLYP		B3LYP		Exp.
			NR	SR	NR	SR	
OsO ₄	T _d	$\omega_1(A_1)$	850	908	921	967	965 ^a
		$\omega_2(E)$	285	314	302	328	333
		$\omega_3(T_2)$	824	879	830	876	960
		$\omega_4(T_2)$	288	307	275	292	323
Pt(O ₂)	C _{2v}	$\omega_1(A_1)$	203	475	198	491	
		$\omega_2(A_1)$	1003	900	1164	1001	928 ^b
		$\omega_3(B_2)$	353	489	342	493	
Cd(CH ₃) ₂	D _{3h}	$\omega_1(A'_1)$	2945	2950	3020	3025	2903 ^c
		$\omega_2(A'_1)$	1118	1133	1157	1173	1127
		$\omega_3(A'_1)$	393	406	415	433	459
		$\omega_4(A''_1)$	74 _i	74 _i	69 _i	69 _i	
		$\omega_5(A''_2)$	2957	2962	3030	3034	2923
		$\omega_6(A''_2)$	1137	1150	1174	1189	1136
		$\omega_7(A''_2)$	457	473	477	497	535
		$\omega_8(E')$	3036	3044	3110	3117	2980
		$\omega_9(E')$	1430	1430	1463	1464	1315
		$\omega_{10}(E')$	688	724	697	733	700
		$\omega_{11}(E')$	111	120	114	122	124
		$\omega_{12}(E'')$	3030	3038	3105	3112	2859
		$\omega_{13}(E'')$	1448	1448	1479	1480	1427
		$\omega_{14}(E'')$	614	648	623	655	634

a) [28] b) [29] c) [30]

on the potential energy surface. When the high-accuracy grid is used, the imaginary frequency becomes much smaller in the non-relativistic case (perhaps simply due to incomplete geometry optimization), whereas in the scalar-relativistic case the torsional frequency becomes real, indicating that this conformer is indeed a minimum on the potential energy hypersurface. It is somewhat worrisome that the chemistry could change as a result of a change in the integration grid, as both grids give a very accurate integrated electron density. Even with the medium grid, the error in integrated electron density is no more than 3×10^{-5} electrons. Therefore, we recommend the use of the more accurate grid in CADPAC whenever calculations are done on the heaviest (third-row) transition metal complexes, especially if the calculations use the non-relativistic potentials.

Table 3.8: Structural parameters and vibrational frequencies calculated using different DFT grids^{a,b}

Compound	Symmetry	Vibration	NR med	NR high	SR med	SR high
ZrF ₄	T _d	r(Zr-F)	1.907	1.901	1.904	1.905
		$\omega_1(A_1)$	634	646	647	638
		$\omega_2(E)$	154	159	158	157
		$\omega_3(T_2)$	635	657	650	647
		$\omega_4(T_2)$	161	167	164	161
HfF ₄	T _d	r(Hf-F)	1.916	1.892	1.895	1.896
		$\omega_1(A_1)$	649	683	675	670
		$\omega_2(E)$	164	186	183	181
		$\omega_3(T_2)$	614	649	645	642
		$\omega_4(T_2)$	158	180	169	168
Hg(CH ₃) ₂	D _{3h}	r(Hg-C)	2.281	2.290	2.160	2.159
		r(C-H)	1.093	1.093	1.093	1.093
		<(Hg-C-H)	110.3	110.4	110.0	110.0
		$\omega_1(A'_1)$	3025	3031	3028	3036
		$\omega_2(A'_1)$	1148	1154	1194	1205
		$\omega_3(A'_1)$	404	435	431	444
		$\omega_4(A''_1)$	68i	10i	66i	27
		$\omega_5(A''_2)$	3034	3034	3038	3038
		$\omega_6(A''_2)$	1163	1160	1208	1208
		$\omega_7(A''_2)$	411	405	435	478
		$\omega_8(E')$	3117	3112	3123	3120
		$\omega_9(E')$	1462	1468	1464	1470
		$\omega_{10}(E')$	689	683	770	773
		$\omega_{11}(E')$	98	100	127	136
$\omega_{12}(E'')$	3112	3112	3118	3120		
$\omega_{13}(E'')$	1477	1471	1479	1474		
$\omega_{14}(E'')$	621	617	686	687		

^{a)} Bond lengths in Å, angles in degrees, frequencies in cm⁻¹

^{b)} All calculations performed using the B3LYP functional.

3.5 Conclusions

The new iMCPs can be used to give semiquantitative agreement with experimental data for the second and third-row transition metal complexes with accuracy comparable to that of our previous work on the first-row transition metals. Through the use of both the non- and scalar-relativistic potentials, the effect of the scalar relativistic corrections on the structures and spectra of transition metal complexes can be determined. The differences between the two functionals used are minor, and although the B3LYP functional tends to give slightly more accurate bond lengths with respect to experiment, the bond angles and vibrational frequencies are more accurate when the BLYP functional is used. We conclude that neither is clearly more suitable for the accurate calculation of structural parameters or vibrational frequencies of heavier transition metal compounds. Increasing the grid size for the DFT integration can have a fairly large effect for the larger atoms, especially when the non-relativistic potentials are used.

Bibliography

- [1] C. C. Lovallo and M. Klobukowski *J. Comput. Chem.* **24** (2003) 1009.
- [2] G. Frenking, I. Antes, M. Böhme, S. Dapprich, A. W. Ehlers, V. Jonas, A. Neuhaus, M. Otto, R. Stegmann, A. Veldkamp, and S.F. Vyboishchikov in *Reviews in Computational Chemistry Vol. 8* VCH: New York, 1996; Chapter 2.
- [3] T. R. Cundari, M. T. Benson, M. Leigh Lutz, and S. O. Sommerer in *Reviews in Computational Chemistry Vol. 8* VCH: New York, 1996; Chapter 3.
- [4] Y. Sakai, E. Miyoshi, M. Klobukowski, and S. Huzinaga *J. Comput. Chem.* **8** (1987) 226.
- [5] Y. Sakai, E. Miyoshi, M. Klobukowski, and S. Huzinaga, *J. Comput. Chem.* **8** (1987) 256.
- [6] W. J. Hehre, R. F. Stewart, and J. A. Pople *J. Chem. Phys.* **51** (1967) 2657.
- [7] J. A. Pople and W. J. Hehre *J. Comput. Phys.* **27** (1978) 161.
- [8] C. Froese-Fischer *Comp. Phys. Comm.* **4** (1972) 107.
- [9] W. C. Martin, A. Musgrove, and S. Kotochigova “Ground Levels and Ionization Energies for the Neutral Atoms” (Web Version 1.2.2), [Online]. Available: <http://physics.nist.gov/IonEnergy> [2003, September 24]. National Institute of Standards and Technology, Gaithersburg, MD.
- [10] S. Huzinaga and M. Klobukowski *Chem. Phys. Lett.* **212** (1993) 260.

- [11] CADPAC version 6.3: The Cambridge Analytic Derivatives Package Issue 6, Cambridge, 1995. A suite of quantum chemistry programs developed by R. D. Amos with contributions from I. L. Alberts, J. S. Andrews, S. M. Colwell, N. C. Handy, D. Jayatilaka, P. J. Knowles, R. Kobayashi, K. E. Laidig, G. Laming, A. M. Lee, P. E. Maslen, C. W. Murray, J. E. Rice, E. D. Simandiras, A. J. Stone, M.-D. Su, and D. J. Tozer.
- [12] M. W. Schmidt, K. K. Baldridge, J. A. Boatz, S. T. Elbert, M. S. Gordon, J. J. Jensen, S. Koseki, N. Matsunaga, K. A. Nguyen, S. Su, T. L. Windus, M. Dupuis, and J. A. Montgomery, *J. Comput. Chem.* **14** (1993) 1347.
- [13] A. D. Becke *Phys. Rev. A* **38** (1988) 3098.
- [14] C. Lee, W. Yang, and R. G. Parr *Phys. Rev. B* **37** (1988) 785.
- [15] A. D. Becke *J. Chem. Phys.* **98** (1993) 5648.
- [16] P. J. Stephens, F. J. Devlin, C. F. Chabalowski, and M. J. Frisch *J. Chem. Phys.* **98** (1994) 11623.
- [17] K. P. Huber and G. Herzberg *Constants of Diatomic Molecules* (data prepared by J.W. Gallagher and R.D. Johnson, III) in NIST Chemistry WebBook, NIST Standard Reference Database Number 69, Eds. P.J. Linstrom and W.G. Mallard, March 2003, National Institute of Standards and Technology, Gaithersburg MD, 20899 (<http://webbook.nist.gov>).
- [18] V. P. Spiridonov, P. A. Akishin, V. I. Tsirel'nikov *J. Struct. Chem. (USSR)* **3** (1962) 311.
- [19] G. V. Girichev, N. I. Giricheva, and T. N. Malysheva *Russ. J. Phys. Chem.* **56** (1982) 1120.
- [20] B. Beagley and D. G. Schmidling *J. Mol. Struct.* **22** (1974) 466.
- [21] W. Beck, T. M. Klapötke, P. Klüfers, G. Kramer, and C. M. Rienäcker *Z. Anorg. Allg. Chem.* **627** (2001) 1669.

- [22] B. Krebs and K. D. Hasse *Acta Crystallogr. B* **32** (1976) 1334.
- [23] K. S. Rao, B. P. Stoicheff, and R. Turner *Can. J. Phys.* **38** (1960) 1516.
- [24] A. Buchler, J. B. Berkowitz-Mattuck, and D. H. Dugre *J. Chem. Phys.* **34** (1961) 2202.
- [25] V. N. Bukhmarina, S. L. Dobyichin, Y. B. Predtechenskii, and V. G. Shklyarik *Russ. J. Phys. Chem.* **60** (1986) 1062.
- [26] L. H. Jones, R. S. McDowell, and M. Goldblatt *Inorg. Chem.* **8** (1969) 2349.
- [27] M. Zhou and L. J. Andrews *J. Phys. Chem. A* **102** (1998) 8251.
- [28] R. S. McDowell and M. Goldblatt *Inorg. Chem.* **10** (1971) 625.
- [29] W. D. Bare, A. Citra, G. V. Chertihin, and L. J. Andrews *J. Phys. Chem. A* **103** (1999) 5456.
- [30] T. J. Shimanouchi *J. Phys. Chem. Ref. Data* **6** (1977) 993.

Chapter 4

Application of the Improved Model Core Potentials to the Thermochemistry of Organoxenon Complexes*

4.1 Introduction

Since the synthesis of the first xenon compound, XeF₂, independently by Bartlett *et al.* [1] and Hoppe *et al.* [2] in 1962 and the synthesis of XeF₄ at Argonne in the same year [3], various other compounds containing xenon bonded to boron, nitrogen, oxygen, fluorine, and chlorine have been synthesized [4, 5, 6]. A binding energy of 43±8 kcal/mol was estimated for the XeCH₃⁺ system as early as 1971 [7]. A more recent study by Hovey and McMahon [8] revised this value to 55 kcal/mol. Although the existence of the first compound with a xenon-carbon bond, Xe(CF₃)₂, was inferred from an infrared spectrum by Lagow *et al.* [9] in 1979, the first structural characterization of a compound with a xenon-carbon bond, the pentafluorophenylxenon(II) cation, was done by Frohn *et al.* via ¹⁹F and ¹²⁹Xe NMR spectroscopy [10] and X-ray crystallography [11] and independently by Naumann *et al.* via ¹⁹F and ¹²⁹Xe NMR [12]. Over the next decade, two major types of cations with a xenon-carbon bond were synthesized: (a) with xenon bonded to a phenyl group substituted with electron-withdrawing substituents [13, 14], and (b) with xenon bonded to a substi-

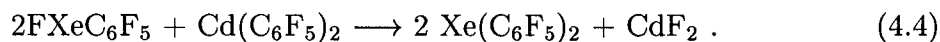
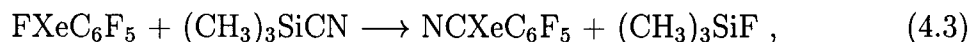
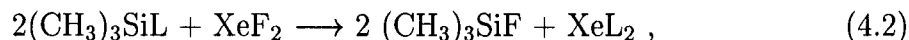
*A version of this chapter was published as: C. C. Lovallo and M. Klobukowski *Int. J. Quant. Chem.* **90** (2002) 1099.

tuted acetylene unit. Using unsubstituted acetylene, Zhdankin *et al.* [15] were unable to synthesize XeCCH^+ , although the related compound ArCCH^+ was predicted to be stable by Frenking *et al.* [16] Mixed two-ligand systems, where there is only one xenon-carbon bond, have also been synthesized [17, 18].

Even though both Frohn *et al.* [19] and Maggiorosa *et al.* [20] have synthesized neutral compounds containing two xenon-carbon covalent bonds, there are still relatively few such systems reported in the literature [21]. There have also been several reports of compounds containing xenon(IV)-carbon bonds [22, 23]. This relative paucity of systems with Xe-C bonds and a lack of computational studies in the area, together with a veritable renaissance of xenon chemistry [21, 24] in recent years, was the motivation of the present study that aimed at elucidating the relative stability of the molecules involved in the reactions leading to xenon-carbon bonds.

Compounds with two xenon-carbon bonds are formed in two steps, with the two fluorides in XeF_2 substituted, one at a time, with the desired ligands via a ligand exchange reaction, typically using substituted trimethylsilanes. To substitute the second ligand, a second equivalent of the silane can be used (or possibly another substituted silane, if a mixed-ligand compound is desired), or another ligand exchange agent can be used. For example, bis(pentafluorophenyl)cadmium can be used as a pentafluorophenylating agent.

In the present work, the energetics of these reactions were studied at the RHF and DFT (B3PW91 and B3LYP) levels to determine which reactions were energetically feasible. The following reactions were studied:



where $\text{L} = \text{CN}, \text{CCH}, \text{CCF}, \text{C}_6\text{H}_5, \text{C}_6\text{F}_5, \text{CF}_3,$ and CH_3 . Reactions (4.3) and (4.4) were studied in order to clear up a question in the literature: Frohn and Theißen [19]

were unable to react FXeC_6F_5 with $(\text{CH}_3)_3\text{SiC}_6\text{F}_5$ to obtain the bis-substituted xenon complex, so they used the cadmium complex as an arylating agent. However, Maggiorosa *et al.* [20] claimed that not only was that reaction possible, but they found it impossible to obtain pure FXeC_6F_5 , because it always contained some $\text{Xe}(\text{C}_6\text{F}_5)_2$. Frohn and Theißen [19] also carried out reaction (4.3), obtaining the first xenon compound with two xenon-carbon bonds to different ligands.

4.2 Computational Methods

In order to simplify our calculations on these systems which contain many chemically inert core electrons, we used the Model Core Potential (MCP) formalism, developed by Huzinaga and coworkers [25]. For more details on the method and the notation used, see Section 2.3. All calculations were done using the recently created new, improved parameterizations of the MCPs (iMCPs). The new L-shell structure of the iMCPs can lead to considerable speedups in integral evaluation; a test calculation on a segment of the solid neon lattice showed an accelerated integral evaluation of more than twofold when compared to the previous MCPs that did not have the advantage of L-shells.

In order to prepare atomic reference data, numerical Hartree-Fock [26] calculations were performed on the state-averaged energy for the ground-state electron configuration of the main-group elements. Up to twenty exponents from the well-tempered basis sets [27] were taken for each core orbital $\bar{\phi}_c$ (1s for C, N, and F, 1s - 4p for Xe). The 4d orbitals for xenon were also treated as valence orbitals, and were represented by six functions. In addition, two d and one f polarization functions were prepared as described in the previous chapters. For the first row elements, two terms with $n_l=0$ were fitted, leading to two A_l and two α_l parameters. For xenon, three terms with $n_l=0$ and three terms with $n_l=1$ were fitted, leading to six A_l and six α_l parameters. Scaling of the f_{proj} parameter can affect the hardness of the potential. The value of f_{proj} for the first-row elements was taken to be 2.0; for xenon, the value of f_{proj} was obtained by scaling to replicate all-electron *ab initio* molecular geometries calculated at the restricted Hartree-Fock level as described previously. The iMCP geometries

most closely reproduced the all-electron ones for $f_{proj} = 2.5$, the same RHF value of f_{proj} was used for the DFT calculations.

The pseudopotential methods can easily reproduce some relativistic effects if these effects are included in the reference core functions as well as the valence orbitals and orbital energies, and consequently will be reflected in the values of the MCP parameters. Scalar-relativistic (SR) numerical calculations (incorporating the Darwin and mass-velocity terms) were performed [26], and SR iMCPs were developed for the elements used here. The difference between the non-relativistic (NR) and SR iMCPs is negligible for the first-row elements, so the NR pseudopotentials were used. For xenon, the SR potential was used.

All calculations were done with CADPAC [28] except for the PCM solvent calculations which were done with the GAMESS program [29]. All structures were optimized using analytical gradients. Harmonic vibrational analysis was performed for all species using analytical second derivatives whenever possible. Whenever software limitations prevented the use of analytical second derivatives, second derivatives were calculated numerically, using a two-point difference model with the default step size ($0.001 a_0$ for RHF and DFT calculations, $0.002 a_0$ for MP2). Calculations were done at the RHF, MP2 [30] (where possible) as well as at the DFT levels using two hybrid functionals: B3LYP [31, 32, 33] and B3PW91 [31]. All valence electrons were correlated in the MP2 calculations using the full orbital space. Cartesian Gaussian functions were used in iMCP calculations, spherical Gaussians in the all-electron ones.

4.3 Results and Discussion

As an initial test of the pseudopotentials, the adiabatic ionization energies of Xe and the methyl radical were calculated as the difference between the energies of the neutral species and the cations. The basis set used (Basis A) contained the s and p spaces of all atoms contracted to triple zeta, while the d space of xenon was fully contracted. In addition, one d polarization function was added to all atoms resulting in a basis set of (511/511/61*) for xenon and (311/311/1*) for the first-row atoms. For hydrogen, the 6-311G(p) [34] basis set was used in Basis A. An extended basis

set, Basis B, was also employed in order to study the effect of polarization space. In Basis B, two d and one f polarization functions were included on xenon and carbon leading to a basis set of (511/511/61*1*/1*) on xenon and (311/311/1*1*/1*) on carbon; the hydrogen basis set was expanded to 6-311G(2pd).

The structural parameters of CH_3 , CH_3^+ , and XeCH_3^+ were calculated at the B3LYP level using the two iMCP basis sets, as well as the well-tempered basis set [27] with polarization functions from basis set A or B. The results, collected in Table 4.1, show that the agreement between the iMCP and WTBS results is very good, with the largest error being 0.024 Å for the Xe-C bond length.

Table 4.1: Structural parameters of CH_3 , CH_3^+ , and XeCH_3^+ ^{a,b}

Molecule	Parameter	iMCP	WTBS	Exp.
CH_3 (D_{3h})	C-H	1.081 (1.077)	1.080 (1.078)	1.0767 ^c
CH_3^+ (D_{3h})	C-H	1.091 (1.090)	1.093 (1.091)	1.095 ^d
XeCH_3^+ (C_{3v})	Xe-C	2.300 (2.288)	2.293 (2.264)	
	C-H	1.083 (1.080)	1.084 (1.080)	
	Xe-C-H	100.8 (100.4)	101.7 (101.7)	
	H-C-H	116.6 (116.8)	116.0 (116.0)	

^{a)} Bond lengths in Å, bond angles in degrees. ^{b)} Results for Basis B in parentheses. ^{c)} [35]. ^{d)} [36].

Table 4.2: Xe and CH_3 ionization energies and methyl cation affinity of Xe (eV).^a

Method	Xe IE	CH_3 IE	ΔH_{aff}	
RHF iMCP	11.6 (11.5)	9.0 (9.0)	0.47 (0.65)	
B3PW91 iMCP	12.5 (12.5)	9.9 (9.9)	1.49 (1.64)	
B3LYP	iMCP	12.4 (12.5)	9.7 (9.8)	1.43 (1.51)
	WTBS	12.4 (12.4)	9.9 (9.9)	1.44 (1.57)
MP2 iMCP	12.1 (12.4)	9.6 (9.7)	1.40 (1.76)	
Exp.	12.1 ^b	9.8 ^c	2.39 ^d	

^{a)} results for Basis B in parentheses. ^{b)} [37]. ^{c)} [38]. ^{d)} [8].

The ionization energies (Table 4.2) are in excellent agreement with experimental values. The methyl cation affinity of xenon, experimentally known to be 55 kcal/mol (2.4 eV) [8] was calculated as the enthalpy of the following reaction at 298K:



The results in Table 4.2 show that the calculated affinity is much too low. With Basis B, the ionization energies are essentially identical; the affinity value is closer to experiment, but it is still too low. Given the excellent results for the ionization energies with Basis A, and the lack of significant improvement in the cation affinity calculated with Basis B, Basis A was used for the remaining calculations, unless indicated otherwise. It should be noted that the results from all-electron calculations with the B3LYP functional are in very good agreement with the ones obtained using the iMCP method.

The iMCPs were further tested for the first-row elements. A number of small molecules with p electrons that could allow bonding to a xenon atom were studied at the RHF, MP2, and DFT levels. The results, shown in Table 4.3, demonstrate that the iMCPs reproduce the experimental geometries of these small molecules very well, especially at the correlated levels.

The bonding in these xenon compounds is similar to the bonding in the trihalides as described by Pimentel [39]. Two singly-occupied p orbitals, one from each of the two ligands, interact with a doubly-occupied p orbital on xenon to form three molecular orbitals: bonding, non-bonding, and anti-bonding, accommodating the four electrons; the bonding can be described as a three-centre four-electron bond. This σ overlap is also possible with s orbitals or sp^3 hybrids. However, π overlap is an additional important contributor to the bonding. This makes it unlikely that a compound without π orbitals on the ligands could bond covalently to a xenon atom, as borne out by calculations on the $\text{Xe}(\text{CF}_3)_2$ system. The calculated bond lengths are very long (over 2.4 Å at the DFT level with Basis A), and recent work in our lab [40] has shown that the IR spectrum measured by Lagow in 1979 [9] is not that of $\text{Xe}(\text{CF}_3)_2$. In fact, no organoxenon systems have been synthesized with xenon bonded to a saturated carbon; in all known systems the carbon bonded to the xenon also participates in either a double or triple bond with another carbon atom. Figures 4.1 and 4.2 show two of the occupied orbitals of $\text{Xe}(\text{C}_6\text{F}_5)_2$. Figure 4.1 shows

Table 4.3: Bond lengths (in Å) of molecules potentially found as xenon ligands

Molecule	Bond	RHF	B3PW91	B3LYP	MP2	Exp.
HF ($C_{\infty v}$)	H-F	0.9000	0.9225	0.9263	0.9170	0.9168 ^a
HCN ($C_{\infty v}$)	H-C	1.060	1.067	1.066	1.062	1.0626 ^b
	C-N	1.127	1.147	1.147	1.167	1.1529 ^b
F ₂ ($D_{\infty h}$)	F-F	1.344	1.410	1.423	1.428	1.4119 ^c
C ₂ H ₂ ($D_{\infty h}$)	C-C	1.189	1.203	1.202	1.217	1.202 ^d
	C-H	1.058	1.064	1.063	1.061	1.0625 ^d
C ₂ F ₂ ($D_{\infty h}$)	C-C	1.167	1.186	1.185	1.200	1.1865 ^e
	C-F	1.271	1.286	1.293	1.291	1.2832 ^e
C ₆ H ₆ (D_{6h})	C-C	1.386	1.390	1.392	1.398	1.396 ^f
	C-H	1.076	1.084	1.083	1.085	1.083 ^f
C ₆ F ₆ (D_{6h})	C-C	1.377	1.386	1.386	1.392	1.401 ^g
	C-F	1.313	1.332	1.340	1.333	1.325 ^g

^{a)} [41]. ^{b)} [42]. ^{c)} [43] ^{d)} [44]. ^{e)} [45] ^{f)} [46]. ^{g)} [47].

orbital 65 (this compound has 136 valence electrons and thus 68 occupied orbitals), that displays σ -antibonding character: it is a d-p σ interaction with the ipso carbon of the pentafluorophenyl ligands. The π overlap that strengthens the xenon-carbon interaction is shown in Figure 4.2 (orbital 60).

Figure 4.1: Sigma antibonding orbital of $\text{Xe}(\text{C}_6\text{F}_5)_2$

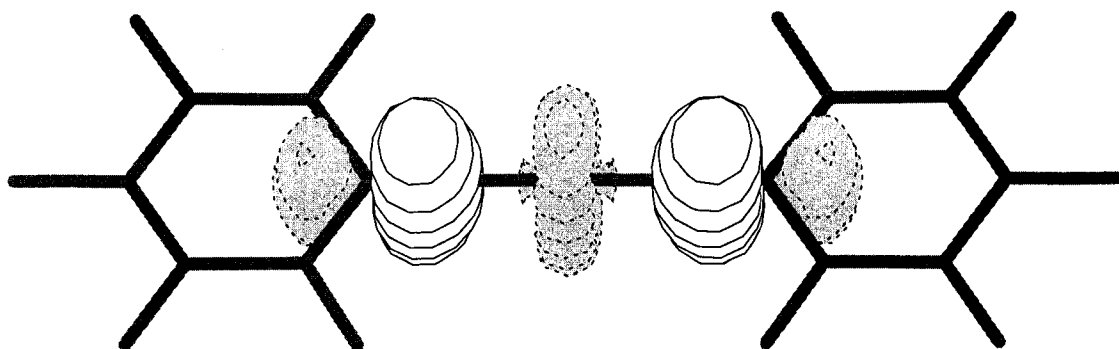
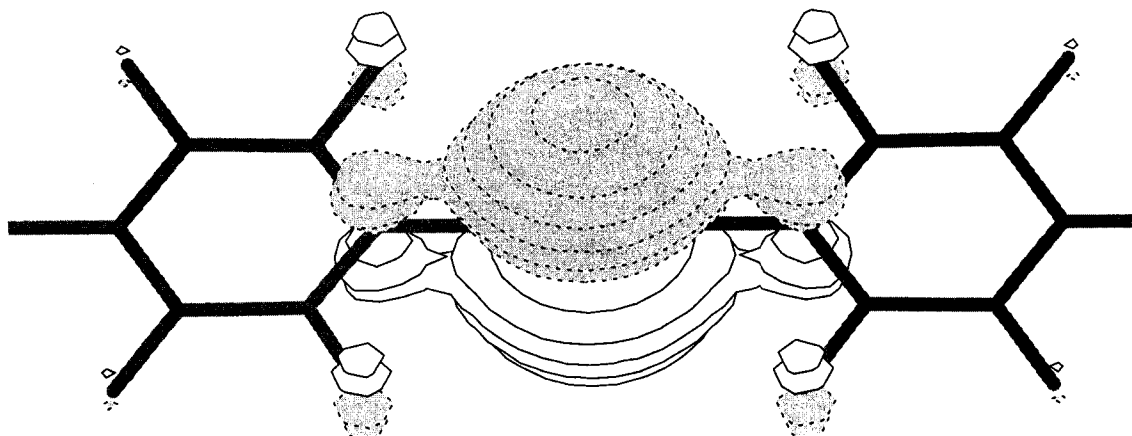


Figure 4.2: Pi bonding orbital of Xe(C₆F₅)₂



The structures of the XeL₂ complexes are given in Table 4.4. The only experimental structure that has been determined is that for XeF₂, with a bond length of 1.974 Å [48]; the iMCPs with a single set of polarization functions overestimate that value by about 0.06 Å. The error is significantly reduced (by 0.02-0.06 Å) with Basis B, which gives a bond length of 1.985 Å at the B3PW91 level. The Xe-F distance of 1.967 Å for XeF₂ at the RHF SRiMCP level agrees fairly well with the value of 2.004 Å obtained at the Dirac-Fock level with finite nuclei [49]. Of the two DFT functionals, B3PW91 tends to give shorter Xe-C bond lengths than B3LYP. The MP2 bond lengths are usually quite similar to the B3LYP values, except that the bond lengths inside the ligands tend to be longer. Harmonic vibrational analysis showed that all structures correspond to minima on the potential energy surface.

For reactions (4.1) and (4.2), where L = CN, CCH, CCF, C₆H₅, C₆F₅, CF₃, and CH₃, the ΔG_{rxn} values were computed at -60°C (213K), and are shown in Tables 4.5 and 4.6. In all cases the reactions are exogonic, with the two DFT functionals giving very similar results that are generally smaller than the RHF values. The addition of the second ligand is less exogonic than that of the first one. Several results are worth noting. Firstly, the CF₃ ligand is strongly bound, despite not having π orbitals available for overlap. In fact, at the DFT level, the reaction substituting two CF₃ ligands for the fluorides in XeF₂ is the most exogonic of the reactions studied.

Table 4.4: Bond lengths (in Å) of xenon complexes

Molecule	Bond	RHF	B3PW91	B3LYP	MP2
XeF_2 ($D_{\infty h}$)	Xe-F	1.967	2.026	2.044	2.036
$\text{Xe}(\text{CN})_2$ ($D_{\infty h}$)	Xe-C	2.202	2.227	2.246	2.233
	C-N	1.133	1.157	1.156	1.180
$\text{Xe}(\text{CCH})_2$ ($D_{\infty h}$)	Xe-C	2.201	2.208	2.227	2.233
	C-C	1.198	1.213	1.212	1.231
	C-H	1.060	1.066	1.065	1.065
$\text{Xe}(\text{CCF})_2$ ($D_{\infty h}$)	Xe-C	2.197	2.197	2.217	2.221
	C-C	1.189	1.208	1.206	1.226
	C-F	1.268	1.284	1.292	1.290
$\text{Xe}(\text{C}_6\text{H}_5)_2$ (D_{2h})	Xe-C	2.291	2.351	2.384	
	C-C (avg)	1.387	1.389	1.392	
	C-H (avg)	1.077	1.086	1.085	
$\text{Xe}(\text{C}_6\text{F}_5)_2$ (D_{2h})	Xe-C	2.291	2.317	2.347	
	C-C (avg)	1.376	1.382	1.383	
	C-F (avg)	1.319	1.340	1.348	
$\text{Xe}(\text{CF}_3)_2$ (D_{3h})	Xe-C	2.301	2.404	2.429	
	C-F	1.325	1.347	1.354	
$\text{Xe}(\text{CH}_3)_2$ (D_{3h})	Xe-C	2.342	2.410	2.467	
	C-H	1.085	1.090	1.089	

The reaction of $(\text{CH}_3)_3\text{SiCF}_3$ with XeF_2 has been attempted, but no evidence for $\text{Xe}(\text{CF}_3)_2$ was found, with C_2F_6 being formed instead. It was postulated that $\text{Xe}(\text{CF}_3)_2$ is initially formed, but that it decomposes very quickly to C_2F_6 [23]. Despite the stability of $\text{Xe}(\text{CF}_3)_2$ with respect to the reactants, the very long Xe-C bond lengths in this compound could make the barrier to CF_3 radical detachment very low, and the formation of C_2F_6 very likely. Secondly, of all the single ligand exchanges, it is the phenyl ligand substitution (one that has not been observed experimentally) that is the most exogonic. However, the second substitution is only slightly exogonic, and

Table 4.5: ΔG_{rxn} (kcal/mol) for reaction (1)

Method	Ligand						
	CN	CCH	CCF	C ₆ H ₅	C ₆ F ₅	CF ₃	CH ₃
RHF	-26.6	-33.3	-36.3	-54.7	-42.9	-41.6	-54.5
B3PW91	-22.0	-24.9	-23.0	-44.1	-36.1	-38.2	-44.0
B3LYP	-22.6	-25.3	-23.4	-46.0	-37.5	-39.2	-45.9

Table 4.6: ΔG_{rxn} (kcal/mol) for reaction (2)

Method	Ligand						
	CN	CCH	CCF	C ₆ H ₅	C ₆ F ₅	CF ₃	CH ₃
RHF	-43.3	-45.8	-54.7	-63.0	-65.3	-59.4	-59.2
B3PW91	-35.5	-34.5	-32.9	-54.5	-57.4	-60.5	-55.0
B3LYP	-37.7	-36.4	-34.6	-58.6	-61.1	-63.9	-59.4

in fact has the smallest exogonicity of any of the reactions studied. The pentafluorophenyl ligand has a very large exogonicity for the second ligand substitution, and this could indicate why Maggiorosa et. al. could not obtain pure FXeC_6F_5 [20].

Reaction (4.3) is also an exogonic reaction, with a ΔG_{rxn} of -14.9, -12.6, and -14.2 kcal/mol at the RHF, B3PW91, and B3LYP levels, respectively. This is comparable with the second step of the double substitution reactions above. The difference in ΔG_{rxn} between reactions (4.1) and (4.2) is between -9 and -23 kcal/mol. However, reaction (4.4) turned out to be endogonic at all levels of theory: 11.7, 8.9, and 8.4 kcal/mol at the RHF, B3PW91, and B3LYP levels, respectively. This is most likely due to the fact that CdF_2 precipitates out in this reaction, and it is the exothermic formation of the CdF_2 lattice (which we are not modeling) that drives this reaction.

The effect of solvent on the reactions was studied via the Polarizable Continuum Method (PCM) [50, 51, 52], as implemented in the GAMESS program [29]. Single-point PCM energy calculations were done at the geometries optimized previously in the gas phase. To simulate the experimental conditions, the PCM parameters were set to reproduce dichloromethane at -60°C (213K). The reaction energies were only very slightly changed (by a maximum of 2 kcal/mol) by the inclusion of solvent. Expansion of the basis set (from Basis A to Basis B) had a similarly small effect (a

maximum of 2 kcal/mol) on the reaction energetics. This leads to the conclusion that the reaction energetics can be accurately modeled at the DFT level using a triple-zeta basis set with a single polarization function and neglecting the effects of solvent.

4.4 Conclusions

We have shown that, from a thermodynamical standpoint, there are many xenon-carbon compounds that could possibly be synthesized. We have found that xenon compounds containing two similar ligands L, where L can be CF_3 , C_6F_5 , CH_3 , CN , CCH , or CCF , should be stable, as well as the mixed NCXeC_6F_5 species. The first ligand substitution is strongly exogonic, with a ΔG_{rxn} of between -22 and -44 kcal/mol at the B3PW91 level of theory. The second substitution is also exogonic, but much less so, with ΔG_{rxn} between -9 and -22 kcal/mol at the same level of theory. In general, the DFT reaction energies are smaller than the RHF ones, with B3PW91 values being smaller than the B3LYP ones. The geometries are similar at the RHF and DFT levels, with electron correlation lengthening the bonds. The iMCPs (especially with the extra polarization functions in Basis B) have been shown to be very good at predicting the structures of both the small ligand molecules, as well as the larger xenon complexes. The predicted energetics seem quite reasonable for these systems. Discrepancies between theoretical predictions and experiment, such as the stability of $\text{Xe}(\text{CF}_3)_2$, could probably be attributed to kinetic effects.

Bibliography

- [1] N. Bartlett *Proc. Chem. Soc.* **112** (1962) 218.
- [2] R. Hoppe, W. Dahne, H. Mattauch, and K. Rodder *Angew. Chem.* **74** (1962) 903.
- [3] H. H. Claasen, H. Selig, and J. G. Malm *J. Am. Chem. Soc.* **84** (1962) 3593.
- [4] C. T. Goetschel and K. R. Loos *J. Am. Chem. Soc.* **94** (1972) 3018.
- [5] K. Seppelt and D. Lentz *Prog. Inorg. Chem.* **29** (1982) 167.
- [6] J. H. Holloway *J. Fluorine Chem.* **33** (1986) 149.
- [7] D. Holtz and J. L. Beauchamp *Science* **24** (1971) 1237.
- [8] J. K. Hovey and T. B. McMahon *J. Am. Chem. Soc.* **108** (1986) 528.
- [9] L. J. Turbini, R. E. Aikman, and R. J. Lagow *J. Am. Chem. Soc.* **101** (1979) 5833.
- [10] H. J. Frohn and S. Jakobs *J. Chem. Soc. Chem. Commun.* (1989) 625.
- [11] H. J. Frohn, S. Jakobs, and G. Henkel *Angew. Chem. Int. Ed.* **28** (1989) 1506.
- [12] D. Naumann and W. Tyrra *J. Chem. Soc. Chem. Commun.* (1989) 47.
- [13] H. J. Frohn and V. V. Bardin *J. Chem. Soc. Chem. Commun.* (1993) 1072.
- [14] D. Naumann, W. Tyrra, R. Gnann, and D. Pfolk *J. Chem. Soc. Chem. Commun.* (1994) 2651.

- [15] V. V. Zhdankin, P. J. Stang, and N. S. Zefirov, *N. S. J. Chem. Soc. Chem. Commun.* (1992) 578.
- [16] G. Frenking, W Koch, F. Reichel, and D. Cremer, *D. J. Am. Chem. Soc.* **112** (1990) 4240.
- [17] H. J. Frohn, A. Klose, and G. Henkel *Angew. Chem. Int. Ed.* **32** (1993) 99.
- [18] H. J. Frohn, T. Schroer, and G. Henkel *Angew. Chem. Int. Ed.* **38** (1999) 2554.
- [19] H. J. Frohn and M. Theißen *Angew. Chem. Int. Ed.* **39** (2000) 4591.
- [20] N. Maggiorosa, D. Naumann, and W. Tyrra *Angew. Chem. Int. Ed.* **39** (2000) 4588.
- [21] K. O. Christe *Angew. Chem. Int. Ed.* **40** (2001) 1419.
- [22] H. J. Frohn, N. LeBlond, K. Lutar, and B. Zemva *Angew. Chem. Int. Ed.* **39** (2000) 391.
- [23] N. Maggiorosa Ph.D. Thesis, University of Cologne, Germany, 1999.
- [24] P. Laszlo and G. J. Schrobilgen *Angew. Chem. Int. Ed.* **27** (1988) 479.
- [25] M. Klobukowski, S. Huzinaga, and Y. Sakai in *Computational Chemistry: Reviews of Current Trends Vol. 3* World Scientific: Singapore, 1999; Chapter 2.
- [26] C. Froese-Fischer *Comp. Phys. Comm.* **4** (1972) 107.
- [27] S. Huzinaga and M. Klobukowski *Chem. Phys. Lett.* **212** (1993) 260.
- [28] CADPAC version 6.3: The Cambridge Analytic Derivatives Package Issue 6, Cambridge, 1995. A suite of quantum chemistry programs developed by R. D. Amos with contributions from I. L. Alberts, J. S. Andrews, S. M. Colwell, N. C. Handy, D. Jayatilaka, P. J. Knowles, R. Kobayashi, K. E. Laidig, G. Laming, A. M. Lee, P. E. Maslen, C. W. Murray, J. E. Rice, E. D. Simandiras, A. J. Stone, M.-D. Su, and D. J. Tozer.

- [29] M. W. Schmidt, K. K. Baldrige, J. A. Boatz, S. T. Elbert, M. S. Gordon, J. J. Jensen, S. Koseki, N. Matsunaga, K. A. Nguyen, S. Su, T. L. Windus, M. Dupuis, and J. A. Montgomery, *J. Comput. Chem.* **14** (1993) 1347.
- [30] C. Møller and M. S. Plesset *Phys. Rev.* **46** (1934) 618.
- [31] A. D. Becke *J. Chem. Phys.* **98** (1993) 5648.
- [32] C. Lee, W. Yang, and R. G. Parr *Phys. Rev. B* **37** (1988) 785.
- [33] P. J. Stephens, F. J. Devlin, C. F. Chabalowski, and M. J. Frisch *J. Chem. Phys.* **98** (1994) 11623.
- [34] R. Krishnan, J. S. Binkley, R. Seeger, and J. A. Pople *J. Chem. Phys.* **72** (1980) 650.
- [35] E. Hirota and C. Yamada *J. Mol. Spectrosc.* **96** (1982) 175.
- [36] M. W. Crofton, M.-F. Jagod, B. D. Reh fuss, W. A. Kreiner, and T. Oka *J. Chem. Phys.* **88** (1988) 666.
- [37] F. Brandi, I. Velchev, W. Horgervorst, and W. Ubachs, *Phys. Rev. A* **64** (2001) 032505.
- [38] J.A. Blush, P. Chen, R.T. Wiedmann and M.G. White, *J. Chem. Phys.* **98** (1993) 3557.
- [39] G. C. Pimentel, G. C. *J. Chem. Phys.* **19** (1951) 446.
- [40] J. Y. Mane and M. Klobukowski, unpublished data.
- [41] D. U. Webb and K. N. Rao *J. Mol. Spectrosc.* **28** (1968) 121.
- [42] E. F. Pearson, R. A. Creswell, M. Winnewisser, and G. Winnewisser *Z. Naturforsch* **31a** (1976) 1394.
- [43] H. G. M. Edwards, E. A. M. Good, and D. A. Long *J. Chem. Soc. Faraday Trans. 2* **72** (1976) 984.

- [44] E. Kostyk and H. L. Welsh *Can. J. Phys.* **58** (1980) 912.
- [45] H. Bürger, W. Schneider, S. Sommer, W. Thiel, and H. Willner *J. Chem. Phys.* **95** (1991) 5660.
- [46] A. Cabana, J. Bachand, and J. Giguère *Can. J. Phys.* **52** (1974) 1949.
- [47] A. Almenningen, O. Bastiansen, R. Seip, and H. M. Seip *Acta Chem. Scand.* **18** (1964) 2115.
- [48] H. Bürger and S. Ma *J. Mol. Spectrosc.* **157** (1993) 536.
- [49] J. Styszynski, X. Cao, G. L. Malli, and L. Visscher *J. Comput. Chem* **18** (1997) 601.
- [50] R. Cammi and J. Tomasi *J. Comput. Chem* **16** (1995) 1449.
- [51] J. Langlet, P. Claverie, J. Caillet, and A. Pullman *J. Phys. Chem* **92** (1988) 1617.
- [52] C. Amovilli and B. Mennucci *J. Phys. Chem B* **101** (1997) 1051.

Chapter 5

Transition Metal - Rare Gas Bonding: The Next Frontier*

5.1 Introduction

In the present chapter, we extend our studies of Chapter 4 to the area of metal-rare gas chemistry. In the past forty years, many covalent compounds of the rare gas atoms have been discovered. Not only have the majority of oxofluorides of xenon been synthesized, up to Xe(VIII) (see [3] and references therein), but compounds with xenon bonding to chlorine [4], nitrogen [5], and even to two carbon atoms have been discovered [6, 7]. Recently, the field has exploded with a number of new discoveries, such as the first covalent argon compound HArF [8], and the discovery that xenon could act as a surprisingly strong ligand. It should come as no surprise that chemical bonding between rare gas and metal atoms should be found.

While attempting to isolate AuF, Seidel and Seppelt [9] discovered a reddish solid that turned out to be AuXe_4^{2+} . Rare gases had previously been known to act only as weak ligands in transition metal systems [10]. For example, the bond dissociation energy (BDE) of the Xe-W bond in $\text{XeW}(\text{CO})_5$ has been calculated to be only 7.6 kcal/mol at the CCSD(T) level [11], in good agreement with the experimental value of 8.2 ± 1.0 kcal/mol obtained via time-resolved infrared spectroscopy in the gas phase [12]. Seidel and Seppelt [9] calculated a BDE of 49.8 kcal/mol for AuXe_4^{2+}

*A version of this chapter was published as: C. C. Lovallo and M. Klobukowski *Chem. Phys. Lett.* **368** (2003) 589.

at the MP2 level, and more recent calculations at the CCSD(T) level have given a value of 57.2 kcal/mol [13]. The BDEs of the Ar-Au bonds in the putative AuAr_4^{2+} have been calculated to be 19.4 kcal/mol [14]. Pyykkö [15, 16] performed calculations on both the gold monocation and the isoelectronic neutral metal (Ni, Pd, Pt) systems. No bound states were found for the NiXe system, but both the PdXe and PtXe systems were bound, by 9.9 and 16.2 kcal/mol, respectively. The Au^+ ion was found to be bound to all of the heavier rare gases at the CCSD(T) level, with counterpoise-corrected BDEs ranging from 0.6 kcal/mol for Ar to 21.0 kcal/mol for Xe. Calculations were also done at the MP2 level, and showed that the bond lengths very nearly identical to the CCSD(T) results, but the BDEs were underestimated by about 10-15%.

In 2000, the first in a series of papers on the microwave spectra of complexes formed by the interaction of a rare gas with a coinage metal monohalide was published by the Gerry group [17]. In that work, basic calculations were done on argon and krypton complexes to predict a value for their rotational constants in order to facilitate the search for spectral lines. Attempting to find the spectral signature of the xenon complexes was much more difficult, as the signals are much weaker due to the fact that there are nine naturally occurring isotopes of xenon, none of which are above 26% natural abundance. A more accurate calculation of the geometries of these species could narrow the search window, aiding in the identification of the desired spectral lines.

In the present work, calculations were done for the systems RgMX ($\text{Rg} = \text{Ar, Kr, Xe}$; $\text{M} = \text{Cu, Ag, Au}$; $\text{X} = \text{F, Cl}$) in order to provide structural parameters for these complexes.

5.2 Computational Methods

We have recently developed a new version of the MCPs based on the large all-electron well-tempered basis set [18] (wtMCPs). They differ from other MCPs in their use of the well-tempered expansion for the reference orbitals [19]. For the work presented in this chapter, the wtMCP potentials were reoptimized using the complete

well-tempered valence basis set, rather than the truncated one as was done previously [19]. In order to obtain the scalar-relativistic corrections for the coinage metals, scalar-relativistic (SR) reference data were obtained using the RESC method [20].

All calculations were done with the GAMESS program [21]. Structures were optimized first on a grid without correcting for basis set superposition error (BSSE). The bond lengths were found by fitting the energies at the grid points to a fourth-order polynomial. Since the BSSE was expected to be small within the MX moiety, the MX distance thus obtained was fixed, and then a search was done to find the rare gas - metal bond length with the interaction energies corrected using the full counterpoise (CP) method [22]; the final values were found by fitting the energies to a fourth-order polynomial.

Calculations were done at the MP2 level, with all valence electrons correlated using the full orbital space. Spherical Gaussian functions were used throughout. Preliminary calculations were done on the xenon fluorides and the coinage metal monohalides to determine the basis set size needed to accurately determine the geometries of the complexes. These calculations indicated that the same basis contraction as used in previous work [23] with a greatly expanded polarization space would be sufficient for our purposes. The metal basis set was augmented with a 2p polarization set to polarize the valence s orbital and a 2f1g polarization set to polarize the valence d orbital; for the rare gas atom a 3d2f1g polarization set was used, and for the halide a 2d1f polarization set was added. The exponents of these p, d, and f polarization functions were obtained by fitting to the valence orbitals as done in previous work [24], while the g function was obtained either from the cc-pVQZ basis set [25] for Ar and Kr, or from a fit to the f polarization set for the other atoms. The final atomic basis set sizes can be found in Table 5.1.

5.3 Results and Discussion

The bond lengths of the coinage metal fluorides and chlorides were calculated at the MP2 level to determine how closely our choice of basis set and method could replicate experimental results. The values are shown in Table 5.2. It can be seen that

Table 5.1: Contraction patterns for basis sets used in calculations^a

Atom	Basis Set
F	(7,8,2,1,2/8,2,1,2/1,1/1)
Cl	(7,11,2,1,2/11,2,1,2/1,1/1)
Ar	(7,8,3,2,1,2/8,3,2,1,2/1,1,1/1,1/1)
Kr	(6,12,3,2,1,2/12,3,2,1,2/14,1,1,1/1,1/1)
Xe	(5,15,3,2,1,2/15,3,2,1,2/17,1,1,1/1,1/1)
Cu	(17,4,2,1,2/17,1,1/7,2,2,1,2/1,1/1)
Ag	(19,5,1,2,1/20,1,1/10,2,2,1,2/1,1/1)
Au	(20,4,1,2,1/21,1,1/12,2,1,2,1/1,1/1)

^a) The first set of numbers represent the s functions, the second set represent the p functions, etc. For example, the basis set for fluorine consists of five s functions (comprised of seven, eight, two, one, and two primitive Gaussians respectively) four p functions, and two d and one f polarization functions

Table 5.2: MP2 Bond lengths of coinage metal monohalides (Å)

Molecule	calc (MP2)	Exp. ^a
CuF	1.751	1.745 ^a
CuCl	2.063	2.051 ^a
AgF	1.992	1.983 ^a
AgCl	2.290	2.281 ^a
AuF	1.924	1.918 ^b
AuCl	2.200	2.199 ^c

^a) [26]. ^b) [27]. ^c) [28].

the computed interatomic distances are always longer than the experimental bond lengths, but only by a maximum of about 0.01 Å; we may expect a similar accuracy in the MX bond length in the complexes.

In all cases, the RgMX complexes were found to be linear, and the resulting bond lengths can be found in Tables 5.3, 5.4, and 5.5, along with the available experimental data. Since all the experimental bond lengths refer to r_0 data, we would expect our calculated r_e values to be somewhat shorter. The calculated values agree fairly well with experiment, but seem to be consistently too long for the Rg-M distances, and too short for the M-X distances. If we assume that our M-X distances should be slightly too long, in accord with our previous discussion of the MX complexes, then this would

imply r_e values of about 0.02 Å shorter than the r_0 ones. If this holds for the Rg-M distances, then our calculations overestimate these bond lengths by about 0.05 Å. It is well known that calculated bond lengths for weak interactions can depend strongly on basis set and method applied, and it seems likely that an extension of the basis set and a higher level of correlation would be necessary for better agreement with the experimental bond lengths. However, the bond lengths do seem to be overestimated by a fairly constant amount (which depends somewhat on the atoms involved), and so it should be possible to predict the bond lengths for those complexes for which no experimental data are present to about 0.01 Å. This should be sufficient for narrowing the spectral range for the search necessary to find these complexes.

Table 5.3: MP2 Bond lengths of argon - coinage metal monohalides (Å)

Molecule	r(Ar-M)		r(M-X)	
	MP2	Exp.	MP2	Exp.
ArCuF	2.238	2.219 ^a	1.727	1.753 ^a
ArCuCl	2.297	2.26 ^a	2.053	2.07 ^a
ArAgF	2.590	2.558 ^b	1.972	1.986 ^b
ArAgCl	2.634	2.597 ^b	2.272	2.285 ^b
ArAuF	2.396	2.391 ^c	1.909	1.918 ^c
ArAuCl	2.472	2.469 ^d	2.196	2.198 ^d

a) [29]. b) [17]. c) [30]. d) [28].

Table 5.4: MP2 Bond lengths of krypton - coinage metal monohalides (Å)

Molecule	r(Kr-M)		r(M-X)	
	MP2	Exp.	MP2	Exp.
KrCuF	2.322		1.730	
KrCuCl	2.369		2.055	
KrAgF	2.609		1.969	
KrAgCl	2.653	2.646 ^a	2.271	2.277 ^a
KrAuF	2.454		1.913	
KrAuCl	2.516	2.522 ^b	2.201	2.210 ^b

a) [31]. b) [28].

Table 5.5: MP2 bond lengths of xenon - coinage metal monohalides (\AA)^a

Molecule	r(Xe-M)	r(M-X)
XeCuF	2.459	1.737
XeCuCl	2.497	2.060
XeAgF	2.684	1.969
XeAgCl	2.728	2.274
XeAuF	2.545	1.922
XeAuCl	2.598	2.213

^a) No experimental data available for these complexes.

Table 5.6: MP2 binding energies (BSSE-corrected) of Rg-MX complexes (kcal/mol)

Molecule	ΔE_{int}	Molecule	ΔE_{int}	Molecule	ΔE_{int}
ArCuF	8.8	KrCuF	11.5	XeCuF	14.2
ArCuCl	6.7	KrCuCl	9.4	XeCuCl	12.3
ArAgF	4.2	KrAgF	6.8	XeAgF	10.2
ArAgCl	3.9	KrAgCl	6.3	XeAgCl	9.4
ArAuF	12.0	KrAuF	16.9	XeAuF	23.3
ArAuCl	9.0	KrAuCl	13.4	XeAuCl	19.1

The binding energies of the rare gas to the metal halide have been calculated, and are collected in Table 5.6. They can probably be considered low estimates, since the rare gas-metal bond lengths are too long, and because as has been seen previously [15], MP2 binding energies tend to be too low when compared to more accurate CCSD(T) results. They cover a fairly wide range, with the weaker interactions being about as strong as a hydrogen bond (which has a bond strength of about 2 - 10 kcal/mol in the gas phase [32]), to the largest bonding energy (for XeAuF) of 23.3 kcal/mol reaching the level of a weak covalent bond. For example, the bond enthalpy of the iodine molecule in the gas phase is 36.1 kcal/mol [33]. Some degree of covalent bonding is also suggested by the short bond lengths: the calculated Xe-Au bond length in XeAuF is 2.545 \AA . This value is much shorter than the sum of the van der Waals radii, which is 3.82 \AA , and even shorter than the sum of the covalent radii, which is 2.74 \AA , or the sum of the covalent radius of Xe and the Pauling ionic radius of Au⁺ which is 2.67 \AA . The calculated bond length in XeAuF clearly indicates the existence

of a stronger, covalent interaction.

5.4 Conclusions

Calculations have been done to determine the structure of the complexes formed by a rare gas and a coinage metal monohalide. The structural parameters have been found to reproduce the known experimental values with acceptable accuracy, and allow for the prediction of bond lengths where no experimental data are available. The predicted parameters should facilitate the search for these currently unknown compounds.

Bibliography

- [1] P. Laszlo and G. J. Schrobilgen *Angew. Chem. Int. Ed.* **27** (1988) 479.
- [2] N. Bartlett *Proc. Chem. Soc.* **112** (1962) 218.
- [3] M. Gerken and G. J. Schrobilgen *Inorg. Chem.* **41** (2002) 198.
- [4] H. J. Frohn and T. Schroer *Angew. Chem. Int. Ed.* **38** (1999) 2554.
- [5] M. Gerken and G. J. Schrobilgen *Coord. Chem. Rev.* **197** (2000) 335.
- [6] H. J. Frohn and M. Theißen *Angew. Chem. Int. Ed.* **39** (2000) 4591.
- [7] N. Maggiorosa, D. Naumann, and W. Tyrre *Angew. Chem. Int. Ed.* **39** (2000) 4588.
- [8] L. Khriachtchev, M. Pettersson, N. Runeberg, J. Lundell, and M. Räsänen *Nature* **406** (2000) 874.
- [9] S. Seidel and K. Seppelt *Science* **290** (2000) 117.
- [10] D. C. Grills and M. W. George *Adv. Inorg. Chem.* **52** (2001) 113.
- [11] A. W. Ehlers, G. Frenking, and E. J. Baerends *Organomet.* **16** (1997) 4896.
- [12] J. R. Wells and E. Weitz *J. Am. Chem. Soc.* **114** (1992) 2783.
- [13] W. Hu and C. Huang *J. Am. Chem. Soc.* **123** (2001) 2340.
- [14] N. R. Walker, R. R. Wright, P. E. Barran, H. Cox, and A. J. Stace *J. Chem. Phys.* **114** (2001) 5562.

- [15] P. Pyykkö *J. Am. Chem. Soc.* **117** (1995) 2067.
- [16] J. V. Burda, N. Runeberg, and P. Pyykkö *Chem. Phys. Lett.* **288** (1998) 635.
- [17] C. J. Evans and M. C. L. Gerry *J. Chem. Phys.* **112** (2000) 1321.
- [18] S. Huzinaga and M. Klobukowski *Chem. Phys. Lett.* **212** (1993) 260.
- [19] J. Y. Mane and M. Klobukowski *J. Mol. Struct. (Theochem)* **547** (2001) 163.
- [20] T. Nakajima and K. Hirao *Chem. Phys. Lett.* **302** (1999) 383.
- [21] M. W. Schmidt, K. K. Baldrige, J. A. Boatz, S. T. Elbert, M. S. Gordon, J. J. Jensen, S. Koseki, N. Matsunaga, K. A. Nguyen, S. Su, T. L. Windus, M. Dupuis, and J. A. Montgomery, *J. Comput. Chem.* **14** (1993) 1347.
- [22] S. F. Boys and F. Bernardi *Mol. Phys.* **37** (1979) 1529.
- [23] J. Y. Mane M.Sc. Thesis, University of Alberta, Edmonton, AB, 2002.
- [24] C. C. Lovallo and M. Klobukowski *Int. J. Quant. Chem.* **90** (2002) 1099.
- [25] T. H. Dunning, Jr. *J. Chem. Phys.* **90** (1989) 1007.
- [26] K. P. Huber and G. Herzberg, in P.J. Linstrom and W.G. Mallard, eds. NIST Chemistry WebBook, NIST Standard Reference Database Number 69, National Institute of Standards and Technology, Gaithersburg MD, July 2001.
- [27] C. J. Evans and M. C. L. Gerry *J. Am. Chem. Soc.* **122** (2000) 1560.
- [28] C. J. Evans, A. Lesarri, and M. C. L. Gerry *J. Am. Chem. Soc.* **122** (2000) 6100.
- [29] C. J. Evans and M. C. L. Gerry *J. Chem. Phys.* **112** (2000) 9363.
- [30] C. J. Evans, D. S. Rubinoff, and M. C. L. Gerry *Chem. Phys. Phys. Chem.* **2** (2000) 3943.
- [31] L. M. Reynard, C. J. Evans, and M. C. L. Gerry *J. Mol. Spectrosc.* **206** (2001) 33.

- [32] J. E. Del Bene and I. Shavitt in S. Scheiner, ed. *Molecular Interactions: From van der Waals to Strongly Bound Complexes*, John Wiley & Sons: Chichester, UK, 1997; p. 157.
- [33] J. W. Tromp, R. J. LeRoy, S. Gerstenkorn, and P. Luc *J. Mol. Spectrosc.* **100** (1983) 82.

Chapter 6

Accurate *ab initio* Alkaline Earth - Helium Pair Potentials*

6.1 Introduction

In this and the following chapter we will present results obtained in the application of the MCP method to the studies of very weakly interacting diatomic systems containing helium, the lightest of the rare gas atoms.

Pair potentials for weakly bound systems are of great interest for theoretical and experimental chemists alike. Weak interactions are very difficult to calculate accurately and thus are an extreme test of basis sets and theoretical methods. The pair potentials themselves are indispensable both to theoreticians who wish to study interactions via molecular dynamics and to spectroscopists who can use the potentials to explain experimental spectra.

Helium nanodroplets can be formed by the expansion of cold helium gas into a vacuum through a narrow nozzle. The resulting droplets under typical experimental conditions contain on the order of 10^4 helium atoms [1]. These droplets are then passed through an oven containing the desired dopant. Depending on conditions, a droplet may pick up one [2] or many [1] dopants as it passes through the oven. These dopants can then be analyzed via spectroscopic means.

Helium nanodroplet spectroscopy allows for the study of the spectroscopic properties of dopants in a very weakly interacting matrix. For extremely weak interactions,

*A version of this chapter was published as: C. C. Lovallo and M. Klobukowski *Chem. Phys. Lett.* **373** (2003) 439.

like those between helium and the ground states of the alkali and alkaline earth metals, the interactions between the dopant and the helium atoms can be even weaker than those between the helium atoms themselves and may cause the dopant to occupy a surface site on the outside of the droplet. This has been shown to occur for the alkali metals both experimentally [3] and theoretically [4]. The alkaline earth metals are bound more strongly to helium than their alkali counterparts [5], but are still less bound than the helium self-interaction. These atoms are of interest because they straddle the line between the very weakly interacting dopants that exist on the surface, and those that exist inside the helium droplet.

Experimental work suggests that the Mg atoms should exist inside a helium droplet [6], however in the case of Ca and Sr, the experimental evidence is not as clear. These elements exhibit much larger shifts and broadening of the spectral lines than are seen for the alkali metals, but only about a third to a half of what is seen in bulk liquid helium [7]. It was suggested that this may indicate a surface site, but with the atom existing in a very deep dimple on the surface to explain the experimental data. A similar conclusion was reached for the Ba atom [8].

Very little theoretical work has been done on the interactions between the ground states of the alkaline earth metals and helium. All of the recent theoretical calculations that we are aware of are summarized in Table 6.1. Accurate *ab initio* calculations have been performed for the BeHe and MgHe pairs. Leung and Breckenridge [9] obtained an interaction energy of 5.7 cm^{-1} at a distance of 4.65 \AA for BeHe at the QCISD(T) level using basis sets with polarization functions up to g on the He atom and f on the Be atom. For MgHe, Funk *et al.* [10] found a well depth of 4.6 cm^{-1} at 5.16 \AA at the MP4 level. Many of the remaining calculations are semiempirical in nature, and predict binding energies that differ by up to 500% (see results for CaHe).

Accurate pair potentials can be used to predict the approximate position of the dopant atom in a helium nanodroplet. Using He density functional theory calculations, Ancilotto *et al.* [11] derived a simple model that relates the gain in interaction energy due to helium-dopant interactions and the cost in energy necessary to carve out a cavity inside the helium droplet for the dopant. This is expressed as a dimensionless parameter λ :

Table 6.1: Previous theoretical calculations of alkaline earth - helium pair potentials

	Method	r_e (Å)	D_e (cm ⁻¹)
BeHe	ACCD[12]	4.84	4.64
	surface integral[5]	4.22	8.22
	QCISD(T)[9]	4.65	5.7
MgHe	ACCD[12]	5.63	2.00
	surface integral[5]	4.70	7.70
	MP2[13]	5.4	2.8
	SCF/CI[14]	5.6	2.3
	HFD[15]	5.4	2.8
	MP4[10]	5.16	4.6
CaHe	surface integral[5]	5.10	10.3
	SCF/CI[14]	7.4	2.9
	HFD[15]	6.6	2.03
	MRCI[16]	5.45	11.6
SrHe	surface integral[5]	5.54	7.11
	MRCI[16]	5.72	12.7
BaHe	surface integral[5]	5.70	8.74
	pseudopotential[17]	6.4	5
	pseudopotential[18]	5.8	3.5

$$\lambda \equiv 2^{-1/6} \sigma^{-1} \rho \varepsilon r_e, \quad (6.1)$$

where σ is the surface tension of liquid helium (0.179 cm⁻¹Å⁻²), ρ is the number density of liquid helium (0.022 Å⁻³), and r_e and ε are the equilibrium bond distance (in Å) and well depth (in cm⁻¹) of the relevant dopant-helium pair potential, respectively. Ancilotto predicted that dopants with values of λ greater than 1.9 should reside inside the droplet, whereas others would reside on the surface. The model is successful in predicting the surface sites of the alkali metals ($\lambda \approx 0.7$) and the interior sites of strongly bound dopants such as Ag ($\lambda \approx 5$) and SF₆ ($\lambda \approx 19$) [6]. However, the alkaline earth atoms yield values of λ very close to this cutoff, so they can be used either as a test of the accuracy of the model and as a test of the pair potential, if the experimental position of the dopant is well-characterized. Therefore, we would

expect values of λ to be greater than 1.9 for Be and Mg, and somewhat below 1.9 for the remaining alkaline earth atoms.

In the present paper, accurate pair potentials are determined for the helium alkaline earth (Be-Ba) pairs. These potentials are used to predict the position of these atoms in a helium nanodroplet, the importance of relativistic effects on the shape of the potentials, and the possible existence of bound states on the potential surfaces.

6.2 Computational Methods

The wtMCPs were used for the work presented in these final two chapters, as the valence basis sets of the iMCPs are much too small to be useful for the calculation of extremely weak interactions such as these. Both non-relativistic and scalar-relativistic (using the RESC method [19]) potentials were developed for the alkaline earth atoms, but the relativistic ones were used only for Sr and Ba.

In order to determine the suitability for pseudopotentials for the calculation of very weak interactions such as these, all-electron calculations were also performed using the well-tempered basis (WTBS) set [20]. The WTBS was also used for the helium atom.

All calculations were done with the GAMESS program [21]. The CCSD(T) method was used, as it was shown [22] to accurately model the interaction energies for weakly bound systems such as these. A recent paper [23] on the related system MgAr used a similar coupled-cluster based method (CC3), and found results that agreed quite well with experiment. In the present work, all electrons were correlated in the full virtual space for the wtMCP calculations. In order to test the effect of core correlation on the potentials, two interaction potentials were determined: one (WTBS) with all electrons correlated in the full virtual space, and the other (FC-WTBS) in which only the valence electrons, including the outermost p shell for Mg-Ba, were correlated.

The basis set expansion used is given in Table 6.2. For the alkaline earth atoms, a set of 3p2d1f polarization functions was added, and a set of 4p3d2f1g polarization functions was added on the helium atom. The polarization functions were determined

Table 6.2: Basis set contraction pattern used in calculations

Atom	Basis Set	Contracted Functions
He	WTBS	11,2,2,1,1/1,1,1,1/1,1,1/1,1/1
Be	wtMCP	15,2,2,1/1,1,1/1,1/1
	WTBS	20,15,2,2,1/1,1,1/1,1/1
Mg	wtMCP	15,4,2,1,1/1,1,1/1,1/1
	WTBS	23,23,15,4,2,1,1/13,1,1,1/1,1/1
Ca	wtMCP	15,4,3,2,1,1/16,1,1,1/1,1/1
	WTBS	26,26,26,15,4,3,2,1,1/16,16,1,1,1/1,1/1
Sr	wtMCP	20,3,2,1,1/20,1,1,1/1,1/1
	WTBS	27,27,27,27,13,3,3,4,2,1,1/20,20,20,1,1,1/17,1,1/1
Ba	wtMCP	20,4,2,1,1/23,1,1,1/1,1/1
	WTBS	30,30,30,30,30,22,4,2,1,1/23,23,23,23,1,1,1/17,17,1,1/1

by fitting to the outermost s orbital as has been discussed in previous chapters. The same contraction pattern and polarization functions were used for the all-electron calculations; the core functions were kept contracted. This yields a valence basis set size equivalent to the cc-VTZ basis of Dunning *et al.* [24] for the alkaline earth atoms, and to the cc-VQZ basis [25] for the helium atom; however, our basis contains larger contractions and is more diffuse, so it probably approaches aug-ccVTZ / aug-ccVQZ [24, 25] in quality. To study the effect of bond functions on basis set convergence, bond functions were added to this basis set for some calculations.

The potentials were found by calculating the interaction energy at 40 points ranging from 2.0 to 12.0 Å. The interaction energies were corrected for basis set superposition error by using the full counterpoise method of Boys and Bernardi [26]. The well depth and the position of the minimum were found by fitting the bottom of the potential well to a fourth-order polynomial. Due to insufficient computing resources, the entire potential surfaces of SrHe and BaHe were not calculated using the all-electron basis set, instead calculations were only performed around the bottom of the well.

Polarizability calculations were done in GAMESS via the finite field method, with a field strength of 0.001 au. The bound-state calculations were performed with the program LEVEL [27]. The potential was extrapolated using a C_6/C_8 sum with the values of C_6 for BeHe, MgHe, and CaHe taken from Standard and Certain [28] (the

middle of the reported range), and the C_8 value determined from the pair potential. To determine the value of C_6 for SrHe and BaHe, an approximate value for C_6 was calculated for CaHe, SrHe, and BaHe using the Slater-Kirkwood formula [29]:

$$C_6 = \frac{3}{2} \frac{\alpha_0^{He} \alpha_0^X}{(\alpha_0^{He}/N_{He})^{1/2} + (\alpha_0^X/N_X)^{1/2}}, \quad (6.2)$$

where α_0^X is the static dipole polarizability of atom X (Ca - Ba, see Table 6.3 for values), and N_X is the number of valence electrons on atom X (here always 2). The results for SrHe and BaHe were then scaled by the ratio of the C_6 coefficient given by Standard and Certain [28] for Ca to that predicted by the Slater-Kirkwood formula.

6.3 Results and Discussion

To determine if our pseudopotentials and basis sets could accurately describe the dispersion forces that hold atoms together, the atomic polarizabilities of the helium atom and the alkaline earth atoms were calculated. The results can be seen in Table 6.3. The dispersion forces depend directly on the calculated polarizabilities, so if the polarizabilities are over- or underestimated, the same may be expected to hold true for the dispersion forces. It can be seen that the polarizabilities for the atoms He, Be, and Mg are all within 2% of the experimental values. The values for the alkaline earth atoms are close to basis set convergence: expanding the basis set up to g functions for the Mg atom lowers the calculated polarizability by only 0.3 au. For the heavier atoms, the calculated polarizabilities are up to 30% too high. There is also a small discrepancy between the wtMCP and the all-electron values, with the pseudopotentials predicting a value up to 5% larger. The all-electron frozen-core calculation (FC-WTBS) for the Sr atom gives an almost identical polarizability (221 versus 222 au), so the error may be in the potential itself, and not a core correlation effect. To see if the large discrepancy with the experimental results was due to relativistic effects, two calculations were performed for Ba and Sr: one using the scalar-relativistic MCP and the other using the RESC [19] method for an all-electron

Table 6.3: Calculated atomic polarizabilities (in au)

Atom		wtMCP	WTBS	Exp.
He	NR	N/A	1.373	1.383 ^a
Be	NR	37.8	37.9	37.8 ^b
Mg	NR	73.0	73.5	71.5 ^c
Ca	NR	170	169	154 ^c / 169 ^d
Sr	NR	230	222	186 ^e
	SR	218	214	
Ba	NR	352	346	268 ^e
	SR	310	323	

a) [30] b) [31] c) [32] d) [33] e) [34]

scalar-relativistic calculation. It is expected that the relativistic contraction of the s orbitals would result in a lower polarizability, and that is what is seen. However, the calculated results are still about 15% too large, indicating that other effects, such as spin-orbit coupling, which are not considered in our calculation, may be affecting our calculated polarizabilities. We may expect our calculated dispersion forces to be accurate for Be and Mg, but our results for Ca-Ba may be slightly overbound. This will of course be offset by any basis set incompleteness in our dimer. These values also allow us to select a polarizability for Ca out of the two reported values [32, 33]: $169 \pm 8\%$ and $154 \pm 2\%$ au. Considering our results for the other alkaline earth atoms, and our neglect of the relativistic effects for this system, our work suggests that the lower value may be more accurate.

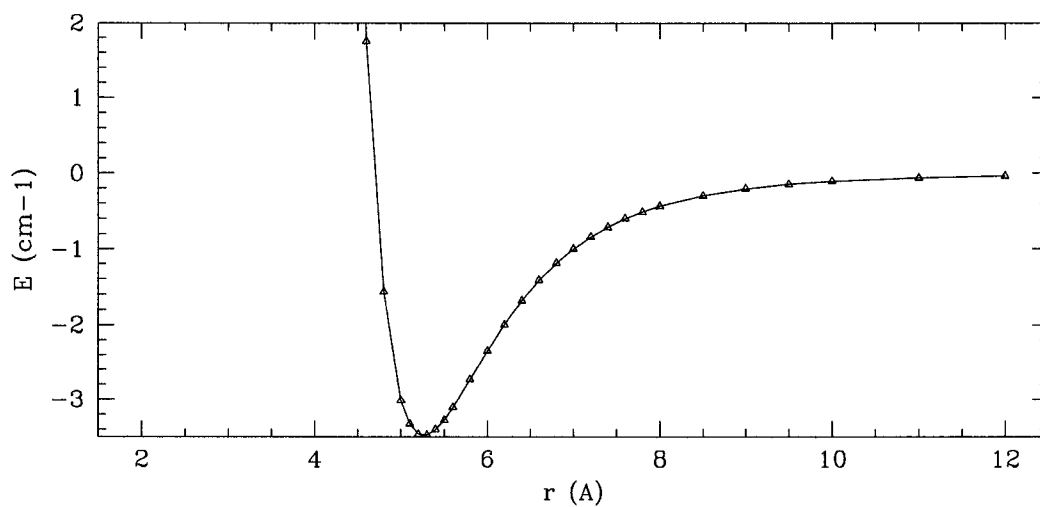
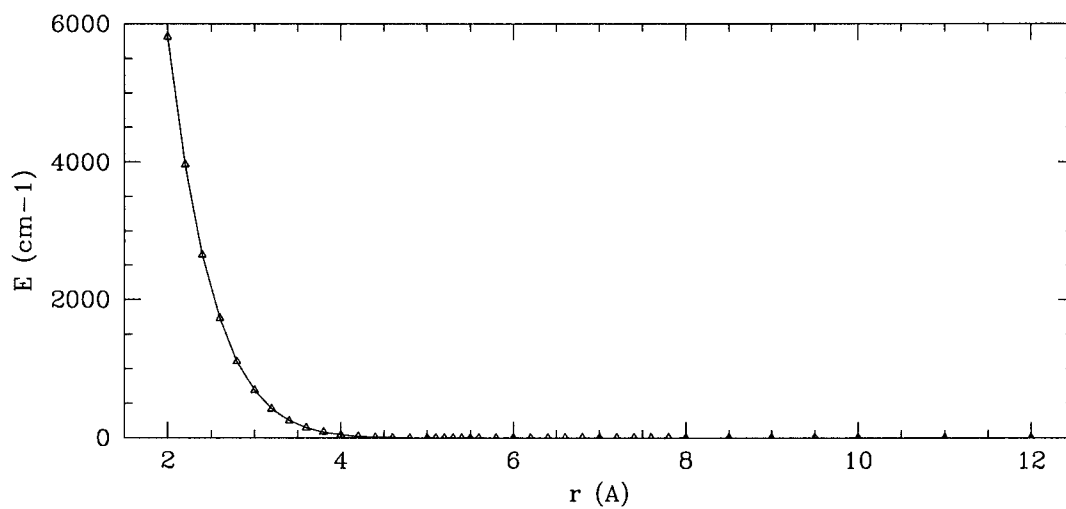
Despite Woon’s previous work showing the validity of the CCSD(T) method for weakly bound rare gas systems [22], some question remained about its applicability to these systems due to the near-degeneracy of the valence s and p orbitals on the alkaline earth atoms. As a test, we performed MRCI calculations on BeHe to compare to our CCSD(T) results. An initial MCSCF calculation was performed with an active space containing the He 1s orbital and the Be 2s and 2p orbitals (4 electrons in 5 orbitals). A MRCI calculation was done considering all of the single and double excitations out of that active space into all of the virtual orbitals. Due to the size-consistency error inherent in CI calculations of less than full-CI quality (see Section 1.3.1), counterpoise

correction was not possible. Therefore, we compared the results to non-CP corrected CCSD(T) calculations. A total of 10 calculations were performed, describing the deepest part of the potential well. The binding energies agreed to within 2% at all points, and to less than 1% at the bottom of the well.

Bond functions are commonly used in calculations of weak interactions in order to improve the description of the electron density between the interacting species without resorting to very high angular momentum or very diffuse atom-centered basis functions. To test the importance of bond functions, we added a set of 3s3p2d bond functions to our basis set, fixed at the midpoint of the bond. The exponents for these functions were taken from the set derived by Cybulski and Toczyłowski [35] for the Ar dimer, and then scaled in order to better describe the different sizes of the complexes studied. The scaling factors used for He₂, BeHe, MgHe, CaHe, SrHe, and BaHe were 1.00, 0.75, 0.50, 0.30, 0.30, and 0.25, respectively. Potentials were determined for all of the atom pairs using bond functions and the wtMCPs, and are shown in the relevant tables (listed as +BF) along with the parameters calculated without bond functions. Hardware limitations prevented us from the calculation of potentials using bond functions and the all-electron basis set, except for the helium dimer.

An example of our calculated pair potentials (for MgHe without bond functions) is shown in Figure 6.1. The well is very shallow, and occurs at large r . The well depths and bond lengths are tabulated in Tables 6.4 - 6.7. The complete CCSD(T) numerical potentials are included in Appendix B. As a by-product of the CCSD(T) calculations, MP2 and CCSD energies are calculated, and they are also shown in the Tables. For the helium dimer, the MP2 and even the CCSD methods give a far too small binding energy, indicating that triple excitations must be considered to obtain an accurate potential. The helium dimer is one of the best-studied weakly interacting systems, and its well depth has been accurately calculated. Our best result underestimates the well depth by about 4%, and overestimates the bond length by about 0.5%. Since our helium basis set contains polarization functions up to g , and our alkaline earth basis set only up to f , it may be expected that this may be a lower bound to the error we may expect in our alkaline earth - helium potentials. A single point calculation for MgHe with the Mg basis set expanded to include a g polarization function yielded

Figure 6.1: CCSD(T) Mg - He interaction potential (without bond functions)



an increase of 11% in the calculated binding energy at a point near the minimum of the potential well. However, if we take the MgHe basis set with bond functions and expand the Mg basis to include a g polarization function, the difference between the binding energies is only about 1%, indicating that the bond functions are indeed very useful in reducing the need for large basis sets on the atoms.

To test this hypothesis, calculations were done on the MgHe complex using a very large basis set containing up to two g functions on each atom, and an expanded set of 3s3p2d2f1g bond functions. The calculated binding energy was only 3% lower than the one obtained with the much smaller basis set (with 3s3p2d bond functions) presented here, while the calculations took an order of magnitude more computational time. Therefore, the use of bond functions can yield results of quality similar to that obtained with much larger atom-centered basis sets. The CP correction is especially important with the use of bond functions, as it is often several times larger than the bonding energy itself.

The potentials calculated with the bond functions are quite different from those calculated without the bond functions. In all cases, the use of bond functions results in much larger binding energies and shorter bond lengths. The effect is more pronounced as one goes down the periodic table, with the BaHe bond length shortening by almost 0.3 Å and the binding energy increasing by about 45%. Even for the He dimer, the binding energy increases by about 11%, yielding results much closer to experiment.

Several trends can be observed in the alkaline earth - helium pair potentials. The well depths at the MP2 level of theory are larger than those at the CCSD level, but smaller than those at the CCSD(T) level of theory. Treatment of triple excitations is very important, as the CCSD(T) well depths are larger than those calculated with CCSD by at least 30%. Core correlation is not important in these systems, as the well depths of the all-electron versus frozen-core all-electron calculations are within 1%. The pseudopotentials do an excellent job of replicating the all-electron calculations, but tend to overbind as the alkaline earth atom gets heavier, which is to be expected from our results of the polarizability calculations. The effect of the scalar-relativistic corrections is to shorten the bond length, and strengthen the bond between the atoms. Due to insufficient computing resources, scalar-relativistic all-electron calculations

Table 6.4: He - He pair potential parameters (r_e in Å, ϵ in cm^{-1}).

Method	r_e	ϵ
MP2	3.10	4.39
CCSD	3.05	5.75
CCSD(T)	3.02	6.60
CCSD(T) + BF	2.97	7.38
ref. [37]	2.965	7.66

Table 6.5: Light alkaline earth (Be - Ca) - He pair potential parameters^{a,b}

System	Method	WTBS		FC-WTBS		wtMCP	
		r_e	ϵ	r_e	ϵ	r_e	ϵ
BeHe	MP2	4.76	3.77	4.76	3.76	4.76	3.75
	CCSD	4.74	3.46	4.74	3.45	4.74	3.47
	CCSD(T)	4.61	4.78	4.61	4.78	4.61 (4.53)	4.79 (5.97)
MgHe	MP2	5.40	2.86	5.39	2.87	5.38	2.94
	CCSD	5.41	2.57	5.40	2.57	5.40	2.58
	CCSD(T)	5.27	3.46	5.27	3.47	5.26 (5.11)	3.49 (4.69)
CaHe	MP2	6.36	2.01	6.36	2.02	6.33	2.11
	CCSD	6.43	1.63	6.43	1.63	6.41	1.69
	CCSD(T)	6.26	2.24	6.26	2.24	6.25 (6.04)	2.30 (3.14)

^{a)} r_e in Å, ϵ in cm^{-1} ^{b)} Results with bond functions (+BF) in parentheses.

Table 6.6: Sr - He pair potential parameters^{a,b}

Method	NR WTBS		NR FC-WTBS		NR wtMCP	
	r_e	ϵ	r_e	ϵ	r_e	ϵ
MP2	6.67	1.96	6.66	1.96	6.74	1.82
CCSD	6.76	1.60	6.75	1.59	6.84	1.48
CCSD(T)	6.59	2.12	6.59	2.12	6.67 (6.44)	1.97 (2.77)*

* The SR wtMCP+BF values for CCSD(T) are $r_e = 6.37$ Å, $\epsilon = 2.87$ cm^{-1}

^{a)} r_e in Å, ϵ in cm^{-1} ^{b)} Results with bond functions (+BF) in parentheses.

Table 6.7: Ba - He pair potential parameters^{a,b}

Method	NR WTBS		NR wtMCP		SR wtMCP	
	r_e	ϵ	r_e	ϵ	r_e	ϵ
MP2	7.36	1.43	7.39	1.41	7.22	1.51
CCSD	7.51	1.07	7.51	1.15	7.31	1.28
CCSD(T)	7.30	1.47	7.33 (7.05)	1.53 (2.23)	7.15 (6.88)	1.68 (2.41)

^{a)} r_e in Å, ϵ in cm^{-1} ^{b)} Results with bond functions (+BF) in parentheses.

were not performed, but the effects are expected to be properly replicated by the pseudopotentials, which have been previously shown to correctly replicate the effects of relativity on bond lengths [36]. It is obvious that the decrease in exchange-repulsion due to the contraction of the outermost s orbital more than overcomes the reduction of dispersion forces upon contraction.

Since these complexes exhibit such weak binding, calculations were done to determine whether these potentials could support any bound rovibrational states. One surprising result was that the He dimer potential supported one bound state despite being almost 0.3 cm^{-1} too shallow with respect to the best currently accepted value [37]. The calculated position of the bound state in the He dimer has been predicted to be about $9 \times 10^{-4} \text{ cm}^{-1}$ [38]. This may then be an indication of how accurate our bound state calculations are. It was found that all of the alkaline earth - helium potentials could support three levels: the $J = 0$, $J = 1$, and $J = 2$ rotational levels of the ground vibrational state, except for the BeHe potential which only supports the $J = 0$ and $J = 1$ levels. This may be expected, as the more weakly bound alkali atoms have been shown to support only one bound state ($v = 0$, $J = 0$) [39]. This contrasts with previous work on MgHe [10], where only two bound states were found for this dimer, although the $J = 2$ state is very close to the dissociation limit and its position is probably very sensitive to the exact shape of the potential. The potentials calculated without bond functions could only support two bound states each, and the energy levels for the MgHe system were very close to those reported by Funk *et al.* [10] The energies of the bound levels (with respect to the dissociation limit) are given in Tables 6.8 - 6.12. For Be-Ca, calculations were done for all of the major (>2% natural abundance) isotopes of the alkaline earth atom. For Mg, Sr and Ba,

only two isotopes are shown; the remaining isotopes cluster in between these energy levels. Since a complete potential was not calculated at the all-electron level for Sr or Ba, no bound state calculations were possible for these atoms at the all-electron level. Judging from the agreement between the pseudopotential and all-electron results for the lighter alkaline earth atoms, the agreement should be of the same order of magnitude. Although the positions of the energy levels change between the all-electron and pseudopotential calculations, the predicted energy of the transitions between the states is quite close, with the largest difference being only 0.003 cm^{-1} for the ^{40}Ca isotope.

Table 6.8: Calculated energies of bound rovibrational states for He_2 and BeHe (in cm^{-1})

(v,J)	He_2		^9Be		
	WTBS	WTBS+BF	WTBS	wtMCP	wtMCP+BF
(0,0)	—	-0.0064	-0.3976	-0.4005	-0.7144
(0,1)	—	—	-0.1156	-0.1178	-0.3768

Table 6.9: Calculated energies of bound rovibrational states for MgHe isotopomers (in cm^{-1})

(v,J)	^{24}Mg			^{26}Mg		
	WTBS	wtMCP	MCP+BF	WTBS	wtMCP	MCP+BF
(0,0)	-0.3877	-0.3950	-0.7686	-0.3956	-0.4029	-0.7805
(0,1)	-0.1922	-0.1979	-0.5308	-0.2008	-0.2067	-0.5442
(0,2)	—	—	-0.0877	—	—	-0.1026

Table 6.10: Calculated energies of bound rovibrational states for CaHe isotopomers (in cm^{-1})

(v,J)	^{40}Ca			^{44}Ca		
	WTBS	wtMCP	wtMCP+BF	WTBS	wtMCP	wtMCP+BF
(0,0)	-0.2192	-0.2364	-0.4793	-0.2229	-0.2402	-0.4852
(0,1)	-0.0934	-0.1077	-0.3213	-0.0974	-0.1118	-0.3279
(0,2)	—	—	-0.0299	—	—	-0.0369

Table 6.11: Calculated energies of bound rovibrational states for SrHe isotopomers (in cm^{-1})

(v,J)	^{86}Sr			^{88}Sr		
	NR	NR+BF	SR+BF	NR	NR+BF	SR+BF
(0,0)	-0.2111	-0.4480	-0.4787	-0.2115	-0.4487	-0.4794
(0,1)	-0.1021	-0.3127	-0.3392	-0.1025	-0.3134	-0.3400
(0,2)	—	-0.0594	-0.0771	—	-0.0602	-0.0780

Table 6.12: Calculated energies of bound rovibrational states for BaHe isotopomers (in cm^{-1})

(v,J)	^{134}Ba				^{138}Ba			
	NR	NR+BF	SR	SR+BF	NR	NR+BF	SR	SR+BF
(0,0)	-0.1440	-0.3402	-0.1751	-0.3918	-0.1442	-0.3404	-0.1753	-0.3920
(0,1)	-0.0591	-0.2307	-0.0827	-0.2749	-0.0593	-0.2310	-0.0830	-0.2751
(0,2)	—	-0.0276	—	-0.0558	—	-0.0278	—	-0.0561

Finally, the value of the Ancilotto λ parameter was calculated in order to determine the position of the alkaline earth atoms in a helium nanodroplet. The values are shown in Table 6.13. The values decrease as one goes down the periodic table. Both Be and Mg are predicted to lie inside a helium droplet ($\lambda \gg 1.9$). The values for Ca and Sr are very slightly higher than 1.9, which may indicate an interior site, but the experimental evidence seems to indicate some sort of hybrid site or very deep dimple on the surface of the droplet [7]. Relativistic effects tend to increase the value of λ as can be seen for Ba, but there seems little doubt that Ba will occupy a surface site, although the λ value of 1.8 indicates that the Ba atom will have a much stronger interaction with the droplet than the alkali atoms.

6.4 Conclusions

Calculations have been done to determine accurate pair potentials between alkaline earth atoms and helium. These potentials have been used to predict three bound rovibrational states for each complex and to predict that Be and Mg would exist inside a helium nanodroplet while the other alkaline earth atoms should occupy surface

Table 6.13: Calculated values of the Ancilotto parameter λ^a

Atom	WTBS	wtMCP	wtMCP+BF
Be	2.41	2.42	2.96
Mg	2.00	2.01	2.62
Ca	1.54	1.57	2.08
Sr	1.53	1.44	1.95
Ba	1.18	1.23 (1.32)	1.72 (1.82)

^{a)} Scalar-relativistic values for Ba shown in parentheses

sites, although with fairly strong atom-droplet interactions. It was also shown that pseudopotentials with sufficiently large valence basis sets can accurately reproduce all-electron results as well as scalar relativistic effects. The use of bond functions allows for quick and accurate calculation of parameters without the use of large atom-centered basis sets. The new interaction potentials are currently being applied in molecular dynamics simulations of the solvation of the alkaline earth atoms in helium.

Bibliography

- [1] A. Bartelt, J. D. Close, F. Federmann, N. Quaas, and J. P. Toennies *Phys. Rev. Lett.* **77** (1996) 3525.
- [2] J. D. Close, F. Federmann, K. Hoffmann, and N. Quaas *Chem. Phys. Lett.* **276** (1997) 393.
- [3] F. Stienkemeier, J. Higgins, C. Callegari, S. I. Kanorsky, W. E. Ernst, and G. Scoles *Z. Phys. D* **38** (1996) 253.
- [4] F. Ancilotto, E. Cheng, M. W. Cole, and F. Toigo *Z. Phys. B* **98** (1995) 323.
- [5] U. Kleinekathöfer *Chem. Phys. Lett.* **324** (2000) 403.
- [6] J. Reho, U. Merker, M. R. Radcliff, K. K. Lehmann, and G. Scoles *J. Chem. Phys.* **112** (2000) 8409.
- [7] F. Stienkemeier, F. Meier, and H. O. Lutz *J. Chem. Phys.* **107** (1997) 10816.
- [8] F. Stienkemeier, F. Meier, and H. O. Lutz *Eur. Phys. J. D* **9** (1999) 313.
- [9] A. W. K. Leung and W. H. Breckenridge *J. Chem. Phys.* **111** (1999) 9198.
- [10] D. J. Funk, W. H. Breckenridge, and J. Simons *J. Chem. Phys.* **91** (1989) 1114.
- [11] F. Ancilotto, P. B. Lerner, and M. W. Cole *J. Low Temp. Phys.* **101** (1995) 1123.
- [12] R. A. Chiles and C. E. Dykstra *Chem. Phys. Lett.* **85** (1982) 447.
- [13] Q. Hui Ph.D. thesis, Graduate School of Science and Engineering, Saitama University, 1997.

- [14] E. Czuchaj, F. Rebenrost, H. Stoll, and H. Preuss *Chem. Phys. Lett.* **182** (1991) 191.
- [15] C. Douketis, G. Scoles, S. Marchetti, M. Zen, and A. Thakkar *J. Chem. Phys.* **76** (1982) 3057.
- [16] F. Stienkemeier, F. Meier, K. Stark, and H. O. Lutz *Faraday Disc.* **108** (1997) 212.
- [17] J. Brust and C. H. Greene *Phys. Rev. A* **56** (1997) 2005.
- [18] E. Czuchaj, F. Rebenrost, H. Stoll, and H. Preuss *Chem. Phys.* **196** (1995) 37.
- [19] T. Nakajima and K. Hirao *Chem. Phys. Lett.* **302** (1999) 383.
- [20] S. Huzinaga and M. Klobukowski *Chem. Phys. Lett.* **212** (1993) 260.
- [21] M. W. Schmidt, K. K. Baldridge, J. A. Boatz, S. T. Elbert, M. S. Gordon, J. J. Jensen, S. Koseki, N. Matsunaga, K. A. Nguyen, S. Su, T. L. Windus, M. Dupuis, and J. A. Montgomery, *J. Comput. Chem.* **14** (1993) 1347.
- [22] D. E. Woon *J. Chem. Phys.* **100** (1994) 2838.
- [23] K. Hald, P. Jørgensen, W. H. Breckenridge, and M. Jaszuński *Chem. Phys. Lett.* **364** (2002) 402.
- [24] T. H. Dunning, Jr. *J. Chem. Phys.* **90** (1989) 1007.
- [25] D. E. Woon and T. H. Dunning, Jr. *J. Chem. Phys.* **100** (1994) 2975.
- [26] S. F. Boys and F. Bernardi *Mol. Phys.* **37** (1979) 1529.
- [27] R. J. LeRoy *LEVEL 7.1: A Computer Program for Solving the Radial Schrödinger Equation for Bound and Quasibound Levels* University of Waterloo Chemical Physics Research Report CP-642R (2000).
- [28] J. M. Standard and P. R. Certain *J. Chem. Phys.* **83** (1985) 3002.

- [29] I. G. Kaplan *Theory of Molecular Interactions* Elsevier: Amsterdam, 1986; p. 41.
- [30] A. D. Buckingham and P. G. Hibbard *Symp. Faraday Soc.* **2** (1968) 41.
- [31] H.-J. Werner and W. Meyer *Phys. Rev. A* **13** (1976) 13.
- [32] E.-A. Reinsch and W. Meyer *Phys. Rev. A* **14** (1976) 915.
- [33] T. M. Miller and B. Bederson *Phys. Rev. A* **14** (1976) 1572.
- [34] H. L. Schwartz, T. M. Miller, and B. Bederson *Phys. Rev. A* **10** (1974) 1924.
- [35] S. M. Cybulski and R. R. Toczyłowski *J. Chem. Phys.* **111** (1999) 10520.
- [36] J. Y. Mane M.Sc. Thesis, University of Alberta, Edmonton, Alberta, 2002.
- [37] A. R. Janzen and R. A. Aziz *J. Chem. Phys.* **107** (1997) 914.
- [38] W. Schöllkopf and J. P. Toennies *J. Chem. Phys.* **104** (1996) 1155.
- [39] U. Kleinekathöfer, M. Lewerenz, and M. Mladenovic *Phys. Rev. Lett.* **83** (1999) 4717.

Chapter 7

Accurate *ab initio* Pair Potentials Between Helium and the Heavier Group 2 Elements*

7.1 Introduction

This chapter is an extension of the work done in the previous chapter. Here, we expand the basis set to near the basis set limit in order to improve the results on the heavier alkaline-earth metals (Ca - Ba). This was done for two reasons. Firstly, the work in Chapter 6 showed that it was for these heavier metals that the expansion of the basis set (via bond functions) gave the most dramatic improvement in the well depths of the potentials. In addition, there is less previous theoretical work done for these metals (especially Sr and Ba), and so the work presented here is the most accurate work available for these systems. All the recent theoretical calculations that we are aware of are summarized in Table 7.1. Most of the previous calculations are semiempirical in nature, and predict binding energies that differ by up to 500%, although the most recent calculations on CaHe [1, 2] are in fairly close agreement.

Our studies in the previous chapter suggested that bond functions were very important in order to accurately predict binding energies for these species and that relativistic effects had to be taken into account for the heavier systems. However, the polarization space and bond functions used were not sufficient to saturate the basis

*A version of this chapter was accepted for publication by the *Journal of Chemical Physics* on October 8, 2003.

Table 7.1: Previous theoretical calculations of heavier alkaline earth - helium pair potential parameters

System	Method	r_e (Å)	ϵ (cm ⁻¹)
CaHe	surface integral[3]	5.10	10.3
	SCF/CI[4]	7.4	2.9
	HFD[5]	6.6	2.03
	MRCI[6]	5.45	11.6
	CCSD(T)[1]	5.85	4.2
	CCSD(T)[2]	5.95	3.3
	CCSD(T)[7]	6.04	3.14
SrHe	surface integral[3]	5.54	7.11
	MRCI[6]	5.72	12.7
	CCSD(T)[7]	6.37	2.87
BaHe	surface integral[3]	5.70	8.74
	pseudopotential[8]	6.4	5
	pseudopotential[9]	5.8	3.5
	CCSD(T)[7]	6.88	2.41

set. With recent advances in computing power available to us, we are now able to remove the basis set limitations and provide definitive answers.

An indication of the position of a dopant atom in or on a helium nanodroplet may be obtained using a simple model [10] derived by Ancilotto *et al.* In that model, the gain in interaction energy due to dopant-helium interactions is balanced with the cost in energy necessary to carve out a cavity inside the helium droplet for the dopant, with a dimensionless parameter λ quantifying this balance:

$$\lambda \equiv 2^{-1/6} \sigma^{-1} \rho \epsilon r_e, \quad (7.1)$$

where σ is the surface tension of liquid helium (0.179 cm⁻¹Å⁻²), ρ is the number density of liquid helium (0.022 Å⁻³), and ϵ and r_e are the well depth (in cm⁻¹) and equilibrium interatomic distance (in Å) of the pair potential respectively. The Ancilotto model predicts that dopants with values of $\lambda > 1.9$ reside inside the droplet, whereas $\lambda < 1.9$ indicates a surface site. The model is successful in predicting the surface sites of the alkali metals ($\lambda \approx 0.7$) and the interior sites of strongly bound dopants such as Ag ($\lambda \approx 5$) and SF₆ ($\lambda \approx 19$) in agreement with experiment [11].

We would like to use the very accurate pair potentials that we will calculate in this chapter to study the suitability of the Ancilotto model, however, any detailed analysis of the usefulness of the model for the systems studied is complicated by the fact that the experiments do not give definitive data about the position of the metal atoms.

In this chapter, the pair potentials for the heavier Group 2 metals (Ca, Sr, and Ba) interacting with helium are calculated using very large basis sets. These potentials are then used to predict the importance of relativistic effects on the shape of the potentials, the possible existence of bound states on the potential surface, and the possible position of these atoms (via the Ancilotto model) in a helium nanodroplet.

7.2 Computational Methods

All calculations were done using the GAMESS program [12]. The coupled-cluster method with single and double excitations and a perturbational treatment of the triple excitations (CCSD(T)) was used, as it has been shown (see Chapter 6 and refs. [7, 13]) to accurately model the interaction energies for weakly bound systems. All electrons outside of the core were correlated using the full virtual space.

The well-tempered basis set was used for the helium atom [14]. The wtMCPs [15] were used as the underlying basis set for all of the Group 2 metals studied in this work because the results in Chapter 6 showed that the wtMCPs were able to accurately reproduce all-electron calculations even on these very weakly bound systems. This basis set was then systematically expanded. First of all, three p, two d, and one f functions were added to all atoms. The exponents of these polarization functions were determined by fitting to the outermost s orbital. Next, a single p, d, and f functions were added, with their exponents determined by continuing the even-tempered sequence formed by the two lowest exponents in each symmetry. A single g function was then added by fitting to the f functions. Finally, a diffuse function of each symmetry (s, p, d, f, and g), with exponents obtained through the continuation of the even-tempered sequence, was added to yield the final basis set used in this work. The structure of the final basis set expansion is given in Table 7.2 and the diffuse and polarization-correlating functions are shown in Table 7.3. This valence

Table 7.2: Basis set contraction pattern used in calculations

Atom	Basis Set	Contraction Scheme
He	WTBS	(18s 5p 4d 3f 2g) / [6s 5p 4d 3f 2g]
Ca	wtMCP	(27s 21p 4d 3f 2g) / [7s 6p 4d 3f 2g]
Sr	wtMCP	(28s 25p 4d 3f 2g) / [6s 6p 4d 3f 2g]
Ba	wtMCP	(29s 28p 4d 3f 2g) / [6s 6p 4d 3f 2g]

basis set is equivalent in size to the aug-cc-V5Z basis of Dunning *et al.* [16] for the helium atom, and of similar quality for the Group 2 atoms. To further improve the basis set, a large set (three s, three p, two d, two f, and one g) of bond functions were added, fixed to the midpoint between the metal and the helium atoms. The exponents for these functions were taken from the set derived by Cybulski and Toczyłowski [17] for the Ar dimer, and then scaled in order to better describe the different sizes of the complexes studied. The scaling factors used for He₂, CaHe, SrHe, and BaHe were 1.00, 0.30, 0.30, and 0.25 respectively.

The potentials were found by calculating the interaction energy at a number of points (usually 15 or 16) covering the range from 2.0 to 14.0 Å. The interaction energies were corrected for basis set superposition error by using the full counterpoise method of Boys and Bernardi [18]. The well depth and the position of the minimum were found by fitting the bottom of the potential well to a fourth-order polynomial.

Polarizability calculations were done in GAMESS using the finite-field model with an applied field of 0.001 au. To check the accuracy of the finite-field method, a test calculation was performed using the analytical TDHF method for the Ca atom. The polarizability obtained with the analytical method agreed with the finite-field result to less than 0.1%. The bound-state calculations were performed with the program LEVEL [19]. The potential was extrapolated to long range using a C₆/C₈ sum with the values of C₆ and C₈ determined by using the last two *ab initio* calculated points.

Table 7.3: Polarization / correlating functions used in calculations

Atom	Symmetry	Exponent
He NR	s	0.043
	p	4.598; 1.567; 0.554; 0.197; 0.070
	d	3.942; 1.192; 0.355; 0.106
	f	3.254; 0.769; 0.182
	g	1.939; 0.458
Ca NR	s	0.008
	p	0.102; 0.036; 0.012; 0.004; 0.001
	d	0.135; 0.047; 0.016; 0.005
	f	0.201; 0.063; 0.020
	g	0.127; 0.040
Sr NR	s	0.007
	p	0.083; 0.030; 0.011; 0.004; 0.001
	d	0.102; 0.035; 0.009; 0.002
	f	0.154; 0.050; 0.016
	g	0.098; 0.032
Sr SR	s	0.007
	p	0.086; 0.031; 0.011; 0.004; 0.001
	d	0.107; 0.036; 0.012; 0.004
	f	0.158; 0.051; 0.016
	g	0.100; 0.033
Ba NR	s	0.004
	p	0.063; 0.024; 0.009; 0.003; 0.001
	d	0.091; 0.032; 0.011; 0.004
	f	0.111; 0.038; 0.013
	g	0.072; 0.025
Ba SR	s	0.003
	p	0.068; 0.025; 0.010; 0.004; 0.002
	d	0.081; 0.029; 0.006; 0.001
	f	0.122; 0.041; 0.013
	g	0.079; 0.026

7.3 Results and Discussion

To determine if our pseudopotentials and basis sets can accurately describe the dispersion forces that hold the complexes together, the atomic polarizabilities of the helium atom and the Group 2 atoms were calculated. The results are shown in Table 7.4. The dispersion forces depend directly on the polarizabilities, so if the calculated polarizabilities are over- or underestimated, the same may be expected to hold true for the dispersion forces. It can be seen that the polarizability for the He atom agrees with experiment to less than 0.2%, however the calculated polarizabilities of the metals are all too large. To see if the discrepancy with the experimental results was due to relativistic effects, calculations were also done with the scalar-relativistic (SR) potentials for Sr and Ba. In accord with expectations, the relativistic contraction of the outermost s orbital results in a lower polarizability. The SR values are closer to experiment, but a fairly significant constant gap of 10-15% (if we assume the lower reported polarizability for Ca) still remains for all of the metals, with Sr showing the greatest error with respect to experiment. There are several possible explanations for these results. Firstly, it is possible that other relativistic effects that we have not considered in this work may further lower the polarizabilities. Furthermore, in the MCP formalism it is assumed that the core electrons perfectly screen the valence electrons leading to the effective nuclear charge of 8 for all of the Group 2 atoms. However, the screening is not perfect, in particular for the outermost s orbital which penetrates into the core region. Therefore, the valence electrons are not bound as tightly as they should be, and the calculated polarizability is too large. The calculated polarizabilities are very similar to those obtained with a much smaller basis set in Chapter 6, see Table 6.3, indicating that they are essentially converged with respect to basis set.

Due to the slightly too large polarizability calculated for the Group 2 metals, our systems may be expected to be slightly overbound. This of course will be offset by any basis set incompleteness in our dimer, as can be demonstrated using the calculated values of C_6 for these systems. By using the C_6 and C_8 constants determined from the final two calculated points, we obtain an upper bound for these values since the effect

Table 7.4: Calculated atomic polarizabilities (in au)

Atom		α	Exp.
He	NR	1.385	1.383 ^a
Ca	NR	169	154 ^b / 169 ^c
Sr	NR	229	–
	SR	217	186 ^d
Ba	NR	344	–
	SR	307	268 ^d

a) [20] b) [21] c) [22] d) [23]

of higher terms is neglected. The calculated values of C_6 and C_8 are shown in Table 7.5. Experimental estimates are available only for He_2 and CaHe . The computed results for He_2 agree very well with experimental values, but the coefficients are too small for CaHe . This is somewhat surprising, given that the calculated polarizability of the Ca atom is too high, and since the calculated value of C_6 is supposed to be an upper bound. It is possible that the exchange repulsion still has a non-zero value even at this long distance, and so our calculated results are too low. To check this hypothesis, interaction energies were calculated for CaHe at 14 and 16 Å, and were used to determine C_6 and C_8 . The calculated C_6 changed by less than 1%, indicating that if the hypothesis were true, then the repulsion must still have a significant value even at these very long ranges, which seems unlikely. In order to obtain a rough estimate of the C_6 values for the other systems, an approximate C_6 was calculated for all of the systems using the Slater-Kirkwood formula [24]:

$$C_6 = \frac{3}{2} \frac{\alpha_0^{\text{He}} \alpha_0^{\text{X}}}{(\alpha_0^{\text{He}}/N_{\text{He}})^{1/2} + (\alpha_0^{\text{X}}/N_{\text{X}})^{1/2}}, \quad (7.2)$$

where α_0^{X} is the static dipole polarizability of atom X, and N_{X} is the number of valence electrons on atom X (here always 2). Calculations were performed for both the experimental values of the polarizability and our calculated values, and the results are included in Table 7.5. It is known that the Slater-Kirkwood formula gives an upper bound to the C_6 value for light systems, and a lower bound for heavier systems. This is the trend that we see with our values, indicating that the values of C_6 and C_8

Table 7.5: Experimental and calculated dispersion coefficients (in au)

System	Calculated ^a		Slater-Kirkwood		Experimental ^d	
	C ₆	C ₈	C ₆ ^b	C ₆ ^c	C ₆	C ₈
He ₂ NR	1.44	14.4	1.72	1.61	1.44-1.47	13.9-14.2
CaHe NR	36.9	2.51×10 ³	33.2	34.9	45.1-48.5	1.48-2.19×10 ³
SrHe NR	45.6	4.05×10 ³		40.3		
SR	45.0	3.70×10 ³	36.9	39.0		
BaHe NR	65.2	4.26×10 ³		49.4		
SR	62.0	3.49×10 ³	44.8	46.3		

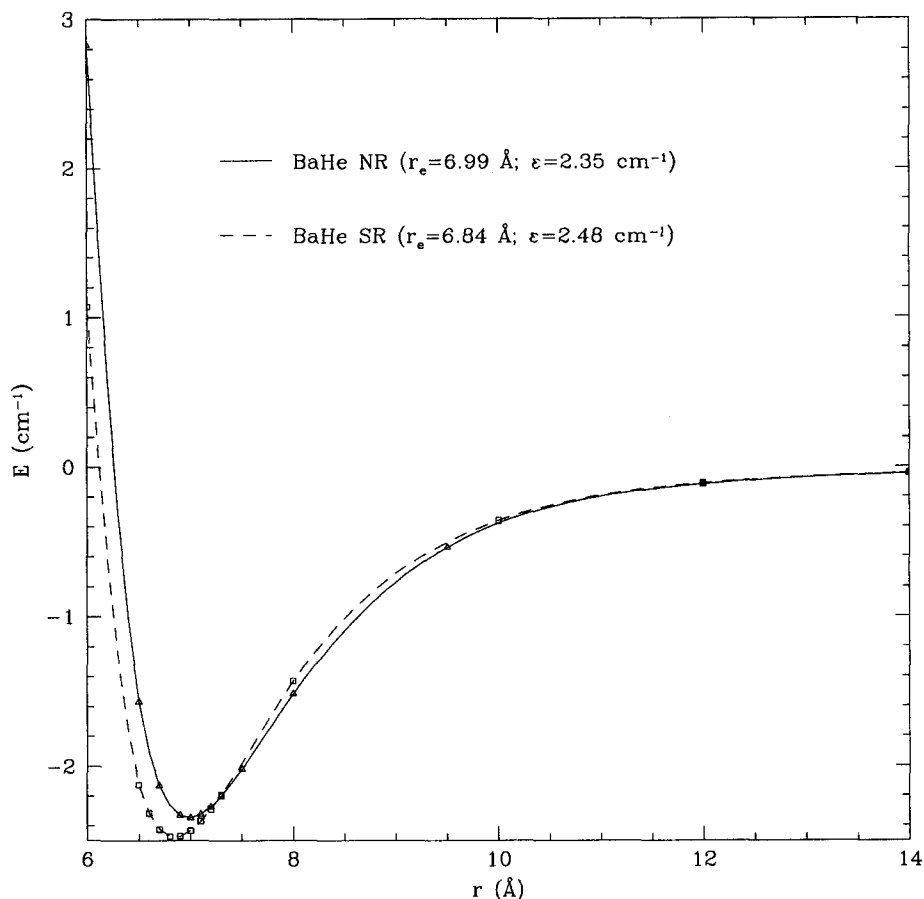
^a from *ab initio* data, this work; ^b Eq. (7.2) using experimental α ;

^c Eq. (7.2) using calculated α ; ^d [25]

obtained from our data are of the right magnitude. Note that our values for C₆ and C₈ were obtained from the last two *ab initio* points on the calculated potential energy curve, so there is no independent way of checking the results. The fact that the C₆ value changes so little when additional *ab initio* points are calculated (see above for CaHe) lends credence to our values being at least fairly accurate. Our calculated value of C₆ for CaHe (36.9 au) is also in good agreement with the value (35.34 au) obtained by Partridge *et al.* [2]

An example of our calculated pair potentials (for BaHe with and without relativistic corrections) is shown in Figure 7.1. The well is very shallow, and occurs at large interatomic distances. The well depths and r_e values for all systems studied are collected in Table 7.6 and the counterpoise-corrected data points are given in Table 7.7. The helium dimer is one of the best-studied weakly interacting systems, and its well depth has been accurately determined. Our result underestimates the well depth by about 3%, and overestimates the bond length by about 0.02 Å. When we compare the parameters to those calculated with a smaller basis set (Table 6.4), we find that the well is deeper, as we expected, but the bond length is longer, further away from the best available value. For the remaining systems, the larger basis set results in a deeper potential well and a shorter internuclear distance, but the effect is small. Typically the internuclear distance shortens by less than 0.1 Å and the well depth increasing by only about 3-5%. The counterpoise correction is especially important

Figure 7.1: Ba - He interaction potentials with respect to the dissociation limit



with the use of bond functions, as the correction is often several times larger than the binding energy itself. Of the two recent calculations for CaHe, our results are in better agreement with those of Partridge [2] than those of Czuchaj *et al.* [1] The bond lengths are approximately equal, but there is a discrepancy in the well depth of almost 30%. In all three cases the same CCSD(T) method was used, but Czuchaj *et al.* [1] used a smaller basis set, together with a pseudopotential for Ca that accounted explicitly for only two valence electrons. We expect that our results are quite close to basis set saturation for the ten active electrons.

The effect of the scalar relativistic corrections is to shorten the bond length and strengthen the bond between atoms. Due to insufficient computing resources, scalar-

Table 7.6: CCSD(T) alkaline-earth metal - helium pair potential parameters^{a,b}

System	Method	r_e	ϵ
He ₂	WTBS	2.985	7.48
	<i>ab initio</i> [26]	2.965	7.69
CaHe	NR wtMCP	6.02	3.32
SrHe	NR wtMCP	6.42	2.85
	SR wtMCP	6.34	2.96
BaHe	NR wtMCP	6.99	2.35
	SR wtMCP	6.84	2.48

^a r_e in Å ^b ϵ in cm⁻¹

relativistic all-electron calculations were not performed, but the scalar-relativistic pseudopotentials have previously been shown [15] to correctly replicate the relativistic effects seen at the all-electron level. It is obvious that the decrease in exchange-repulsion due to the contraction of the outermost s orbital more than overcomes the reduction of dispersion forces upon contraction (due to a lowered polarizability), resulting in shorter bond lengths.

Calculations were done to determine whether these potentials could support any bound rovibrational states. The energies (with respect to the dissociation limit) are given in Table 7.8. Despite an earlier prediction of a bound state in the He dimer (Table 6.8), we do not expect the He dimer potential to support a bound state, since our potential is too shallow and the calculated position of the bound state in the He dimer has been predicted to be about 9×10^{-4} cm⁻¹ [27]. The fact that no bound state was found for the He dimer with the current pair potential, despite it having a deeper potential well than the one derived in Chapter 6, suggests that the previous potential may have had the incorrect shape, as it predicted a bound state contrary to our expectations.

For all of the heavier Group 2 metal - helium potentials, it was found that three levels could be supported, the $J = 0$, $J = 1$, and $J = 2$ rotational levels of the ground vibrational state. It was expected that there should be more than one bound level, as the more weakly bound alkali atoms were found to support one bound state ($v = 0$, $J = 0$) [28]. The potentials calculated in Chapter 6 (with a smaller basis set) were

Table 7.7: Counterpoise-corrected CCSD(T) interaction energies (in cm^{-1})

Interatomic distance (\AA)	CaHe	SrHe NR	SrHe SR	BaHe NR	BaHe SR
2.0	6833.27	8182.32	8455.25	10730.72	11591.06
3.0	1329.94	1575.11	1547.31	1796.72	1820.07
4.0	174.50	264.63	248.18	422.04	380.34
5.0	9.23	24.45	21.29	60.22	49.39
5.3	1.02	9.03	7.28		
5.6		1.65	0.73		
5.7	-2.77				
5.8	-3.08				
5.9	-3.24				
6.0	-3.36	-2.10	-2.46	2.83	1.07
6.1	-3.27				
6.2	-3.19				
6.3	-3.08	-2.81	-2.73		
6.4		-2.85	-2.89		
6.5		-2.83	-2.96	-1.57	-2.12
6.6		-2.77	-2.95		-2.31
6.7		-2.68	-2.90	-2.13	-2.42
6.8		-2.57	-2.81		-2.47
6.9		-2.44	-2.30	-2.33	-2.47
7.0	-1.98			-2.35	-2.43
7.1				-2.32	-2.37
7.2				-2.27	-2.29
7.3				-2.20	-2.19
7.5	-1.34	-1.64	-1.63	-2.02	
8.0	-0.90	-1.15	-1.12	-1.52	-1.43
9.0	-0.42	-0.55	-0.53		
9.5				-0.54	
10.0	-0.21	-0.27	-0.27		-0.36
12.0	-0.07	-0.09	-0.08	-0.12	-0.11
14.0	-0.03			-0.05	-0.04
16.0	-0.01				

also able to support three bound states. For all metals, the two isotopomers with the highest natural abundance are shown; the results for the remaining isotopes would cluster closely around these energy levels. The complexes are so weakly bound that the expectation values $\langle r \rangle$ (shown in Table 7.8) are very different from the r_e values (as tabulated in Table 7.6), and vary considerably between the bound states. The $\langle r \rangle$ values are 2 - 3 Å larger than the corresponding r_e values, and range from 8 to 10 Å, indicating a very weakly bound system. In fact, the bound state that is the most strongly bound, the $v = 0, J = 0$ state of CaHe, is only bound by about one half of a wavenumber with respect to the separated atoms. When the positions and spacing of the states is compared between the current potentials and those calculated in Chapter 6 (see Tables 6.10 - 6.12), a couple of conclusions can be drawn. Firstly, the bound states are more tightly bound in the potentials derived here. This may be expected from the greater depth of these potentials. The spacing between the levels is also larger for the deeper potentials, which would result in different predictions for the spectroscopic constants of these complexes. The differences are small, on the order of a few percent, but this underlines the importance of using the best possible potentials if highly accurate predictions of molecular properties are desired.

Finally, the value of the Ancilotto λ parameter was calculated. The values are shown in Table 7.9. The values decrease as expected as one goes down the periodic table, indicating a smaller helium-metal interaction. Experimental evidence appears to indicate a hybrid site or a very deep dimple on the surface of the droplet [29] for both Ca and Sr. However, our calculated value of λ for Ca is 2.2, larger than the cutoff value of 1.9. The neglected relativistic effects could further increase this number slightly, as seen for Sr and Ba. Considering that our pair potentials are quite accurate, the values of λ suggest that the Ancilotto model should be viewed more as a progression from dopants on the outside of the droplet (e.g. Na) to those fully inside the droplet (e.g. Ag). As the value of λ is increased, the interaction between the dopant and the helium atoms becomes gradually stronger and the dopant occupies a progressively deeper dimple on the surface until finally the dopant is completely solvated by helium. This occurs at a value of λ larger than 1.9, as the Ca atom is not fully solvated at a value of 2.2. It is not surprising that the Ancilotto model

Table 7.8: Calculated energies (in cm^{-1}) and radial expectation values (in \AA) of bound rovibrational states

State (v,J)	E	$\langle r \rangle$	E	$\langle r \rangle$
	$^{40}\text{Ca}^4\text{He}$ NR		$^{44}\text{Ca}^4\text{He}$ NR	
(0,0)	-0.5417	7.95	-0.5479	7.94
(0,1)	-0.3784	8.15	-0.3854	8.13
(0,2)	-0.0730	8.97	-0.0808	8.90
	$^{86}\text{Sr}^4\text{He}$ NR		$^{86}\text{Sr}^4\text{He}$ SR	
(0,0)	-0.4805	8.43	-0.4728	8.39
(0,1)	-0.3426	8.62	-0.3332	8.59
(0,2)	-0.0831	9.36	-0.0716	9.40
	$^{88}\text{Sr}^4\text{He}$ NR		$^{88}\text{Sr}^4\text{He}$ SR	
(0,0)	-0.4812	8.43	-0.4735	8.39
(0,1)	-0.3433	8.62	-0.3339	8.59
(0,2)	-0.0838	9.35	-0.0724	9.39
	$^{137}\text{Ba}^4\text{He}$ NR		$^{137}\text{Ba}^4\text{He}$ SR	
(0,0)	-0.3894	9.18	-0.4280	8.94
(0,1)	-0.2750	9.40	-0.3075	9.14
(0,2)	-0.0602	10.26	-0.0802	9.87
	$^{138}\text{Ba}^4\text{He}$ NR		$^{138}\text{Ba}^4\text{He}$ SR	
(0,0)	-0.3895	9.18	-0.4281	8.94
(0,1)	-0.2751	9.40	-0.3076	9.14
(0,2)	-0.0604	10.26	-0.0804	9.87

does not give a clearer picture of the dopant-helium interaction in a nanodroplet as it is a very simple model, best used for distinguishing between obvious cases like the alkali metals and the silver atom. A much more advanced model would be needed to describe the borderline cases.

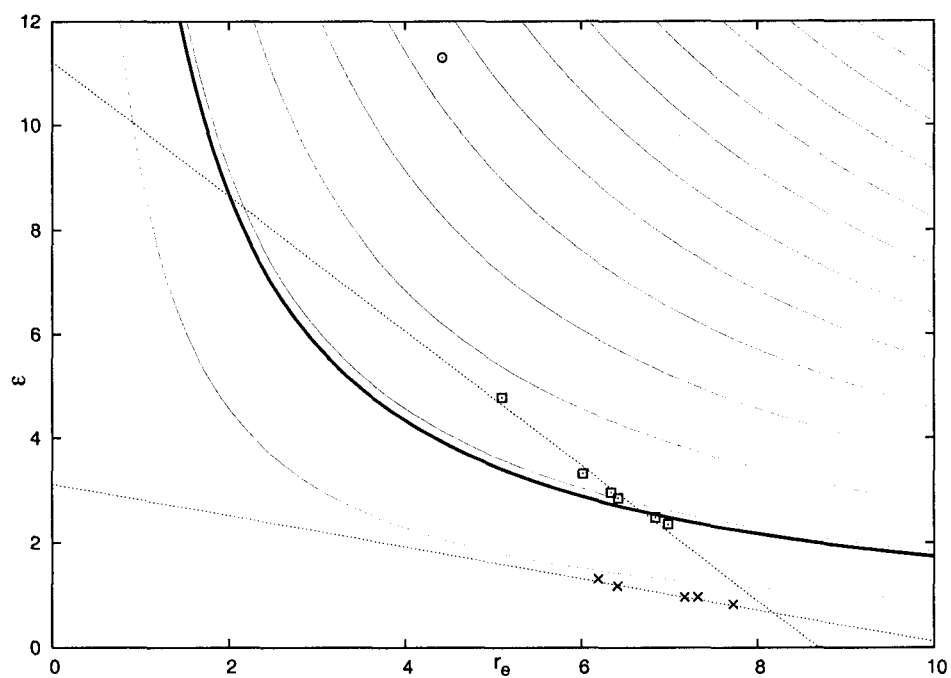
Table 7.9: Calculated values of the Ancilotto parameter λ (Eqn. 7.1)

System	Method	λ
CaHe	NR wtMCP	2.19
SrHe	NR wtMCP	2.00
	SR wtMCP	2.05
BaHe	NR wtMCP	1.80
	SR wtMCP	1.86

The larger basis set used in the present work leads to a deeper interaction potential when compared with those of Chapter 6. In consequence, the present values of λ are larger than the ones shown there (see Table 6.13). The largest increase occurs for the Ca atom, and the effect is smaller for the heavier atoms. The difference between the non-relativistic and the scalar-relativistic values decreases with the larger basis set. This suggests that the results are nearly converged with basis set, and further basis set enlargement would be unnecessary.

Figure 7.2 shows the relationship between the well depth and the interatomic distance for interaction potentials that involve Group 1 and Group 2 atoms. The light contours are plots of the Ancilotto parameter; the first contour corresponds to $\lambda = 1$, the second contour to $\lambda = 2$ and so on. The thicker, darker contour is the cutoff of $\lambda = 1.9$. The crosses are the results for the alkali metals (Li - Cs, ref [10]), which all have values of $\lambda < 1$. The circle near the top of the plot is an example of a strongly bound dopant, the silver atom[10]. The squares that cross the cutoff contour are the results for the alkaline-earth metals calculated in this work. Both the non- and scalar-relativistic values are shown. Linear regression reveals a straight-line relationship between the well depth and the interatomic distance for both sets of data with a high correlation coefficient ($R^2 > 0.97$ in both cases).

Figure 7.2: Contour plot of the Ancilotto equation and the correlation between the well depths (in cm^{-1}) and equilibrium interatomic distances (in \AA) for the alkali and alkaline earth metals



7.4 Conclusions

Very accurate pair potentials were calculated for the interaction between helium and the heavier Group 2 metals. These potentials were used to predict the existence of three bound rovibrational states for each complex, and, in conjunction with the Ancilotto model, were used to predict the location of these metals in a helium nanodroplet. We have shown the Ancilotto model to be useful in describing dopant-helium interactions when it is viewed as a progression leading from nearly unsolvated to fully solvated dopants. The current results improve upon the earlier ones, and suggest that basis set convergence has been reached for both atomic (polarizabilities) and molecular interaction potential (r_e , ε) parameters. These potentials are currently being applied in molecular dynamics simulations of the Group 2 metals in liquid helium.

Bibliography

- [1] E. Czuchaj, M. Krośnicki, and H. Stoll *Chem. Phys.* **292** (2003) 101.
- [2] H. Partridge, J. R. Stallcop, and E. Levin *J. Chem. Phys.* **115** (2001) 6471.
- [3] U. Kleinekathöfer *Chem. Phys. Lett.* **324** (2000) 403.
- [4] E. Czuchaj, F. Rebentrost, H. Stoll, and H. Preuss *Chem. Phys. Lett.* **182** (1991) 191.
- [5] C. Douketis, G. Scoles, S. Marchetti, M. Zen, and A. Thakkar *J. Chem. Phys.* **76** (1982) 3057.
- [6] F. Stienkemeier, F. Meier, K. Stark, and H. O. Lutz *Faraday Disc.* **108** (1997) 212.
- [7] C. C. Lovallo and M. Klobukowski *Chem. Phys. Lett.* **373** (2003) 439.
- [8] J. Brust and C. H. Greene *Phys. Rev. A* **56** (1997) 2005.
- [9] E. Czuchaj, F. Rebentrost, H. Stoll, and H. Preuss *Chem. Phys.* **196** (1995) 37.
- [10] F. Ancilotto, P. B. Lerner, and M. W. Cole *J. Low Temp. Phys.* **101** (1995) 1123.
- [11] J. Reho, U. Merker, M. R. Radcliff, K. K. Lehmann, and G. Scoles *J. Chem. Phys.* **112** (2000) 8409.
- [12] M. W. Schmidt, K. K. Baldridge, J. A. Boatz, S. T. Elbert, M. S. Gordon, J. J. Jensen, S. Koseki, N. Matsunaga, K. A. Nguyen, S. Su, T. L. Windus, M. Dupuis, and J. A. Montgomery, *J. Comput. Chem.* **14** (1993) 1347.

- [13] D. E. Woon *J. Chem. Phys.* **100** (1994) 2838.
- [14] S. Huzinaga and M. Klobukowski *Chem. Phys. Lett.* **212** (1993) 260.
- [15] J. Y. Mane M.Sc. Thesis, University of Alberta, Edmonton, Alberta, 2002.
- [16] T. H. Dunning, Jr. *J. Chem. Phys.* **90** (1989) 1007.
- [17] S. M. Cybulski and R. R. Toczyłowski *J. Chem. Phys.* **111** (1999) 10520.
- [18] S. F. Boys and F. Bernardi *Mol. Phys.* **37** (1979) 1529.
- [19] R. J. LeRoy *LEVEL 7.1: A Computer Program for Solving the Radial Schrödinger Equation for Bound and Quasibound Levels* University of Waterloo Chemical Physics Research Report CP-642R (2000).
- [20] A. D. Buckingham and P. G. Hibbard *Symp. Faraday Soc.* **2** (1968) 41.
- [21] E.-A. Reinsch and W. Meyer *Phys. Rev. A* **14** (1976) 915.
- [22] T. M. Miller and B. Bederson *Phys. Rev. A* **14** (1976) 1572.
- [23] H. L. Schwartz, T. M. Miller, and B. Bederson *Phys. Rev. A* **10** (1974) 1924.
- [24] I. G. Kaplan *Theory of Molecular Interactions* Elsevier: Amsterdam, 1986; p. 41.
- [25] J. M. Standard and P. R. Certain *J. Chem. Phys.* **83** (1985) 3002.
- [26] A. R. Janzen and R. A. Aziz *J. Chem. Phys.* **107** (1997) 914.
- [27] W. Schöllkopf and J. P. Toennies *J. Chem. Phys.* **104** (1996) 1155.
- [28] U. Kleinekathöfer, M. Lewerenz, and M. Mladenovic *Phys. Rev. Lett.* **83** (1999) 4717.
- [29] F. Stienkemeier, F. Meier, and H. O. Lutz *J. Chem. Phys.* **107** (1997) 10816.

Chapter 8

Final Conclusions

Although the chapters in this thesis cover a very wide range, there is a common thread throughout: the application of pseudopotential methods to calculate molecular properties. The applicability of the Model Core Potential formalism to several types of compounds, as well as its ability to study a wide variety of atomic and molecular properties, is the core focus of this thesis.

A number of conclusions can be drawn from the work presented here. The development of the iMCPs for the transition metals showed that a better parameterization method and much better atomic property calculations do not always result in greatly improved results on molecules. However, the iMCPs for the transition metals are now internally consistent with those derived for the main group elements, and the L-shell structure that these basis sets entail do give results of at least equal (and in most cases better) quality than the previous MCPs in less time. The DFT methods are not a black box, and care must be taken with the choice of functional. Several functionals should be tested in order to obtain the best results for the system under study. There is not a clear prescription for which functional is best; for example one may be superior for bond lengths, while another one for angles. There are a number of other factors that must be considered when studying transition metal complexes. Even for the first-row transition metals, relativistic effects were found to be important, especially for the metal-ligand bond lengths. The calculated vibrational frequencies are also greatly affected by relativity, but in many cases, the scalar-relativistic frequencies are further from experiment than the non-relativistic ones. This can be attributed to

the deficiencies in the approximate DFT functionals and in the use of a fairly small basis set. The potentially large effect of the underlying DFT integration grid was also studied. The use of larger grids can easily increase the required time for the calculation by an order of magnitude or more, but the results presented here indicate that this effect should at least be checked, especially for the heavier transition metals.

The iMCPs can give fairly accurate bond lengths and energetic properties for both transition metal and main group complexes with only a triple-zeta basis set and a small (2d1f or even 1d) set of polarization functions. A higher level of theory than DFT or MP2 is required for very accurate energetics, but the trends shown at the DFT level agree well with both experiment and chemical intuition. The accuracy is sufficient for complexes that contain fairly strong bonds (*e.g.* weak covalent bonds like the Xe-C bonds in $\text{Xe}(\text{C}_6\text{F}_5)_2$), and studies have shown [1, 2] the DFT method to be able to predict binding energies even for hydrogen bonds to a good degree of accuracy, if modern functionals are used.

In addition to their use on quick and fairly accurate calculations on large clusters, the MCP formalism can also be applied to high-accuracy calculations on very weakly-bonded molecules. The initial study on the rare gas-coinage metal monohalides showed that geometries calculated at the MP2 level for weakly-bound complexes showed good agreement with available experimental data, and the method could be applied to unknown compounds to predict geometries, and thus spectroscopic parameters. The wtMCPs were then pushed to the limit of current computational methodology in order to predict geometries and binding energies of very weakly bound van der Waals systems. Even when the binding energies were of the order of wavenumbers, the MCP formalism still performed very well, giving results that were very close to other high-level all-electron calculations on the systems. The work on the heavier Group 2 elements interacting with helium is the most accurate work yet available for these systems.

8.1 Future Work

There is still a lot of work that has to be done with the MCP formalism. Although all of the transition metals, and many of the main group elements have been parameterized, iMCPs have not yet been optimized for many of the main group elements or the f-block elements. The iMCPs also need to be further tested on larger systems; such a project, on antimony-oxygen-sulfur clusters, is in progress.

Well-tempered MCPs had been derived for all of the main group elements [3, 4], but these have been reoptimized for certain elements in this work in order to improve the description of the valence s orbital. The remaining main group elements will have to be covered, and the optimization of wtMCPs must be done for the transition metals. While wtMCPs were prepared for the coinage metals (Cu, Ag, and Au) wtMCPs in the studies of their monohalides, no other metal wtMCPs are available. Some additional data points may need to be calculated for the pair potentials between the heavier Group 2 metals and helium in order to minimize the extent of interpolation in the potential. This will help increase the accuracy of any molecular dynamics calculations done using these potentials. A recent paper [5] showed the importance of including iterative triples in a coupled-cluster calculation on the lighter systems (*e.g.* a full CCSDT instead of CCSD(T)), and this would be an interesting aspect to study for the heavier systems as well.

Increasing the availability of the MCPs in computational chemistry programs is also a priority. At this moment, the MCPs are only included in CADPAC [6] and the newest version of the GAMESS [7] program. The current version in the GAMESS program does not have analytical gradients implemented, so geometry optimizations either have to be done by finite difference (implemented in a development version we have on-site) or by a non-gradient TRUDGE algorithm. Development versions of both HONDO [8] and deMon [9] also include MCPs, but they are not widely available. Implementation of analytical gradients in GAMESS and the inclusion of the MCPs in the next release of deMon are the current priorities, and work is ongoing in both areas.

Implementation of the MCPs in deMon, a DFT-only program, requires a further

development in the MCPs. Currently, both the iMCPs and the wtMCPs are derived for Hartree-Fock wavefunctions (either scalar- or non-relativistic). When calculations are done using the MCPs at a correlated level, the valence electrons are correlated, but the core remains frozen in its uncorrelated state. It was suggested [10], that pseudopotentials derived at the DFT level give different bond lengths and molecular properties than those derived at the HF level. To test this hypothesis, we are about to parameterize both iMCPs and wtMCPs using a DFT method. This will allow us to test the effect of core correlation on molecular properties.

8.2 Final Comments

The explosive growth of computational chemistry is primarily due to two factors: growth in computing power, and availability of software for fast, accurate calculations on molecular systems. Development of methods that improve the reliability and speed of calculations is thus very important to further growth of the field. The MCP methods have the potential to accelerate all types of calculations, from high-accuracy calculations on atoms and diatomic molecules, to transition metal complexes, to hybrid quantum mechanics/molecular mechanics (QM/MM) studies of proteins. It is this sort of developments that will facilitate the further growth of computational chemistry well into the future.

Bibliography

- [1] H. Guo, N. Gresh, B. P. Roques, and D. R. Salahub *J. Phys. Chem. B* **104** (2000) 9746.
- [2] O. Lukin and J. Leszczynski *J. Phys. Chem. A* **106** (2002) 6775.
- [3] J. Y. Mane M.Sc. Thesis, University of Alberta, Edmonton, Alberta, 2002.
- [4] J. Y. Mane and M. Klobukowski *J. Mol. Struct. (Theochem)* **547** (2001) 163.
- [5] R. J. Hinde *J. Phys. B* **36** (2003) 3119.
- [6] CADPAC version 6.3: The Cambridge Analytic Derivatives Package Issue 6, Cambridge, 1995. A suite of quantum chemistry programs developed by R. D. Amos with contributions from I. L. Alberts, J. S. Andrews, S. M. Colwell, N. C. Handy, D. Jayatilaka, P. J. Knowles, R. Kobayashi, K. E. Laidig, G. Laming, A. M. Lee, P. E. Maslen, C. W. Murray, J. E. Rice, E. D. Simandiras, A. J. Stone, M.-D. Su, and D. J. Tozer.
- [7] M. W. Schmidt, K. K. Baldridge, J. A. Boatz, S. T. Elbert, M. S. Gordon, J. J. Jensen, S. Koseki, N. Matsunaga, K. A. Nguyen, S. Su, T. L. Windus, M. Dupuis, and J. A. Montgomery *J. Comput. Chem.* **14** (1993) 1347.
- [8] M. Dupuis, A. Marquez, and E.R. Davidson, "HONDO 2000", 2000, based on HONDO 95.3, M. Dupuis, A. Marquez, and E.R. Davidson Quantum Chemistry Program Exchange (QCPE), Indiana University, Bloomington, IN 47405.
- [9] StoBe-deMon version 1.0, K. Hermann and L. G. M. Pettersson, M. E. Casida, C. Daul, A. Goursot, A. Koester, E. Proynov, A. St-Amant, and D. R. Salahub. Contributing authors: V. Carravetta, H. Duarte, N. Godbout, J. Guan, C. Jamorski,

M. Leboeuf, V. Malkin, O. Malkina, M. Nyberg, L. Pedocchi, F. Sim, L. Triguero, and A. Vela StoBe Software, 2002.

- [10] P. Calaminici, A. M. Köster, T. Carrington, Jr., P.-N. Roy, N. Russo, and D. R. Salahub *J. Chem. Phys.* **114** (2001) 4036.

Appendix A

Parameterization and Testing Data for the Improved Model Core Potentials

A.1 Reference Data for the First-Row Transition Metals

The optimized values of f_{proj} (see Eqn. (1.77)) for the iMCPs are shown in parentheses.

ScO	
WTBS	1.656 Å
iMCP (5.0)	1.667 Å
sMCP	1.619 Å

ScF	
WTBS	1.819 Å
iMCP (5.0)	1.814 Å
sMCP	1.815 Å

ScF ₃	
WTBS	1.852 Å
iMCP (5.0)	1.849 Å
sMCP	1.845 Å

TiN		
WTBS		1.502 Å
iMCP (4.5)		1.506 Å
sMCP		1.476 Å

TiF ₄		
WTBS		1.736 Å
iMCP (4.5)		1.737 Å
sMCP		1.722 Å

TiCl ₄		
WTBS		2.179 Å
iMCP (4.5)		2.182 Å
sMCP		2.167 Å

VOF ₃			
WTBS	V-O		1.489 Å
	V-F		1.711 Å
iMCP (2.5)	V-O		1.494 Å
	V-F		1.709 Å
sMCP	V-O		1.467 Å
	V-F		1.709 Å

VF ₅			
WTBS	V-F _{ax}		1.720 Å
	V-F _{eq}		1.673 Å
iMCP (2.5)	V-F _{ax}		1.720 Å
	V-F _{eq}		1.670 Å
sMCP	V-F _{ax}		1.715 Å
	V-F _{eq}		1.667 Å

VOCl ₃			
WTBS	V-O		1.488 Å
	V-Cl		2.148 Å
iMCP (2.5)	V-O		1.492 Å
	V-Cl		2.147 Å
sMCP	V-O		1.466 Å
	V-Cl		2.150 Å

Cr(NO) ₄			
WTBS	Cr-N		1.701 Å
	N-O		1.112 Å
iMCP (1.4)	Cr-N		1.701 Å
	N-O		1.110 Å
sMCP	Cr-N		1.706 Å
	N-O		1.110 Å

CrO ₄ ²⁻	
WTBS	1.606 Å
iMCP (1.4)	1.609 Å
sMCP	1.603 Å

CrO ₂ F ₂			
WTBS	Cr-O		1.483 Å
	Cr-F		1.699 Å
iMCP (1.4)	Cr-O		1.479 Å
	Cr-F		1.700 Å
sMCP	Cr-O		1.475 Å
	Cr-F		1.700 Å

CrO ₂ Cl ₂			
WTBS	Cr-O		1.486 Å
	Cr-Cl		2.130 Å
iMCP (1.4)	Cr-O		1.483 Å
	Cr-Cl		2.132 Å
sMCP	Cr-O		1.478 Å
	Cr-Cl		2.141 Å

MnO ₄ ⁻	
WTBS	1.550 Å
iMCP (1.05)	1.548 Å
sMCP	1.540 Å

MnO ₃ F			
WTBS	Mn-O	1.505 Å	
	Mn-F	1.745 Å	
iMCP (1.4)	Mn-O	1.505 Å	
	Mn-F	1.762 Å	
sMCP	Mn-O	1.494 Å	
	Mn-F	1.737 Å	

MnO	
WTBS	1.754 Å
iMCP (1.05)	1.748 Å
sMCP	1.729 Å

Fe(CO) ₅			
WTBS	Fe-C _{ax}	2.077 Å	
	Fe-C _{eq}	1.891 Å	
	C-O _{ax}	1.102 Å	
iMCP(2.1)	C-O _{eq}	1.113 Å	
	Fe-C _{ax}	2.081 Å	
	Fe-C _{eq}	1.904 Å	
sMCP	C-O _{ax}	1.102 Å	
	C-O _{eq}	1.113 Å	
	Fe-C _{ax}	2.070 Å	
	Fe-C _{eq}	1.908 Å	
	C-O _{ax}	1.098 Å	
	C-O _{eq}	1.108 Å	

FeF ₂	
WTBS	1.758 Å
iMCP (2.1)	1.752 Å
sMCP	1.742 Å

FeCl ₂	
WTBS	2.197 Å
iMCP (2.1)	2.191 Å
sMCP	2.197 Å

FeO ₂	
WTBS	1.513 Å
iMCP (2.1)	1.517 Å
sMCP	1.499 Å

FeN	
WTBS	1.505 Å
iMCP (2.1)	1.499 Å
sMCP	1.488 Å

CoO	
WTBS	1.731 Å
iMCP (1.8)	1.738 Å
sMCP	1.721 Å

CoF ₃	
WTBS	1.742 Å
iMCP (1.8)	1.739 Å
sMCP	1.736 Å

CoH(CO) ₄			
WTBS	Co-C _{ax}	2.078 Å	
	Co-C _{eq}	2.035 Å	
	Co-H	1.655 Å	
	C-O _{ax}	1.099 Å	
	C-O _{eq}	1.104 Å	
iMCP (1.8)	Co-C _{ax}	2.079 Å	
	Co-C _{eq}	2.054 Å	
	Co-H	1.653 Å	
	C-O _{ax}	1.099 Å	
	C-O _{eq}	1.104 Å	
sMCP	Co-C _{ax}	2.080 Å	
	Co-C _{eq}	2.062 Å	
	Co-H	1.645 Å	
	C-O _{ax}	1.095 Å	
	C-O _{eq}	1.099 Å	

CoNO(CO) ₃			
WTBS	Co-C	1.968 Å	
	Co-N	1.598 Å	
	C-O	1.101 Å	
	N-O	1.145 Å	
iMCP (1.8)	Co-C	1.974 Å	
	Co-N	1.595 Å	
	C-O	1.102 Å	
	N-O	1.140 Å	
sMCP	Co-C	1.990 Å	
	Co-N	1.592 Å	
	C-O	1.097 Å	
	N-O	1.140 Å	

NiO	
WTBS	1.702 Å
iMCP (1.5)	1.704 Å
sMCP	1.695 Å

NiCl ₃ ⁻	
WTBS	2.299 Å
iMCP (1.5)	2.291 Å
sMCP	2.308 Å

NiF ₆ ²⁻	
WTBS	1.762 Å
iMCP (1.5)	1.762 Å
sMCP	1.765 Å

Ni(CO) ₄		
WTBS	Ni-C	1.927 Å
	C-O	1.106 Å
iMCP (1.5)	Ni-C	1.931 Å
	C-O	1.107 Å
sMCP	Ni-C	1.952 Å
	C-O	1.102 Å

CuH	
WTBS	1.568 Å
iMCP (2.3)	1.568 Å
sMCP	1.567 Å

CuF	
WTBS	1.838 Å
iMCP (2.3)	1.842 Å
sMCP	1.841 Å

CuCl	
WTBS	2.188 Å
iMCP (2.3)	2.183 Å
sMCP	2.191 Å

CuO (² Σ)	
WTBS	1.882 Å
iMCP (2.3)	1.884 Å
sMCP	1.872 Å

CuO (² Π)	
WTBS	1.885 Å
iMCP (2.3)	1.890 Å
sMCP	1.886 Å

Cu(CH ₃) ₂ ⁻			
WTBS	Cu-C	2.072 Å	
	C-H	1.096 Å	
iMCP (2.3)	Cu-C	2.072 Å	
	C-H	1.099 Å	
sMCP	Cu-C	2.078 Å	
	C-H	1.096 Å	

ZnH	
WTBS	1.619 Å
iMCP (1.3)	1.621 Å
sMCP	1.632 Å

ZnH ⁺	
WTBS	1.549 Å
iMCP (1.3)	1.551 Å
sMCP	1.546 Å

ZnF	
WTBS	1.798 Å
iMCP (1.3)	1.800 Å
sMCP	1.807 Å

ZnCl	
WTBS	2.195 Å
iMCP (1.3)	2.188 Å
sMCP	2.205 Å

ZnO	
WTBS	1.763 Å
iMCP (1.3)	1.770 Å
sMCP	1.785 Å

Zn(CH ₃) ₂		
WTBS	Zn-C	1.999 Å
	C-H	1.087 Å
iMCP (1.3)	Zn-C	1.996 Å
	C-H	1.089 Å
sMCP	Zn-C	2.002 Å
	C-H	1.087 Å

A.2 Testing Data for the First-Row Transition Metals

Doubly and triply degenerate vibrations are indicated by x2 and x3, respectively. Axial and equatorial bonds are denoted by ax and eq, respectively. The tables also contain data calculated using other pseudopotentials. The CEP column refers to the Compact Effective Potentials of Stevens *et al.* and SDB refers to the potentials derived by the groups at Stuttgart-Dresden-Bonn. Both types of potentials are described in more detail in Section 1.5.1.

ScF geom		NR iMCP	SR iMCP	NR sMCP	CEP	SDB
Exp.	1.788					
RHF		1.799	1.798	1.794	1.819	1.817
B3P86		1.752	1.750	1.737	1.792	1.749
MP2		1.776	1.777	1.763	1.805	1.799

ScF freq		NR iMCP	SR iMCP	NR sMCP	CEP	SDB
Exp.	736					
RHF		754	761	705	716	748
B3P86		784	790	741	714	738
MP2		789	790	747	718	760

ScF ₃ geom		NR iMCP	SR iMCP	NR sMCP	CEP	SDB
Exp.	1.847					
RHF		1.841	1.841	1.836	1.858	1.851
B3P86		1.816	1.815	1.803	1.847	1.836
MP2		1.850	1.850	1.840	1.864	1.851

ScF ₃ freq		NR iMCP	SR iMCP	NR sMCP	CEP	SDB
Exp.		119				
	x2	165				
		634				
	x2	723				
RHF		146	147	147	143	128
	x2	187	186	183	181	168
		675	676	644	627	649
	x2	767	770	730	730	766
B3P86		21	31	77	94	79
	x2	174	174	178	165	164
		661	663	638	615	652
	x2	752	755	723	719	774
MP2		140	85	108	122	108
	x2	181	167	172	164	160
		645	644	625	605	636
	x2	732	730	709	704	749

TiF ₄ geom		NR iMCP	SR iMCP	NR sMCP	CEP	SDB
Exp.	1.745					
RHF		1.727	1.727	1.716	1.742	1.740
B3P86		1.725	1.725	1.709	1.751	1.743
MP2		1.746	1.746	1.731	1.759	1.754

TiF ₄ freq		NR iMCP	SR iMCP	NR sMCP	CEP	SDB
Exp.	x2	185				
	x3	209				
		712				
	x3	793				
RHF	x2	221	221	224	204	197
	x3	266	266	266	250	238
		825	826	775	746	768
	x3	889	892	826	820	861
B3P86	x2	202	202	205	195	178
	x3	227	227	228	226	200
		768	768	739	705	736
	x3	841	844	803	797	843
MP2	x2	194	215	201	187	187
	x3	217	248	225	216	214
		752	755	723	697	727
	x3	830	839	792	781	829

TiCl ₄ geom		NR iMCP	SR iMCP	NR sMCP	CEP	SDB
Exp.	2.170					
RHF		2.184	2.183	2.168	2.187	2.155
B3P86		2.153	2.151	2.138	2.180	2.151
MP2		2.193	2.191	2.171	2.181	2.144

TiCl ₄ freq		NR iMCP	SR iMCP	NR sMCP	CEP	SDB
Exp.	x2	114				
	x3	136				
		389				
RHF	x3	498				
	x2	125	125	128	123	125
	x3	156	156	158	155	156
B3P86		421	420	423	410	417
	x3	518	518	515	515	515
	x2	116	116	119	117	121
	x3	135	135	139	141	144
		397	398	401	386	394
MP2	x3	511	512	510	504	508
	x2	117	112	119	114	122
	x3	138	130	137	131	142
		383	381	387	388	402
	x3	506	504	506	508	527

VOF ₃ geom		NR iMCP	SR iMCP	NR sMCP	CEP	SDB
Exp.	V-O	1.569				
	V-F	1.729				
RHF	V-O	1.504	1.509	1.477	1.499	1.498
	V-F	1.686	1.693	1.700	1.712	1.708
B3P86	V-O	1.542	1.542	1.520	1.555	1.551
	V-F	1.695	1.694	1.695	1.723	1.715
MP2	V-O	1.594	1.600	1.592	1.611	
	V-F	1.749	1.747	1.748	1.765	

VOF ₃ freq		NR iMCP	SR iMCP	NR sMCP	CEP	SDB
Exp.	x2	204				
		256				
	x2	304				
		720				
	x2	801				
		1055				
RHF	x2	237	238	235	245	220
		300	301	292	289	280
	x2	369	363	379	367	354
		829	833	780	773	793
	x2	889	894	841	849	873
		1307	1313	1332	1323	1304
B3P86	x2	212	214	221	203	202
		266	268	272	255	255
	x2	326	327	335	315	313
		781	785	765	719	746
	x2	854	859	845	804	836
		1178	1185	1184	1151	1159
MP2	x2					
	x2					
	x2					

VF ₅ geom		NR iMCP	SR iMCP	NR sMCP	CEP	SDB
Exp.	ax	1.734				
	eq	1.703				
RHF	ax	1.709	1.708	1.707	1.721	1.722
	eq	1.660	1.659	1.658	1.677	1.678
B3P86	ax	1.722	1.721	1.718	1.749	1.740
	eq	1.680	1.679	1.677	1.711	1.703
MP2	ax	1.746	1.744	1.742	1.756	1.758
	eq	1.715	1.712	1.713	1.730	1.732

VF ₅ freq		NR iMCP	SR iMCP	NR sMCP	CEP	SDB	
Exp.	x2	110					
		282					
		331					
	x2	336					
		608					
		718					
		784					
RHF	x2	810					
	x2	157	157	159	180	132	
	x2	334	335	335	352	311	
		381	383	377	381	368	
	x2	382	384	382	381	369	
		695	698	656	664	669	
		783	784	776	814	821	
		878	882	833	843	835	
	x2	937	942	876	896	908	
		120	121	124	126	104	
B3P86	x2	292	293	292	308	272	
		348	350	347	291	336	
	x2	354	356	355	343	339	
		641	645	632	611	629	
		746	748	751	726	743	
		787	791	765	775	802	
	x2	864	868	845	813	845	
	MP2	x2	136	91	95	154	105
		x2	297	274	274	311	271
			344	337	332	355	338
x2		346	343	340	355	338	
		624	618	600	610	607	
		721	719	703	687	700	
		722	727	739	793	792	
x2		828	817	782	805	810	

VOCl ₃ geom		NR iMCP	SR iMCP	NR sMCP	CEP	SDB
Exp.	V-O	1.570				
	V-Cl	2.142				
RHF	V-O	1.501	1.502	1.473	1.499	1.496
	V-Cl	2.142	2.141	2.145	2.151	2.124
B3P86	V-O	1.538	1.538	1.516	1.555	1.550
	V-Cl	2.111	2.110	2.116	2.145	2.120
MP2	V-O	1.621	1.626	1.616	1.641	
	V-Cl	2.185	2.185	2.182	2.185	

VOCl ₃ freq		NR iMCP	SR iMCP	NR sMCP	CEP	SDB		
Exp.	x2	129						
		165						
	x2	249						
		408						
	x2	504						
RHF	x2	1035						
		146	147	145	142	141		
		180	181	185	187	185		
		x2	288	288	298	297	295	
		437	437	438	445	437		
	x2	529	530	534	535	524		
		1294	1301	1311	1300	1286		
		B3P86	x2	131	132	129	128	133
			176	177	173	168	172	
			x2	264	265	267	258	261
427	428		420	415	420			
MP2	x2	523	524	517	511	515		
		1167	1173	1170	1131	1141		
	x2			124	121			
				166	162			
				259	236			
x2			375	383				
x2			491	487				
			1137	1135				

CrO ₄ ²⁻ geom		NR iMCP	SR iMCP	NR sMCP	CEP	SDB
Exp.	1.66					
RHF		1.601	1.599	1.602	1.612	1.603
B3P86		1.628	1.625	1.629	1.657	1.643
MP2		1.675	1.677	1.680	1.702	

CrO ₄ ²⁻ freq		NR iMCP	SR iMCP	NR sMCP	CEP	SDB
Exp.	x2	349				
	x3	378				
		846				
RHF	x3	890				
	x2	403	406	413	408	396
	x3	455	457	464	458	452
		1032	1038	1028	1003	1004
B3P86	x3	983	991	987	978	981
	x2	353	355	354	342	335
	x3	398	400	397	385	385
		914	918	921	873	889
MP2	x3	909	914	923	898	919
	x2	331	329		313	
	x3	374	374		362	
		1095	1064		989	
	x3	1088	1072		1045	

CrO ₂ F ₂ geom		NR iMCP	SR iMCP	NR sMCP	CEP	SDB
Exp.	Cr-O	1.575				
	Cr-F	1.720				
RHF	Cr-O	1.485	1.485	1.480	1.495	1.487
	Cr-F	1.678	1.675	1.690	1.695	1.694
B3P86	Cr-O	1.524	1.522	1.522	1.551	1.542
	Cr-F	1.682	1.678	1.688	1.712	1.702
MP2	Cr-O	1.642	1.642		1.671	
	Cr-F	1.753	1.753		1.788	

CrO ₂ F ₂ freq	NR iMCP	SR iMCP	NR sMCP	CEP	SDB
Exp.	208				
	259				
	274				
	304				
	364				
	727				
	789				
	1006				
	1016				
RHF	254	255	257	250	243
	331	333	355	336	323
	368	365	365	355	341
	392	385	435	404	381
	505	490	535	502	493
	825	831	812	808	811
	852	856	848	846	849
	1273	1278	1268	1272	1260
	1313	1322	1327	1307	1296
B3P86	235	237	230	223	221
	300	303	301	288	286
	323	325	312	305	297
	340	341	346	328	324
	441	443	453	429	429
	771	773	763	747	760
	813	814	808	803	817
	1158	1164	1152	1120	1131
	1159	1165	1158	1133	1145

CrO ₂ Cl ₂ geom	NR iMCP	SR iMCP	NR sMCP	CEP	SDB
Exp.	Cr-O 1.581				
	Cr-Cl 2.126				
RHF	Cr-O 1.485	1.485	1.481	1.497	1.489
	Cr-Cl 2.119	2.118	2.129	2.126	2.104
B3P86	Cr-O	1.523	1.523	1.553	1.544
	Cr-Cl	2.093	2.097	2.120	2.098
MP2	Cr-O 1.689	1.695	1.689	1.711	
	Cr-Cl 2.114	2.107	2.114	2.131	

CrO ₂ Cl ₂ freq	NR iMCP	SR iMCP	NR sMCP	CEP	SDB
Exp.	140				
	215				
	224				
	257				
	356				
	475				
	500				
	995				
	1002				
RHF	148	150	149	153	156
	261	262	276	272	260
	270	273	304	283	272
	301	302	347	332	318
	398	400	404	413	405
	516	517	559	548	526
	548	550	576	560	554
	1237	1242	1236	1247	1228
	1303	1314	1312	1292	1279
B3P86		149	146	143	149
		233	233	228	229
		245	245	237	241
		286	284	279	281
		385	385	377	375
		503	506	488	492
		524	527	517	511
		1147	1129	1103	1118
		1153	1149	1115	1127

MnO ₄ ⁻ geom	NR iMCP	SR iMCP	NR sMCP	CEP	SDB
Exp.	1.629				
RHF	1.535	1.533	1.538	1.550	1.542
B3P86	1.567	1.565	1.569	1.599	1.587
MP2	1.566	1.570	1.570	1.589	

MnO ₄ ⁻ freq		NR iMCP	SR iMCP	NR sMCP	CEP	SDB
Exp.	x2	346				
	x3	386				
		834				
RHF	x3	902				
	x2	443	433	428	425	415
	x3	501	484	480	477	474
		1092	1076	1063	1057	1029
B3P86	x3	1055	975	958	1025	968
	x2	391	394	391	372	371
	x3	441	441	438	419	423
		998	988	982	936	949
	x3	1022	1007	997	992	1005

Fe(CO) ₅ geom		NR iMCP	SR iMCP	NR sMCP	CEP	SDB
Exp.	Fe-C _{ax}	1.807				
	Fe-C _{eq}	1.827				
	C-O _{ax}	1.152				
	C-O _{eq}	1.152				
RHF	Fe-C _{ax}	2.060	2.038	2.045	2.052	2.063
	Fe-C _{eq}	1.897	1.882	1.898	1.880	1.879
	C-O _{ax}	1.103	1.103	1.097	1.106	1.096
	C-O _{eq}	1.114	1.114	1.107	1.117	1.107
B3P86	Fe-C _{ax}	1.788	1.783	1.794	1.813	1.804
	Fe-C _{eq}	1.785	1.780	1.787	1.805	1.795
	C-O _{ax}	1.136	1.136	1.130	1.142	1.132
	C-O _{eq}	1.140	1.140	1.134	1.146	1.136
MP2	Fe-C _{ax}	1.694	1.693	1.704	1.693	
	Fe-C _{eq}	1.778	1.775	1.768	1.784	
	C-O _{ax}	1.165	1.165	1.155	1.185	
	C-O _{eq}	1.156	1.156	1.147	1.173	

Fe(CO) ₅ freq		NR iMCP	SR iMCP	NR sMCP	CEP	SDB
Exp.	x2	74				
	x2	97				
		100				
	x2	105				
	x2	375				
		383				
		413				
	x2	429				
		443				
		475				
	x2	493				
	x2	553				
		619				
	x2	645				
	x2	2013				
		2034				
		2042				
	2121					
RHF	x2	76	77	70	75	84
	x2	104	107	107	102	111
		122	125	121	123	150
	x2	127	129	133	118	135
	x2	240	253	257	251	248
		346	359	355	349	361
		400	414	400	423	418
	x2	407	421	409	441	433
		402	416	401	432	422
		410	417	402	438	443
	x2	486	499	490	507	506
	x2	532	547	530	548	543
		555	572	547	577	566
	x2	558	573	554	588	586
	x2	2261	2257	2289	2267	2300
		2330	2328	2353	2323	2389
		2399	2395	2419	2396	2469
	2423	2421	2441	2412	2489	

Fe(CO) ₅ freq (cont'd.)		NR iMCP	SR iMCP	NR sMCP	CEP	SDB
B3P86	x2	58	61	58	58	57
	x2	104	104	109	106	106
		111	111	111	121	114
	x2	112	115	121	111	112
	x2	383	397	393	387	384
		392	402	394	390	388
		422	433	444	429	428
	x2	450	465	463	461	461
		460	468	470	455	451
		461	477	486	495	489
	x2	485	495	507	501	500
	x2	594	601	584	576	584
		637	650	640	641	639
	x2	675	682	683	676	679
	x2	2060	2061	2093	2083	2114
		2080	2079	2113	2098	2146
		2090	2090	2123	2111	2148
	2170	2171	2188	2170	2225	

CoH(CO) ₄ geom		NR iMCP	SR iMCP	NR sMCP	CEP	SDB
Exp.	Co-H	1.556				
	Co-C _{ax}	1.764				
	Co-C _{eq}	1.818				
	C-O _{ax}	1.141				
	C-O _{eq}	1.141				
RHF	Co-H	1.654	1.633	1.647	1.631	1.643
	Co-C _{ax}	2.049	2.019	2.050	2.041	2.056
	Co-C _{eq}	2.046	1.998	2.051	1.992	2.012
	C-O _{ax}	1.100	1.101	1.095	1.104	1.093
	C-O _{eq}	1.104	1.105	1.099	1.108	1.098
B3P86	Co-H	1.475	1.455	1.459	1.472	1.471
	Co-C _{ax}	1.791	1.762	1.793	1.804	1.799
	Co-C _{eq}	1.791	1.760	1.782	1.793	1.784
	C-O _{ax}	1.148	1.137	1.128	1.140	1.130
	C-O _{eq}	1.149	1.135	1.131	1.142	1.133

CoH(CO) ₄ freq		NR iMCP	SR iMCP	NR sMCP	CEP	SDB
RHF	x2	90	84	85	91	88
	x2	115	112	112	117	113
		126	119	128	138	123
		202	218	198	231	213
		256	272	263	282	262
	x2	241	272	243	297	274
		334	356	351	376	337
	x2	377	405	390	423	395
	x2	413	425	415	445	413
		436	466	435	468	449
	x2	472	485	473	486	463
	x2	810	844	822	853	829
		1542	1588	1557	1610	1585
	x2	2388	2379	2412	2374	2447
		2409	2404	2426	2389	2469
		2446	2443	2464	2432	2513
	B3P86	x2	66	74	71	71
x2		96	101	99	96	97
		100	112	109	106	108
		344	379	363	362	357
		400	435	432	425	424
x2		325	371	357	353	346
		437	483	480	481	472
x2		384	432	423	437	427
x2		490	530	520	517	517
		550	591	560	569	563
x2		562	601	569	572	577
x2		713	762	772	760	753
		1943	2062	2059	2060	2025
x2		1960	2084	2105	2111	2142
		2008	2125	2139	2118	2172
		2047	2168	2181	2168	2228

Ni(CO) ₄ geom		NR iMCP	SR iMCP	NR sMCP	CEP	SDB
Exp.	Ni-C	1.838				
	C-O	1.141				
RHF	Ni-C	1.927	1.899	1.947	1.909	1.904
	C-O	1.107	1.108	1.101	1.111	1.100
B3P86	Ni-C	1.809	1.793	1.827	1.827	1.817
	C-O	1.134	1.135	1.128	1.140	1.131
MP2	Ni-C			1.784	1.799	
	C-O			1.143	1.171	

Ni(CO) ₄ freq		NR iMCP	SR iMCP	NR sMCP	CEP	SDB	
Exp.	x2	62					
	x3	79					
	x3	300					
		371					
	x2	380					
	x3	423					
	x3	459					
	x3	2092					
		2154					
	RHF	x2	97	91	95	90	60
		x3	122	117	120	115	76
		x3	260	294	237	330	302
			284	303	288	322	303
x2		427	454	406	465	445	
x3		313	329	291	358	306	
x3		413	440	394	457	432	
x3		2347	2343	2368	2339	2407	
		2408	2408	2430	2405	2474	
B3P86		x2	63	66	64	75	64
	x3	81	84	78	98	81	
	x3	311	325	287	310	298	
		373	388	375	395	384	
	x2	487	504	465	480	486	
	x3	407	424	407	442	439	
	x3	479	494	459	478	474	
	x3	2111	2111	2120	2127	2173	
		2173	2174	2184	2171	2237	

CuH geom		NR iMCP	SR iMCP	NR sMCP	CEP	SDB
Exp.	1.462					
RHF		1.568	1.540	1.567	1.539	1.538
B3P86		1.468	1.444	1.458	1.458	1.456
MP2		1.459	1.432	1.443	1.443	

CuH freq		NR iMCP	SR iMCP	NR sMCP	CEP	SDB
Exp.	1941					
RHF		1636	1693	1621	1706	1732
B3P86		1872	1953	1886	1968	1934
MP2		1795	1894	1789	2058	

CuF geom		NR iMCP	SR iMCP	NR sMCP	CEP	SDB
Exp.	1.745					
RHF		1.830	1.812	1.828	1.808	1.801
B3P86		1.762	1.741	1.749	1.745	1.745
MP2		1.785	1.757	1.773	1.747	

CuF freq		NR iMCP	SR iMCP	NR sMCP	CEP	SDB
Exp.	623					
RHF		552	561	555	570	601
B3P86		588	610	591	628	633
MP2		568	590	548	613	

CuCl geom		NR iMCP	SR iMCP	NR sMCP	CEP	SDB
Exp.	2.051					
RHF		2.179	2.159	2.191	2.166	2.149
B3P86		2.070	2.049	2.080	2.071	2.065
MP2		2.109	2.082	2.122	2.081	

CuCl freq		NR iMCP	SR iMCP	NR sMCP	CEP	SDB
Exp.	415					
RHF		358	366	353	362	373
B3P86		400	415	392	407	410
MP2		396	408	382	397	

Cu(CH ₃) ₂ ⁻ geom		NR iMCP	SR iMCP	NR sMCP	CEP	SDB
Exp.	Cu-C	1.935				
	C-H					
RHF	Cu-C	2.068	2.050	2.078	2.044	2.022
	C-H	1.097	1.097	1.096	1.099	1.092
B3P86	Cu-C	1.954	1.940	1.962	1.957	1.946
	C-H	1.104	1.105	1.104	1.107	1.101
MP2	Cu-C	1.944	1.932	1.950	1.927	
	C-H	1.102	1.102	1.101	1.103	

Cu(CH ₃) ₂ ⁻ freq		NR iMCP	SR iMCP	NR sMCP	CEP	SDB
RHF		15	130	156	99	107
	x2	126	136	134	146	146
		375	383	375	396	414
		434	444	433	453	485
	x2	511	519	522	550	559
	x2	588	600	599	626	649
		1188	1195	1204	1209	1249
		1191	1197	1207	1217	1254
	x2	1561	1562	1569	1565	1596
	x2	1561	1562	1570	1566	1597
		3040	3041	3028	3022	3084
		3044	3045	3032	3027	3090
	x2	3080	3079	3061	3050	3122
	x2	3080	3080	3062	3051	3123
B3P86		23	22	30	-11	13
	x2	136	139	136	142	152
		443	453	441	452	463
		489	496	482	512	511
	x2	514	520	515	528	542
	x2	611	619	616	626	661
		1106	1111	1120	1111	1140
		1111	1116	1124	1122	1144
	x2	1442	1441	1447	1438	1463
	x2	1443	1442	1448	1438	1463
		2917	2915	2901	2905	2956
		2923	2921	2911	2911	2965
	x2	2977	2974	2957	2957	3029
	x2	2978	2975	2957	2957	3031
MP2		-38	-41	21		
	x2	138	139	140		
		468	485	472		
		510	527	498		
	x2	558	566	561		
	x2	658	668	664		
		1155	1160	1182		
		1200	1202	1183		
	x2	1461	1460	1468		
	x2	1462	1462	1469		
		2977	2975	2970		
		2980	2978	2975		
	x2	3053	3051	3038		
	x2	3055	3053	3040		

Zn(CH ₃) ₂ geom		NR iMCP	SR iMCP	NR sMCP	CEP	SDB
Exp.	Zn-C	1.929				
	C-H	1.090				
RHF	Zn-C	1.993	1.977	2.001	1.977	1.973
	C-H	1.088	1.088	1.086	1.086	1.083
B3P86	Zn-C	1.933	1.917	1.948	1.932	1.932
	C-H	1.094	1.094	1.093	1.094	1.093
MP2	Zn-C	1.944	1.928	1.954	1.929	
	C-H	1.093	1.093	1.092	1.092	

Zn(CH ₃) ₂ freq		NR iMCP	SR iMCP	NR sMCP	CEP	SDB
Exp.		0				
	x2	134				
		503				
		613				
	x2	620				
	x2	704				
		1157				
		1183				
	x2	1301				
	x2	1434				
	x2	2843				
		2900				
		2915				
	x2					
RHF		38	39	189	199	85
	x2	134	134	144	151	142
		488	496	491	498	502
		583	591	590	602	608
	x2	666	663	671	689	683
	x2	744	746	751	768	770
		1304	1310	1306	1317	1344
		1307	1312	1309	1318	1346
	x2	1570	1570	1572	1573	1587
	x2	1572	1573	1575	1577	1591
	x2	3206	3208	3190	3188	3251
		3135	3135	3124	3126	3176
		3138	3139	3128	3130	3181
	x2	3207	3209	3192	3192	3251
B3P86		58	58	116	52	51
	x2	137	140	140	144	148
		493	501	491	523	510
		582	586	593	614	615
	x2	632	638	634	638	651
	x2	725	736	726	731	747
		1199	1204	1198	1189	1219
		1199	1205	1201	1211	1232
	x2	1454	1454	1451	1451	1461
	x2	1455	1455	1457	1457	1466
	x2	3106	3106	3090	3083	3146
		3021	3022	3003	3005	3055
		3024	3024	3011	3010	3062
	x2	3106	3106	3091	3084	3148

Zn(CH ₃) ₂ freq (cont'd.)		NR iMCP	SR iMCP	NR sMCP	CEP	SDB
MP2		18	-9	-24		
	x2	123	127	142		
		503	514	514		
		591	600	613		
	x2	650	657	648		
	x2	736	747	739		
		1236	1240	1247		

Zn(CH ₃) ₂ freq		NR iMCP	SR iMCP	NR sMCP	CEP	SDB
MP2		1236	1242	1248		
	x2	1474	1476	1475		
	x2	1474	1477	1481		
	x2	3158	3162	3146		
		3059	3064	3056		
		3061	3064	3057		
	x2	3159	3162	3146		

Zn(CH ₃) ₄ ²⁻ geom		NR iMCP	SR iMCP	NR sMCP	CEP	SDB
Exp.	Zn-C	2.07				
	C-H					
RHF	Zn-C	2.253	2.240	2.261	2.237	2.233
	C-H	1.100	1.100	1.100	1.100	1.096
B3P86	Zn-C	2.166	2.151	2.187	2.165	2.176
	C-H	1.107	1.107	1.108	1.108	1.105
MP2	Zn-C		2.144	2.175	2.164	
	C-H		1.104	1.104	1.111	

Zn(CH ₃) ₄ ²⁻ freq	NR iMCP	SR iMCP	NR sMCP	CEP	SDB
RHF	75	77	195	77	99
x3	82	84	141	84	102
x2	101	102	113	106	101
x3	123	124	190	132	127
x3	292	290	288	297	294
	334	336	329	341	339
x3	430	436	477	449	454
x2	553	560	588	578	594
x3	570	576	613	597	612
x3	1112	1113	1164	1150	1199
	1117	1118	1167	1155	1208
x2	1545	1545	1557	1555	1590
x3	1545	1545	1557	1556	1590
x3	1552	1552	1566	1566	1598
x3	3006	3006	3006	2983	3045
	3011	3011	3013	2992	3053
x3	3042	3042	3007	3009	3071
x2	3044	3044	3009	3013	3074
x3	3050	3050	3014	3019	3081
B3P86	44	49	47	60	86
x3	53	58	57	72	90
x2	105	106	96	100	97
x3	125	127	116	122	122
x3	320	321	304	323	304
	338	343	340	345	348
x3	432	438	424	455	431
x2	551	558	545	570	584
x3	561	566	562	585	591
x3	1018	1020	1054	1066	1063
	1035	1035	1058	1075	1081
x2	1430	1429	1444	1444	1462
x3	1430	1430	1445	1445	1463
x3	1438	1438	1455	1456	1472
x3	2890	2889	2851	2849	2931
	2898	2897	2864	2863	2938
x3	2961	2959	2915	2910	2989
x2	2963	2961	2917	2912	2992
x3	2968	2967	2923	2918	2997

A.3 Reference Data for the Second- and Third-Row Transition Metals

YO	
WTBS	1.793 Å
iMCP (2.2)	1.792 Å
sMCP	1.795 Å

ZrN	
WTBS	1.654 Å
iMCP (1.9)	1.653 Å
sMCP	1.661 Å

NbN	
WTBS	1.612 Å
iMCP (1.4)	1.613 Å
sMCP	1.619 Å

MoO ₂	
WTBS	1.707 Å
iMCP (1.3)	1.709 Å
sMCP	1.702 Å

TcO	
WTBS	1.742 Å
iMCP (1.05)	1.743 Å
sMCP	1.752 Å

RuCO ⁻		
WTBS	Ru-C	1.871 Å
	C-O	1.124 Å
iMCP (1.8)	Ru-C	1.873 Å
	C-O	1.125 Å
sMCP	Ru-C	1.858 Å
	C-O	1.126 Å

RhC	
WTBS	1.584 Å
iMCP (2.0)	1.584 Å
sMCP	1.591 Å

WF ₆	
WTBS	1.848 Å
iMCP (1.6)	1.847 Å

PdCO		
WTBS	Pd-C	2.204 Å
	C-O	1.104 Å
iMCP (1.4)	Pd-C	2.204 Å
	C-O	1.105 Å
sMCP	Pd-C	2.115 Å
	C-O	1.101 Å

ReClO ₃		
WTBS	Re-Cl	2.316 Å
	Re-O	1.689 Å
iMCP (1.2)	Re-Cl	2.328 Å
	Re-O	1.680 Å

OsO ₄	
WTBS	1.699 Å
iMCP (1.5)	1.700 Å

AgH	
WTBS	1.776 Å
iMCP (1.4)	1.776 Å
sMCP	1.740 Å

IrC	
WTBS	1.867 Å
iMCP (1.8)	1.869 Å

CdH	
WTBS	1.811 Å
iMCP (1.3)	1.813 Å
sMCP	1.829 Å

PtC	
WTBS	2.009 Å
iMCP (1.3)	2.009 Å

CdH ⁺	
WTBS	1.735 Å
iMCP (1.3)	1.732 Å
sMCP	1.712 Å

AuH	
WTBS	1.825 Å
iMCP (1.3)	1.824 Å

HfF ₄	
WTBS	1.921 Å
iMCP (2.9)	1.921 Å
sMCP	1.901 Å

HgCl ₂	
WTBS	2.449 Å
iMCP (1.9)	2.450 Å

TaO	
WTBS	1.714 Å
iMCP (2.5)	1.713 Å

A.4 Testing Data for the Second- and Third-Row Transition Metals

YF					
	NR BLYP	SR BLYP	NR B3LYP	SR B3LYP	Exp.
r (Y-F)	1.904	1.915	1.907	1.914	1.926
ω	682	592	389	605	631

ZrF ₄ med grid					
	NR BLYP	SR BLYP	NR B3LYP	SR B3LYP	Exp.
r (Zr-F)	1.919	1.916	1.907	1.904	1.901
ω_1 x2	152	156	154	158	150
ω_2 x3	155	158	161	164	190
ω_3	605	621	634	647	600
ω_4 x3	608	625	635	650	668

ZrF ₄ high grid					
	NR BLYP	SR BLYP	NR B3LYP	SR B3LYP	Exp.
r (Zr-F)	1.911	1.917	1.901	1.905	1.901
ω_1 x2	157	156	159	157	150
ω_2 x3	161	157	167	161	190
ω_3	620	611	646	638	600
ω_4 x3	635	624	657	647	668

ZrCl ₄					
	NR BLYP	SR BLYP	NR B3LYP	SR B3LYP	Exp.
r (Zr-Cl)	2.327	2.324	2.322	2.321	2.320
ω_1 x2	80	82	89	91	98
ω_2 x3	82	84	92	94	113
ω_3	317	327	340	347	377
ω_4 x3	355	369	380	391	418

Mo(CO) ₆	NR BLYP	SR BLYP	NR B3LYP	SR B3LYP	Exp.
r (Mo-C)	2.067	2.056	2.069	2.057	2.063
r (C-O)	1.149	1.150	1.137	1.138	1.145
ω_1 x3	58	59	62	64	60
ω_2 x3	79	82	82	86	79
ω_3 x3	83	85	88	91	82
ω_4 x3	325	334	335	349	342
ω_5 x3	351	368	359	372	367
ω_6 x2	369	375	371	380	381
ω_7	385	393	386	397	391
ω_8 x3	476	483	490	500	477
ω_9 x3	512	518	523	532	507
ω_{10} x3	597	605	611	621	596
ω_{11} x3	1945	1946	2047	2044	2000
ω_{12} x2	1962	1958	2070	2065	2025
ω_{13}	2057	2059	2164	2165	2121

Ag(N ₃) ₄ ⁻	NR BLYP	NR B3LYP	SR B3LYP
r (Ag-N1)	2.197	2.167	2.123
r (N1-N2)	1.214	1.203	1.206
r (N2-N3)	1.167	1.149	1.148
< (Ag-N1-N2)	117.4	116.4	117.2
< (N1-N2-N3)	176.0	176.7	176.0
ω_1	32	35	
ω_2	48	47	
ω_3 x2	56	58	
ω_4	64	66	
ω_5	70	83	
ω_6 x2	87	88	
ω_7	127	137	
ω_8	137	152	
ω_9	145	153	
ω_{10} x2	175	187	
ω_{11}	248	276	
ω_{12}	283	301	
ω_{13} x2	327	358	
ω_{14}	529	548	
ω_{15}	530	549	
ω_{16} x2	532	552	
ω_{17}	575	613	
ω_{18}	575	613	
ω_{19} x2	579	618	
ω_{20}	1248	1324	
ω_{21}	1248	1326	
ω_{22} x2	1250	1328	
ω_{23}	1902	2026	
ω_{24} x2	1903	2029	
ω_{25}	1903	2030	

Cd(CH ₃) ₂ D _{3h} symmetry medium grid					
	NR BLYP	SR BLYP	NR B3LYP	SR B3LYP	Exp.
r (Cd-C)	2.195	2.157	2.182	2.141	2.112
r (C-H)	1.098	1.098	1.093	1.093	1.09
< (Cd-C-H)	110.2	109.8	110.5	110.1	108.4
ω_1	-74	-74	-69	-69	0
ω_2 x2	111	120	114	122	124
ω_4	457	473	477	497	459
ω_5 x2	614	648	623	655	634
ω_6 x2	688	724	697	733	700
ω_7	1118	1133	1157	1173	1127
ω_8	1137	1150	1174	1189	1136
ω_9 x2	1430	1430	1463	1464	1315
ω_{10} x2	1448	1448	1479	1480	1427
ω_{11}	2945	2950	3020	3025	2903
ω_{12}	2957	2962	3030	3034	2923
ω_{13} x2	3030	3038	3105	3112	2859
ω_{14} x2	3036	3044	3110	3117	2980

Cd(CH ₃) ₂ D _{3h} symmetry high grid					
	NR BLYP	SR BLYP	NR B3LYP	SR B3LYP	Exp.
r (Cd-C)	2.194	2.137	2.181	2.129	2.112
r (C-H)	1.099	1.099	1.093	1.093	1.09
< (Cd-C-H)	110.1	110.1	110.4	110.4	108.4
ω_1	21	8	13	-22	0
ω_2 x2	104	120	108	122	124
ω_4	471	506	492	522	459
ω_5 x2	624	643	632	652	634
ω_6 x2	692	719	702	729	700
ω_7	1132	1154	1170	1190	1127
ω_8	1138	1158	1175	1193	1136
ω_9 x2	1439	1440	1471	1471	1315
ω_{10} x2	1442	1443	1474	1475	1427
ω_{11}	2959	2959	3030	3031	2903
ω_{12}	2962	2962	3032	3034	2923
ω_{13} x2	3037	3037	3109	3111	2859
ω_{14} x2	3037	3037	3109	3111	2980

Cd(CH ₃) ₂ D _{3d} symmetry medium grid				
	NR BLYP	SR BLYP	NR B3LYP	SR B3LYP
r (Cd-C)	2.195	2.158	2.182	2.142
r (C-H)	1.099	1.093	1.094	1.093
< (Cd-C-H)	110.2	109.8	110.5	110.2
ω ₁	-74	-70	-68	-66
ω ₂ x2	103	112	107	116
ω ₄	457	472	477	497
ω ₅ x2	609	643	621	653
ω ₆ x2	674	710	687	722
ω ₇	1123	1136	1162	1178
ω ₈	1128	1141	1167	1181
ω ₉ x2	1440	1440	1472	1472
ω ₁₀ x2	1442	1442	1473	1474
ω ₁₁	2946	2951	3021	3026
ω ₁₂	2949	2954	3024	3028
ω ₁₃ x2	3033	3041	3108	3115
ω ₁₄ x2	3034	3042	3108	3115

Cd(CH ₃) ₂ D _{3d} symmetry high grid				
	NR BLYP	SR BLYP	NR B3LYP	SR B3LYP
r (Cd-C)	2.194	2.137	2.181	2.129
r (C-H)	1.098	1.099	1.093	1.093
< (Cd-C-H)	110.1	110.1	110.4	110.4
ω ₁	-23	-31	-23	-36
ω ₂ x2	106	122	110	124
ω ₄	471	506	492	522
ω ₅ x2	629	648	637	656
ω ₆ x2	695	721	705	731
ω ₇	1133	1155	1171	1191
ω ₈	1139	1159	1176	1194
ω ₉ x2	1441	1442	1472	1473
ω ₁₀ x2	1442	1443	1474	1474
ω ₁₁	2959	2960	3030	3031
ω ₁₂	2962	2962	3032	3034
ω ₁₃ x2	3037	3037	3110	3111
ω ₁₄ x2	3037	3037	3110	3111

HfF ₄ med grid					
	NR BLYP	SR BLYP	NR B3LYP	SR B3LYP	Exp.
r (Hf-F)	1.926	1.903	1.916	1.895	1.910
ω_1 x2	155	166	158	169	164
ω_2 x3	162	182	164	183	173
ω_3	590	623	614	645	650
ω_4 x3	617	650	649	675	677

HfF ₄ high grid					
	NR BLYP	SR BLYP	NR B3LYP	SR B3LYP	Exp.
r (Hf-F)	1.897	1.905	1.892	1.896	1.910
ω_1 x2	179	165	180	168	164
ω_2 x3	188	181	186	181	173
ω_3	632	620	649	642	650
ω_4 x3	662	643	683	670	677

HfCl ₄					
	NR BLYP	SR BLYP	NR B3LYP	SR B3LYP	Exp.
r (Hf-Cl)	2.351	2.307	2.348	2.307	2.316
ω_1 x2	77	90	86	98	101
ω_2 x3	86	97	91	102	112
ω_3	323	423	344	435	382
ω_4 x3	333	450	351	460	390

TaO ₃ ⁻					
	NR BLYP	SR BLYP	NR B3LYP	SR B3LYP	Exp.
r (Ta-O)	1.856	1.832	1.843	1.818	
< (O-Ta-O)	106.9	103.4	109.0	104.8	
ω_1	228	273	186	245	
ω_2 x2	282	316	270	310	
ω_3 x2	752	784	737	767	807
ω_4	841	884	860	894	

W(CO) ₆					
	NR BLYP	SR BLYP	NR B3LYP	SR B3LYP	Exp.
r (W-C)	2.118	2.071	2.119	2.070	2.058
r (C-O)	1.149	1.151	1.137	1.139	1.148
ω_1 x3	57	60	60	63	61
ω_2 x3	75	82	68	73	81
ω_3 x3	76	83	78	86	82
ω_4 x3	301	333	268	302	362
ω_5 x3	318	336	327	350	374
ω_6 x2	365	395	368	401	410
ω_7	384	412	386	418	426
ω_8 x3	457	471	471	489	482
ω_9 x3	514	523	524	539	521
ω_{10} x3	567	587	555	582	587
ω_{11} x3	1942	1933	2049	2036	1998
ω_{12} x2	1967	1962	2073	2066	2021
ω_{13}	2059	2058	2166	2166	2126

ReO ₄ ⁻					
	NR BLYP	SR BLYP	NR B3LYP	SR B3LYP	Exp.
r (Re-O)	1.792	1.752	1.771	1.735	
ω_1 x3	288	304	278	291	
ω_2 x2	285	312	299	326	
ω_3 x3	786	835	785	822	907
ω_4	844	891	907	952	

OsO ₄ ⁻					
	NR BLYP	SR BLYP	NR B3LYP	SR B3LYP	Exp.
r (Os-O)	1.776	1.734	1.752	1.713	1.711
ω_1 x3	288	307	275	292	323
ω_2 x2	285	314	302	328	333
ω_3 x3	824	879	830	876	960
ω_4	850	908	921	967	965

$\text{Ir}(\text{CO})_2^-$	NR BLYP	SR BLYP	NR B3LYP	SR B3LYP	Exp.
r (Ir-C)	1.953	1.834	1.953	1.831	
r (C-O)	1.178	1.187	1.163	1.172	
< (C-Ir-C)	131.4	132.8	132.0	133.1	
< (Ir-C-O)	160.6	161.2	161.3	162.1	
ω_1	56	76	50	71	
ω_2	263	335	259	345	
ω_3	265	352	263	362	
ω_4	363	482	346	471	
ω_5	379	504	363	490	
ω_6	409	511	376	498	
ω_7	520	659	518	667	
ω_8	1772	1750	1875	1846	1818
ω_9	1840	1843	1944	1944	

$\text{Pt}(\text{O}_2)$	NR BLYP	SR BLYP	NR B3LYP	SR B3LYP	Exp.
r (Pt-O)	2.116	1.966	2.126	1.960	
r (O-O)	1.362	1.446	1.312	1.391	
ω_1	203	475	198	491	
ω_2	353	489	342	493	
ω_3	1023	900	1164	1001	928

$\text{Au}(\text{N}_3)_4^-$	NR BLYP	SR BLYP	NR B3LYP	SR B3LYP	Exp.
r (Au-N1)	2.213	2.127	2.191	2.093	2.033
r (N1-N2)	1.217	1.224	1.206	1.212	1.220
r (N2-N3)	1.165	1.160	1.148	1.143	1.133
< (Au-N1-N2)	117.3	117.2	116.8	117.3	116.9
< (N1-N2-N3)	175.5	173.8	176.2	174.6	174.4
ω_1	34	28	35	30	
ω_2	45	41	36	33	
ω_3 x2	61	70	56	71	
ω_4	74	81	74	73	
ω_5 x2	82	74	84	85	
ω_6	91	95	101	111	
ω_7	140	148	142	144	
ω_8	150	152	146	160	
ω_9	152	172	160	187	172
ω_{10} x2	178	200	164	190	188
ω_{11}	283	297	306	339	220
ω_{12}	296	326	315	356	236
ω_{13} x2	330	349	332	362	402
ω_{14}	531	513	553	536	414
ω_{15}	532	514	553	537	427
ω_{16} x2	531	515	554	540	575
ω_{17}	563	613	600	653	614
ω_{18}	575	617	613	654	
ω_{19} x2	586	627	621	663	683
ω_{20}	1237	1226	1319	1309	1250
ω_{21}	1245	1226	1322	1309	1261
ω_{22} x2	1243	1229	1322	1307	
ω_{23}	1916	1950	2041	2093	2027
ω_{24} x2	1913	1952	2041	2085	
ω_{25}	1919	1952	2046	2096	2049

Hg(CH ₃) ₂ D _{3h} symmetry medium grid					
	NR BLYP	SR BLYP	NR B3LYP	SR B3LYP	Exp.
r (Hg-C)	2.300	2.186	2.281	2.160	2.083
r (C-H)	1.098	1.097	1.093	1.093	1.106
< (Hg-C-H)	109.9	109.6	110.3	110.0	
ω_1	-73	-71	-68	-66	
ω_2 x2	96	130	98	127	
ω_4	397	439	411	435	
ω_5 x2	612	670	621	686	
ω_6 x2	678	753	689	770	
ω_7	1108	1149	1148	1194	
ω_8	1126	1165	1163	1208	
ω_9 x2	1429	1430	1462	1464	
ω_{10} x2	1446	1448	1477	1479	
ω_{11}	2951	2954	3025	3028	
ω_{12}	2962	2966	3034	3038	
ω_{13} x2	3039	3046	3112	3118	
ω_{14} x2	3044	3051	3117	3123	

Hg(CH ₃) ₂ D _{3h} symmetry high grid					
	NR BLYP	SR BLYP	NR B3LYP	SR B3LYP	Exp.
r (Hg-C)	2.311	2.183	2.290	2.159	2.083
r (C-H)	1.098	1.098	1.093	1.093	1.106
< (Hg-C-H)	110	109.6	110.4	110.0	
ω_1	20	31	-10	27	
ω_2 x2	88	131	100	136	
ω_4	386	454	435	478	
ω_5 x2	606	669	617	687	
ω_6 x2	667	752	683	773	
ω_7	1113	1160	1154	1205	
ω_8	1121	1166	1160	1208	
ω_9 x2	1436	1437	1468	1470	
ω_{10} x2	1440	1442	1471	1474	
ω_{11}	2961	2966	3031	3036	
ω_{12}	2964	2969	3034	3038	
ω_{13} x2	3040	3049	3112	3120	
ω_{14} x2	3040	3049	3112	3120	

Hg(CH ₃) ₂ D _{3d} symmetry medium grid				
	NR BLYP	SR BLYP	NR B3LYP	SR B3LYP
r (Hg-C)	2.301	2.186	2.281	2.160
r (C-H)	1.098	1.098	1.093	1.093
< (Hg-C-H)	109.9	109.6	110.3	110.0
ω_1	-57	-64	-55	-60
ω_2 x2	94	122	98	130
ω_4	426	440	441	466
ω_5 x2	605	664	617	683
ω_6 x2	666	741	680	764
ω_7	1108	1151	1150	1198
ω_8	1115	1155	1156	1201
ω_9 x2	1438	1439	1470	1472
ω_{10} x2	1440	1442	1472	1474
ω_{11}	2952	2956	3025	3029
ω_{12}	2955	2958	3028	3032
ω_{13} x2	3042	3049	3115	3121
ω_{14} x2	3042	3049	3115	3121

Hg(CH ₃) ₂ D _{3d} symmetry high grid				
	NR BLYP	SR BLYP	NR B3LYP	SR B3LYP
r (Hg-C)	2.311	2.183	2.290	2.160
r (C-H)	1.098	1.098	1.093	1.093
< (Hg-C-H)	110.0	109.6	110.4	110.0
ω_1	-32	-19	-30	-20
ω_2 x2	97	133	102	138
ω_4	414	453	434	478
ω_5 x2	610	673	621	690
ω_6 x2	671	753	685	774
ω_7	1114	1161	1155	1206
ω_8	1121	1167	1161	1209
ω_9 x2	1438	1440	1470	1472
ω_{10} x2	1439	1441	1471	1474
ω_{11}	2962	2966	3031	3036
ω_{12}	2965	2969	3034	3039
ω_{13} x2	3041	3049	3112	3120
ω_{14} x2	3042	3050	3113	3120

Appendix B

CCSD(T) Alkaline Earth Metal - Helium Pair Potentials

All of the pair potentials on the next pages were calculated using the CCSD(T) method. The basis set contractions used can be found in Table 6.2, and the exponents, contraction coefficients, and wtMCP potential parameters are available as a preprint. The helium-helium pair potentials calculated with the same well-tempered basis set used in the mixed dimers is included at the end of this Appendix. The following abbreviations are used in the tables:

wtMCP	well-tempered Model Core Potential basis set
WTBS	all-electron well-tempered basis set
FC-WTBS	frozen-core all-electron calculation (only valence electrons correlated)
BF	bond functions used (3s3p2d set)
no BF	no bond functions (just atom-centered basis set)

Table B.1: Be-He CCSD(T) pair potentials

wtMCP no BF		wtMCP BF		WTBS no BF		FC-WTBS no BF	
r (Å)	E_{int} (cm ⁻¹)	r (Å)	E_{int} (cm ⁻¹)	r (Å)	E_{int} (cm ⁻¹)	r (Å)	E_{int} (cm ⁻¹)
2.0	4483.04	2.0	4450.25	2.0	4476.45	2.0	4476.79
2.2	2797.12	2.2	2777.33	2.2	2797.17	2.2	2796.28
2.4	1692.27	2.4	1675.36	2.4	1693.74	2.4	1692.61
2.6	994.89	2.6	980.14	2.6	996.29	2.6	995.31
2.8	568.03	2.8	556.49	2.8	569.03	2.8	568.31
3.0	314.06	3.0	305.53	3.0	314.69	3.0	314.20
3.2	167.05	3.2	160.76	3.2	167.42	3.2	167.11
3.4	84.29	3.4	79.54	3.4	84.50	3.4	84.31
3.6	39.08	3.6	35.40	3.6	39.20	3.6	39.09
3.8	15.28	3.8	12.38	3.8	15.35	3.8	15.29
4.0	3.38	4.0	1.07	4.0	3.42	4.0	3.38
4.2	-2.11	4.2	-3.95	4.2	-2.09	4.2	-2.10
4.4	-4.27	4.3	-5.12	4.4	-4.25	4.4	-4.26
4.5	-4.66	4.4	-5.73	4.5	-4.65	4.5	-4.65
4.6	-4.77	4.5	-5.95	4.6	-4.76	4.6	-4.76
4.7	-4.71	4.6	-5.92	4.7	-4.70	4.7	-4.70
4.8	-4.53	4.7	-5.72	4.8	-4.52	4.8	-4.52
4.9	-4.28	4.8	-5.42	4.9	-4.28	4.9	-4.27
5.0	-4.00	5.0	-4.68	5.0	-3.99	5.0	-3.99
5.2	-3.40	5.2	-3.92	5.2	-3.40	5.2	-3.39
5.4	-2.83	5.4	-3.23	5.4	-2.83	5.4	-2.83
5.6	-2.34	5.6	-2.63	5.6	-2.34	5.6	-2.33
5.8	-1.92	5.8	-2.14	5.8	-1.92	5.8	-1.92
6.0	-1.58	6.0	-1.74	6.0	-1.58	6.0	-1.57
6.2	-1.30	6.2	-1.42	6.2	-1.30	6.2	-1.29
6.4	-1.07	6.4	-1.16	6.4	-1.07	6.4	-1.07
6.6	-0.89	6.6	-0.96	6.6	-0.88	6.6	-0.88
6.8	-0.74	6.8	-0.79	6.8	-0.74	6.8	-0.73
7.0	-0.62	7.0	-0.66	7.0	-0.61	7.0	-0.61
7.2	-0.52	7.2	-0.55	7.2	-0.52	7.2	-0.52
7.4	-0.44	7.4	-0.46	7.4	-0.44	7.4	-0.43
7.6	-0.37	7.6	-0.39	7.6	-0.37	7.6	-0.37
7.8	-0.31	7.8	-0.33	7.8	-0.31	7.8	-0.31
8.0	-0.27	8.0	-0.28	8.0	-0.27	8.0	-0.27
8.5	-0.18	8.5	-0.19	8.5	-0.18	8.5	-0.18
9.0	-0.13	9.0	-0.13	9.0	-0.13	9.0	-0.13
9.5	-0.09	9.5	-0.09	9.5	-0.09	9.5	-0.09
10.0	-0.07	10.0	-0.07	10.0	-0.07	10.0	-0.07
11.0	-0.04	11.0	-0.04	11.0	-0.04	11.0	-0.04
12.0	-0.02	12.0	-0.02	12.0	-0.02	12.0	-0.02
20.0	0.00						

Table B.2: Mg-He CCSD(T) pair potentials

wtMCP no BF		wtMCP BF		WTBS no BF		FC-WTBS no BF	
r (Å)	E_{int} (cm ⁻¹)	r (Å)	E_{int} (cm ⁻¹)	r (Å)	E_{int} (cm ⁻¹)	r (Å)	E_{int} (cm ⁻¹)
2.0	5811.65	2.0	5750.92	2.0	5877.23	2.0	5876.53
2.2	3960.82	2.2	3917.13	2.2	3997.87	2.2	3995.22
2.4	2647.60	2.4	2615.78	2.4	2671.03	2.4	2667.77
2.6	1729.11	2.6	1703.36	2.6	1744.73	2.6	1741.68
2.8	1103.48	2.8	1081.53	2.8	1114.05	2.8	1111.54
3.0	688.70	3.0	670.03	3.0	695.88	3.0	693.95
3.2	420.35	3.2	404.67	3.2	425.22	3.2	423.81
3.4	250.45	3.4	237.52	3.4	253.75	3.4	252.76
3.6	145.05	3.6	134.62	3.6	147.25	3.6	146.58
3.8	80.97	3.8	72.76	3.8	82.42	3.8	81.98
4.0	42.86	4.0	36.53	4.0	43.80	4.0	43.52
4.2	20.78	4.2	15.96	4.2	21.37	4.2	21.20
4.4	8.39	4.4	4.75	4.4	8.76	4.4	8.66
4.6	1.76	4.6	-0.99	4.6	1.98	4.6	1.92
4.8	-1.56	4.8	-3.63	4.8	-1.43	4.8	-1.47
5.0	-3.02	4.9	-4.26	5.0	-2.94	5.0	-2.96
5.1	-3.33	5.0	-4.58	5.1	-3.28	5.1	-3.29
5.2	-3.46	5.1	-4.69	5.2	-3.43	5.2	-3.43
5.3	-3.48	5.2	-4.65	5.3	-3.45	5.3	-3.46
5.4	-3.40	5.3	-4.51	5.4	-3.39	5.4	-3.39
5.5	-3.28	5.4	-4.31	5.5	-3.26	5.5	-3.26
5.6	-3.11	5.6	-3.80	5.6	-3.10	5.6	-3.10
5.8	-2.73	5.8	-3.26	5.8	-2.73	5.8	-2.73
6.0	-2.35	6.0	-2.75	6.0	-2.35	6.0	-2.35
6.2	-2.00	6.2	-2.29	6.2	-2.00	6.2	-2.00
6.4	-1.68	6.4	-1.91	6.4	-1.69	6.4	-1.68
6.6	-1.42	6.6	-1.58	6.6	-1.42	6.6	-1.42
6.8	-1.19	6.8	-1.31	6.8	-1.19	6.8	-1.19
7.0	-1.00	7.0	-1.10	7.0	-1.01	7.0	-1.00
7.2	-0.84	7.2	-0.91	7.2	-0.85	7.2	-0.85
7.4	-0.71	7.4	-0.77	7.4	-0.72	7.4	-0.71
7.6	-0.61	7.6	-0.65	7.6	-0.61	7.6	-0.61
7.8	-0.52	7.8	-0.55	7.8	-0.52	7.8	-0.52
8.0	-0.44	8.0	-0.46	8.0	-0.44	8.0	-0.44
8.5	-0.30	8.5	-0.31	8.5	-0.30	8.5	-0.30
9.0	-0.21	9.0	-0.22	9.0	-0.21	9.0	-0.21
9.5	-0.15	9.5	-0.15	9.5	-0.15	9.5	-0.15
10.0	-0.11	10.0	-0.11	10.0	-0.11	10.0	-0.11
11.0	-0.06	11.0	-0.06	11.0	-0.06	11.0	-0.06
12.0	-0.04	12.0	-0.04	12.0	-0.04	12.0	-0.04

Table B.3: Ca-He CCSD(T) pair potentials

wtMCP no BF		wtMCP BF		WTBS no BF		FC-WTBS no BF	
r (Å)	E_{int} (cm ⁻¹)	r (Å)	E_{int} (cm ⁻¹)	r (Å)	E_{int} (cm ⁻¹)	r (Å)	E_{int} (cm ⁻¹)
2.0	7143.79	2.0	6968.95	2.0	7486.09	2.0	7499.32
2.2	4985.19	2.4	3539.05	2.2	5138.62	2.2	5143.71
2.4	3638.10	2.6	2604.19	2.4	3705.71	2.4	3707.10
2.6	2674.37	2.8	1896.54	2.6	2706.00	2.6	2705.64
2.8	1944.37	3.0	1356.05	2.8	1960.90	2.8	1959.71
3.0	1387.80	3.2	948.34	3.0	1397.47	3.0	1395.97
3.2	970.60	3.4	647.84	3.2	976.72	3.2	975.22
3.4	665.43	3.6	432.40	3.4	669.47	3.4	668.13
3.6	447.65	3.8	282.06	3.6	450.35	3.6	449.25
3.8	295.66	4.0	179.76	3.8	297.50	3.8	296.63
4.0	191.66	4.2	111.71	4.0	192.93	4.0	192.28
4.2	121.74	4.4	67.32	4.2	122.63	4.2	122.16
4.4	75.49	4.6	38.88	4.4	76.13	4.4	75.79
4.6	45.39	4.8	21.01	4.6	45.85	4.6	45.62
4.8	26.13	5.0	10.08	4.8	26.47	4.8	26.32
5.0	14.05	5.2	3.60	5.0	14.31	5.0	14.21
5.2	6.66	5.4	-0.06	5.2	6.86	5.2	6.79
5.4	2.28	5.6	-1.98	5.4	2.43	5.4	2.39
5.6	-0.20	5.8	-2.86	5.6	-0.08	5.6	-0.10
5.8	-1.50	5.9	-3.05	5.8	-1.41	5.8	-1.42
6.0	-2.10	6.0	-3.13	6.0	-2.03	6.0	-2.03
6.1	-2.23	6.1	-3.13	6.1	-2.16	6.1	-2.17
6.2	-2.29	6.2	-3.07	6.2	-2.23	6.2	-2.23
6.3	-2.29	6.3	-2.97	6.3	-2.23	6.3	-2.23
6.4	-2.25	6.4	-2.84	6.4	-2.20	6.4	-2.20
6.5	-2.18	6.6	-2.55	6.5	-2.13	6.5	-2.13
6.6	-2.09	6.8	-2.23	6.6	-2.05	6.6	-2.05
6.8	-1.89	7.0	-1.93	6.8	-1.85	6.8	-1.85
7.0	-1.67	7.2	-1.66	7.0	-1.64	7.0	-1.64
7.2	-1.46	7.4	-1.42	7.2	-1.43	7.2	-1.43
7.4	-1.26	7.6	-1.21	7.4	-1.24	7.4	-1.24
7.6	-1.09	7.8	-1.04	7.6	-1.07	7.6	-1.07
7.8	-0.94	8.0	-0.88	7.8	-0.92	7.8	-0.92
8.0	-0.81	8.5	-0.60	8.0	-0.80	8.0	-0.79
8.5	-0.56	9.0	-0.41	8.5	-0.55	8.5	-0.55
9.0	-0.39	9.5	-0.29	9.0	-0.39	9.0	-0.38
9.5	-0.28	10.0	-0.21	9.5	-0.27	9.5	-0.27
10.0	-0.20	11.0	-0.11	10.0	-0.20	10.0	-0.20
11.0	-0.11	12.0	-0.07	11.0	-0.11	11.0	-0.11
12.0	-0.06	13.0	-0.04	12.0	-0.06	12.0	-0.06
		14.0	-0.03				

Table B.4: Sr-He CCSD(T) pair potentials

wtMCP no BF		wtMCP BF		WTBS no BF		FC-WTBS no BF	
r (Å)	E_{int} (cm ⁻¹)	r (Å)	E_{int} (cm ⁻¹)	r (Å)	E_{int} (cm ⁻¹)	r (Å)	E_{int} (cm ⁻¹)
2.0	8958.16	2.0	8718.78	6.2	-1.64	2.0	9950.62
2.2	5788.18	2.6	2904.06	6.4	-2.02	2.6	3094.00
2.4	4092.68	2.8	2147.37	6.5	-2.10	3.2	1211.99
2.6	3018.45	3.0	1581.72	6.6	-2.12	3.8	430.24
2.8	2248.26	3.2	1149.48	6.7	-2.10	4.4	130.45
3.0	1663.83	3.4	818.60	6.8	-2.05	5.0	33.07
3.2	1214.12	3.6	569.82	6.9	-1.98	5.6	5.61
3.4	871.00	3.8	387.74	7.0	-1.90	6.2	-0.77
3.6	613.96	4.0	258.19	7.2	-1.71	6.4	-1.32
3.8	425.42	4.2	168.40			6.6	-1.55
4.0	289.90	4.4	107.49			6.7	-1.59
4.2	194.29	4.6	66.81			6.8	-1.59
4.4	127.95	4.8	40.05			6.9	-1.57
4.6	82.61	5.0	22.74			7.0	-1.52
4.8	52.08	5.2	11.79			7.1	-1.47
5.0	31.82	5.4	5.06			7.2	-1.41
5.2	18.59	5.6	1.07			7.4	-1.27
5.4	10.12	5.8	-1.16			8.0	-0.87
5.6	4.81	6.0	-2.30			10.0	-0.23
5.8	1.59	6.1	-2.60			12.0	-0.07
6.0	-0.29	6.2	-2.78				
6.2	-1.31	6.3	-2.86				
6.4	-1.79	6.4	-2.87				
6.6	-1.96	6.5	-2.83				
6.7	-1.97	6.6	-2.75				
6.8	-1.95	6.8	-2.52				
6.9	-1.90	7.0	-2.26				
7.0	-1.84	7.2	-1.99				
7.1	-1.76	7.4	-1.73				
7.2	-1.67	7.6	-1.49				
7.4	-1.50	7.8	-1.29				
7.6	-1.32	8.0	-1.11				
7.8	-1.16	8.5	-0.76				
8.0	-1.01	9.0	-0.53				
8.5	-0.71	9.5	-0.37				
9.0	-0.50	10.0	-0.26				
9.5	-0.36	11.0	-0.14				
10.0	-0.26	12.0	-0.08				
11.0	-0.14	13.0	-0.05				
12.0	-0.08	14.0	-0.03				
		15.0	-0.02				

Table B.5: Ba-He non-relativistic CCSD(T) pair potentials

wtMCP no BF		wtMCP BF		WTBS no BF		FC-WTBS no BF	
r (Å)	E_{int} (cm ⁻¹)	r (Å)	E_{int} (cm ⁻¹)	r (Å)	E_{int} (cm ⁻¹)	r (Å)	E_{int} (cm ⁻¹)
2.0	12208.79	2.0	11083.91	6.8	-0.98	6.8	-0.98
2.4	4671.45	3.0	1864.69	6.9	-1.18	7.0	-1.32
2.6	3354.64	3.2	1446.90	7.0	-1.32	7.1	-1.41
2.8	2544.57	3.4	1112.89	7.1	-1.41	7.2	-1.45
3.0	1963.80	3.6	843.19	7.2	-1.46	7.3	-1.47
3.2	1512.40	3.8	625.70	7.3	-1.47	7.4	-1.46
3.4	1152.01	4.0	453.79	7.4	-1.46	7.5	-1.43
3.6	864.55	4.2	321.83	7.5	-1.43	7.6	-1.39
3.8	638.45	4.4	223.56	7.6	-1.39	7.8	-1.29
4.0	463.95	4.6	152.36	7.8	-1.29		
4.2	331.96	4.8	101.95				
4.4	234.01	5.0	66.88				
4.6	162.54	5.2	42.79				
4.8	111.22	5.4	26.45				
5.0	74.86	5.6	15.52				
5.2	49.45	5.8	8.36				
5.4	31.91	6.0	3.78				
5.6	19.97	6.2	0.94				
5.8	11.95	6.4	-0.73				
6.0	6.66	6.6	-1.65				
6.2	3.24	6.8	-2.09				
6.4	1.08	6.9	-2.18				
6.6	-0.22	7.0	-2.23				
6.8	-0.96	7.1	-2.22				
7.0	-1.35	7.2	-2.19				
7.1	-1.45	7.3	-2.13				
7.2	-1.51	7.4	-2.06				
7.3	-1.53	7.6	-1.88				
7.4	-1.52	7.8	-1.69				
7.5	-1.50	8.0	-1.50				
7.6	-1.46	8.5	-1.08				
7.8	-1.36	9.0	-0.76				
8.0	-1.24	9.5	-0.54				
8.5	-0.93	10.0	-0.39				
9.0	-0.68	11.0	-0.21				
9.5	-0.49	12.0	-0.12				
10.0	-0.36	13.0	-0.07				
11.0	-0.20	14.0	-0.04				
12.0	-0.11	15.0	-0.03				
13.0	-0.07	16.0	-0.02				
15.0	-0.03	17.0	-0.01				

Table B.6: Ba-He scalar-relativistic CCSD(T) pair potentials

wtMCP no BF		wtMCP BF	
r (Å)	E_{int} (cm ⁻¹)	r (Å)	E_{int} (cm ⁻¹)
2.0	12856.87	2.0	11880.01
2.4	4925.00	3.0	1869.11
2.6	3486.70	3.2	1414.48
2.8	2588.69	3.4	1060.81
3.0	1952.48	3.6	784.17
3.2	1470.60	3.8	568.95
3.4	1096.78	4.0	404.52
3.6	806.81	4.2	281.82
3.8	584.59	4.4	192.42
4.0	417.15	4.6	128.77
4.2	293.24	4.8	84.40
4.4	203.10	5.0	53.98
4.6	138.56	5.2	33.43
4.8	93.01	5.4	19.77
5.0	61.28	5.6	10.84
5.2	39.48	5.8	5.14
5.4	24.69	6.0	1.61
5.6	14.81	6.2	-0.48
5.8	8.31	6.4	-1.63
6.0	4.13	6.6	-2.20
6.2	1.51	6.7	-2.33
6.4	-0.07	6.8	-2.40
6.6	-0.98	6.9	-2.41
6.8	-1.45	7.0	-2.38
6.9	-1.57	7.1	-2.33
7.0	-1.64	7.2	-2.25
7.1	-1.67	7.4	-2.06
7.2	-1.67	7.6	-1.85
7.3	-1.65	7.8	-1.64
7.4	-1.61	8.0	-1.44
7.6	-1.49	8.5	-1.02
7.8	-1.36	9.0	-0.72
8.0	-1.22	9.5	-0.51
8.5	-0.89	10.0	-0.36
9.0	-0.64	11.0	-0.19
9.5	-0.46	12.0	-0.11
10.0	-0.34	13.0	-0.07
11.0	-0.19	14.0	-0.04
12.0	-0.11	15.0	-0.03
13.0	-0.07	16.0	-0.02
15.0	-0.03	17.0	-0.01

Table B.7: He-He CCSD(T) pair potentials

WTBS no BF		WTBS BF	
r (Å)	E_{int} (cm ⁻¹)	r (Å)	E_{int} (cm ⁻¹)
1.0	31950.93	1.0	31937.49
1.2	14031.31	1.2	14021.48
1.4	6006.85	1.4	5998.38
1.6	2498.93	1.6	2491.51
1.8	1002.89	1.8	996.85
2.0	382.59	2.0	377.88
2.2	134.13	2.2	130.61
2.4	39.18	2.4	36.67
2.6	5.53	2.6	3.81
2.8	-4.70	2.8	-5.85
2.9	-6.20	2.9	-7.14
3.0	-6.59	3.0	-7.35
3.1	-6.38	3.1	-7.00
3.2	-5.88	3.2	-6.39
3.3	-5.26	3.3	-5.67
3.4	-4.63	3.4	-4.96
3.6	-3.48	3.8	-2.72
3.8	-2.57	4.2	-1.48
4.0	-1.90	4.6	-0.84
4.2	-1.42	5.0	-0.50
4.4	-1.06	5.2	-0.39
4.6	-0.81	5.4	-0.31
4.8	-0.62	5.8	-0.20
5.0	-0.48	6.2	-0.13
5.2	-0.38	6.6	-0.09
5.4	-0.30	7.0	-0.06
5.6	-0.24	9.0	-0.01
5.8	-0.19	11.0	0.00
6.0	-0.16		
6.2	-0.13		
6.4	-0.11		
6.6	-0.09		
6.8	-0.07		
7.0	-0.06		
7.5	-0.04		
8.0	-0.03		
8.5	-0.02		
9.0	-0.01		
10.0	-0.01		
11.0	0.00		
12.0	0.00		